THE UNIVERSITY
of EDINBURGH

Synthesis and Applications of Carbon Dots

Andrew Nolan

Doctor of Philosophy

The University of Edinburgh

2014

Declaration

I, Andrew Nolan, confirm that this thesis and the work presented in it are my own and the research described in this thesis was carried out under the supervision of Professor Mark Bradley at the University of Edinburgh between September 2010 and November 2014. Where work has been performed either jointly or wholly by others, this is clearly attributed and where I have quoted the work of others, the source is always given. No part of this thesis has been previously submitted for any other degree or professional qualification.

Parts of this thesis were published previously as:

Jiang, Z., Nolan, A., Walton, J. G. A., Lilienkampf, A., Zhang, R., and Bradley, M., Photoluminescent Carbon Dots from 1,4-Addition Polymers, Chemistry A European Journal 2014, 20, 10926–10931. The author of this thesis was joint first author.

Signed: Date:

Abstract

The use of non-invasive methods to visualise and monitor processes inside living organisms is vital in the understanding and diagnosis of disease. The work in this thesis details the synthesis and applications of a new imaging modality; carbon dots, whose inherent fluorescence and non-toxic nature makes them attractive alternatives to more traditional ‘quantum dots’.

In this thesis, different methods of carbon dot synthesis were attempted in order to produce carbon dots of the desired size and morphology. Nitrogen-containing carbon dots generated from 1,4-addition polymers provided the most successful route with optical and structural characteristics studied by TEM, UV-Vis and fluorescence spectroscopy and XPS. The biological behaviour of the carbon dots produced by this method were also evaluated. The ability of these carbon dots to up-convert when excited at long excitation wavelengths was studied.

A number of biologically relevant applications of the carbon dots were studied. Using amine-functionalised carbon dots, cell targeting cargoes were conjugated and the effects of the carbon dot-cargo conjugates on cell lines were studied.

Lay Summary

Monitoring and visualising processes within cells is crucial in understanding the way diseases work and ultimately in diagnosing and treating these diseases. Techniques which enable this to happen without the need for invasive surgery are generally termed ‘molecular imaging’. This wide-ranging field covers everything from X-Rays and MRI scans to lesser known techniques such as PET and SPECT.

Optical imaging is a technique that relies on light to interrogate molecules. In order to visualise the process of interest, fluorescent molecules are attached to a probe, which can give an indication of where the probe is located within a body or a cell. The work in this thesis describes a new carbon nanoparticle-based imaging probe that is inherently fluorescent, therefore removing the need to use additional fluorophores. The synthesis of these carbon nanoparticles from carbon rich polymer starting materials is reported and their optical and structural properties are described. The carbon nanoparticles were shown to be non-toxic and readily taken up by cells. To test the biological relevance of these carbon nanoparticles, they were attached to compounds which targeted the carbon nanoparticles to certain cellular locations. Fluorescence microscopy was used to verify the location of the nanoparticles within the cells.

These new fluorescent carbon nanoparticles are a non-toxic alternative to other fluorescent molecules (fluorophores, quantum dots, etc) and have potential use in a variety of optical imaging scenarios.

Acknowledgements

Firstly, I would like to thank Professor Mark Bradley for the support and guidance he has given me over the course of my PhD in his group – it has been a rewarding experience and I have learnt a lot, personally as well as academically. Thanks also to all the postdocs in the group, especially Nicos, Nanna, Sunay, Tashfeen, Jeff, Ana and Michael, without whom my reactions and writing just would not have progressed. A further thanks must go to Matthew, whose semi-confocal wizardry helped me get published. Additional thanks must go to the EPSRC and the MRC for funding this PhD.

My time in the group has been punctuated by a series of friendships, from the old guard (Neil, Aurélie, Holly, Martha, Matt and Martin) to the new crew (Fiammetta, Eugenio, Claudia, Andrea, Jess, Liz), everyone in the office over the last 4 years has created such as welcoming environment in which to learn – thank you.

My thanks also go to those outisde of the lab who have spurred me on to achieve what is written on these pages. To my parents, Michael and Heather, for their constant encouragement even when they did not understand the science, for their financial help and for many supportive phone calls. To James and David, for keeping me grounded. Thanks also to Elaine for her wisdom, honesty and long lasting friendship which has helped me finish. Finally to all my new friends in Edinburgh, especially Garry, Jürgen and Anne whose day to day help and genuine friendship are much appreciated.

Abbreviations

Ac_2O	Acetic anhydride
BHEDA	Bis(2-hydroxyethyl)ethylenediamine
Boc	*tert*-Butoxycarbonyl
Chloranil	Tetrachloro-1,4-benzoquinone
d	Doublet
Da	Daltons
DCM	Dichloromethane
DIC	Diisopropylcarbodiimide
DLS	Dynamic Light Scattering
DMEM	Dulbecco's Modified Essential Medium
DIC	*N*,*N'*-Diisopropylcarbodiimide
DIPEA	*N*,*N*-Diisopropylethylamine
DMF	*N*,*N*-Dimethylformamide
DTT	Dithiothreitol
ELSD	Evaporative light scattering detector
ES	Electrospray
Et_2O	Diethyl ether
FACS	Fluorescence-activated cell sorting
Fmoc	Fluorenylmethoxycarbonyl
GPC	Gel-permeation chromatography
HNE	Human neutrophil elastase
HPLC	High-performance liquid chromatography
IR	Infrared
J	Coupling constant
m	multiplet
MALDI-TOF	Matrix-assisted laser desorption/ionization – time of flight
MBA	Methylene bisacrylamide
MCF7	Human adenocarcinomic mammary gland epithelial cells
MeOH	Methanol

NHS	*N*-Hydroxysuccinimide
Ninhydrin	2,2-Dihydroxy-1,3-indandione
Oxyma	Ethyl 2-cyano-2-(hydroxyimino)acetate
Pbf	2,2,4,6,7-Pentamethyldihydrobenzofuran-5-sulfonyl
PBS	Phosphate-buffered saline
PC3	Human adenocarcinomic prostate cells
PDI	Polydispersity index
PEG	Poly(ethylene) glycol
RAW	Abelson murine leukemia virus-induced macrophages
t	triplet
TEGDA	Tetraethyleneglycol diacrylate
TEM	Transmission Electron Microscopy
TFA	Trifluoroacetic acid
TIS	Triisopropylsilane
δ	Chemical shift in ppm
λ	Wavelength
λ_{em}	Emission wavelength
λ_{ex}	Excitation wavelength
μW	microwave
Φ	Quantum yield

Table of Contents

Chapter 1:

Introduction

1.1 Nanoparticles

Defined by the National Nanotechnology Initiative as "the manipulation of matter with at least one dimension sized from 1 to 100 nanometres",[1] nanotechnology covers subjects as diverse as semiconductors and surface science[2] to biological chemistry.[3] Although it has its detractors, nanotechnology continues to attract widespread investment due to the diversity of potential applications.[4]

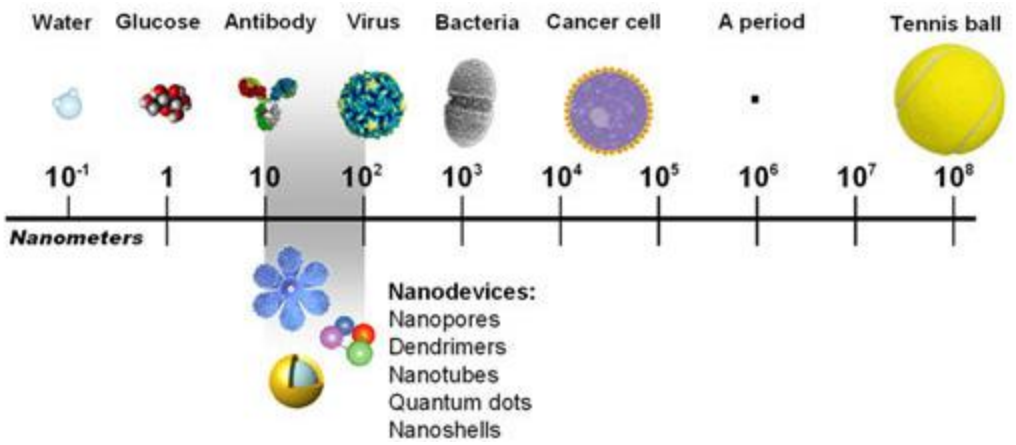

Figure 1: Nanoparticles between 1-100 nm include dendrimers, gold nanoshells, quantum dots and liposomes and are shown in comparison to molecules for size comparison. Reprinted with permission from the National Cancer Institute, Office of Cancer Nanotechnology research.[5]

Nanoparticles are particles having at least one dimension sized between 1 and 100 nm (**Figure 1**) which can display properties not seen in larger-sized particles of the same material.[6] In larger particles, there are relatively few atoms on the surface compared with the bulk whereas in nanoparticles, the large surface area to volume

ratio dominates the chemistry. Due to their small size, quantum mechanical effects have an important bearing on the properties of nanoparticles, in particular novel optical properties due to the 'confinement of electrons'.[7] The diameter of large particles is much larger than the electron wave function, therefore the distance between the conduction and valence bands (bandgap) remains constant. In nanoparticles however, the diameter is of the same magnitude as the electron wave function, therefore the energy levels become discrete (rather than continuous).[8] The bandgap is dependent on the size of the nanoparticle which results in different optical and electronic properties compared to larger particles or bulk material (**Figure 2**). Many applications take advantage of these unique properties ranging from paint formulations[9] to sunscreens[10] and cosmetics.[11]

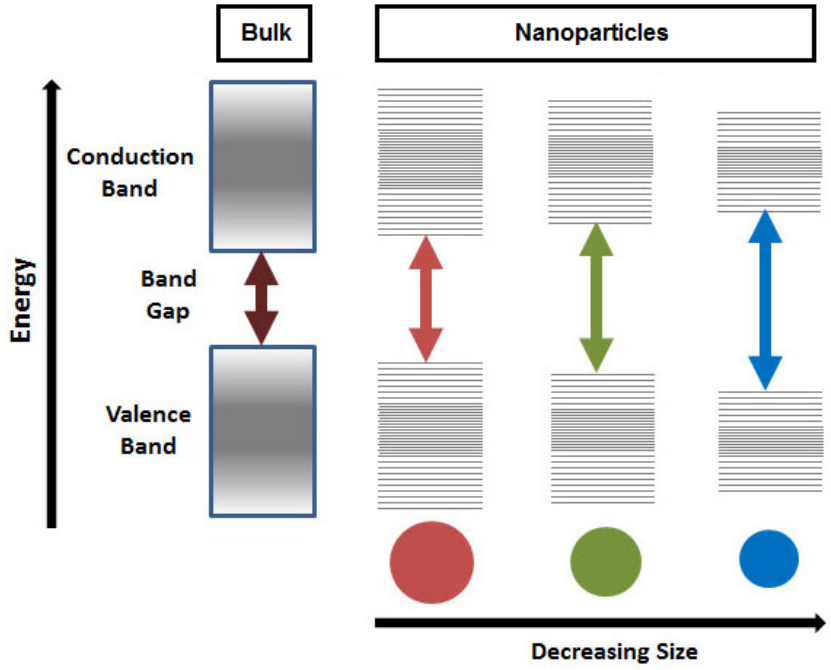

Figure 2: Differences in band gap energy between bulk materials and nanoparticles of different sizes. As the size of the nanoparticle decreases, the band gap widens resulting in fluorescence. Reprinted with permission from Sigma Aldrich.[12]

Nanoparticles based on various materials such as gold and other d- or f-block metals, e.g. iron, silver, and lanthanum have been reported with applications across molecular imaging platforms.[13–15] Gold nanoparticles are widely studied and a range

of applications developed. A typical 3 nm nanoparticle will contain ~500 gold atoms[16] with the size of the gold nanoparticles depending greatly on the method of synthesis - most applications focussing on gold nanoparticles <10 nm. A popular and simple method for gold nanoparticle fabrication is the citrate reduction of $HAuCl_4$ first developed by Turkevich.[17] In this process, Au^{3+} ions are reduced to neutral gold atoms which precipitate from the supersaturated solution as nanoparticles. Compared to small molecule fluorophores which can be degraded by light, gold nanoparticles do not undergo photobleaching.[18]

Gold nanoparticles have been widely studied due to their unique surface properties. For example, the electrons at the surface of gold nanoparticles are in resonance with the frequency of light, in a process known as surface plasmon resonance.[19] This phenomenon depends on the size of the nanoparticle (~30 nm nanoparticles appear red whereas larger particles or aggregates appear blue to purple), and can be used to tailor the optical properties of these nanoparticles for different applications.[20,21] Surface modification of gold nanoparticles is achieved via Au-S chemistry which has been used to introduce polyethylene glycol (PEG) and other polymers to stabilise the nanoparticles and make them suitable for biological applications, i.e. detection of biomarkers.[22] Functionalising gold nanoparticles is the basis of many widely used assays, e.g. the home pregnancy test.[23] Gold nanoparticles tagged with antibodies specific to the β-subunit of human chorionic gonadotropin (hCG) travel via capillary action across strips coated with immobilised α-subunits. On binding of the β-subunit in the urine of the pregnant woman to the antibody-functionalised gold nanoparticle and subsequent binding of the two subunits, a red line will appear if the hCG concentration is high enough. This colour change property has been exploited in mercury sensing when gold nanoparticles are functionalised with nitrogen rich ligands which chelate the mercury ions.[24] On binding of mercury ions, the individual red nanoparticles aggregate and become blue in colour (**Figure 3**).

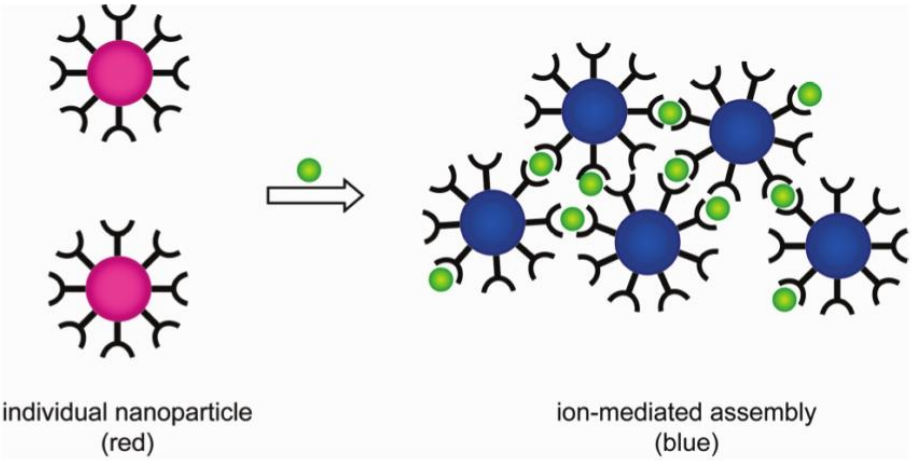

Figure 3: Red-to-blue colorimetric sensing of mercury ions using gold nanoparticles functionalised with chelating ligands. Reprinted with permission from Rotello.[25] Copyright 2012 American Chemical Society.

Gold nanoparticles have been widely used in clinical applications.[26] Qian used gold nanoparticles functionalised with Raman reporters and single chain variable fragment (ScFv) antibodies to target epithelial growth factor receptors (EGFR) found on cancer cells.[27] Over time the nanoparticles accumulated in the tumours and their location was detected using Surface Enhanced Raman Spectroscopy (SERS) (**Figure 4**) (laser irradiation λ_{ex} 785 nm). On irradiation with light, localised surface plasmons in gold (and silver) nanoparticles are excited and resonate with similar frequencies to the incident radiation, thus enhancing the Raman scattering of Raman-active molecules (Raman reporters) adsorbed onto the surface of the metallic nanostructure.[20]

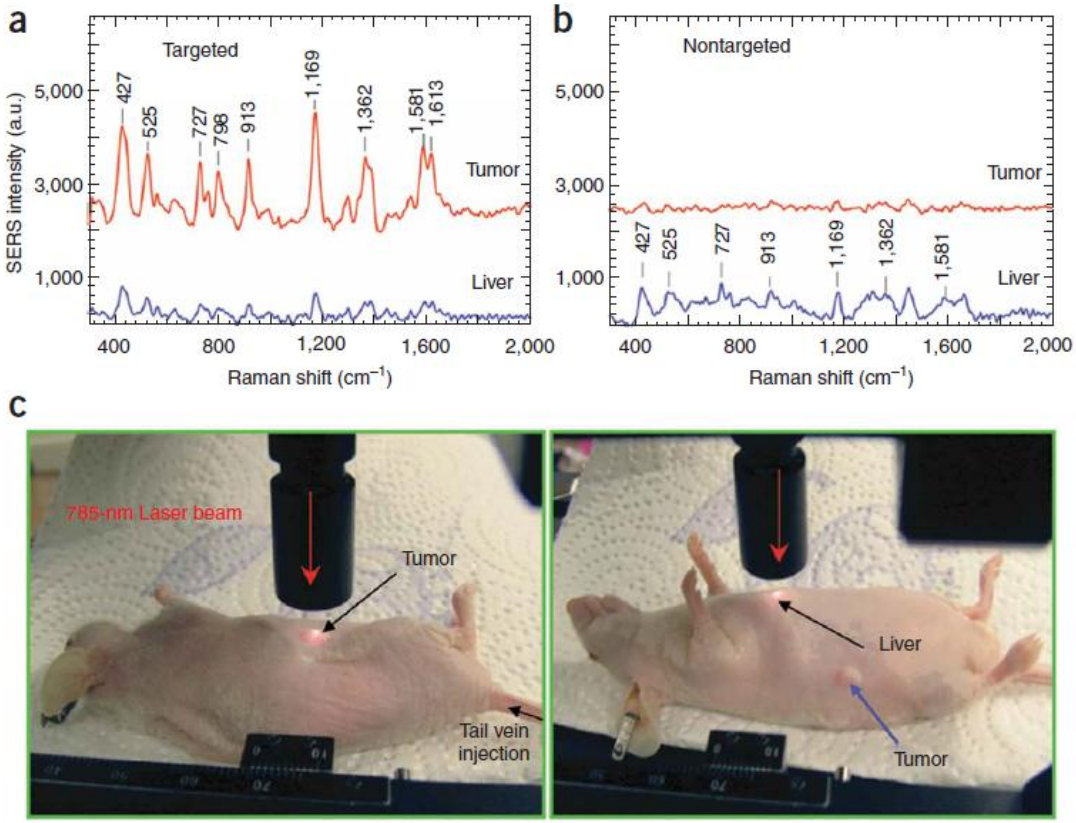

Figure 4: SERS spectra obtained from the tumour (red lines) and liver (blue lines) using (a) targeted and (b) non-targeted gold nanoparticles administered to nude mice by tail vein injection; (c) laser irradiation of the tumour site and liver (λ_{ex} 785 nm). Raman reporter used was Malachite green. Reprinted with permission from Qian.[27] Copyright 2008 Nature Publishing Group.

Once a tumour has been detected, gold nanoparticles themselves can be used for photothermal ablation. Thus, Huang irradiated the area using a near infrared (NIR) laser causing the nanoparticles to absorb the incident energy and generate heat sufficient enough to kill the tumour cells.[28] Aside from their clinical applications, gold nanoparticles have also been used to identify if foods are suitable for consumption.[29] A DNA sequence complimentary to that present in pork (but not beef or chicken) was incubated with gold nanoparticles. When challenged with DNA extracts from beef or chicken products, no duplex was formed and as such the gold nanoparticles remained dispersed in solution. On binding with the complimentary sequence present in pork products (or products adulterated with pork), aggregation of the gold nanoparticles resulted in a colour change from pink to grey.

Silver nanoparticles (AgNPs), in similarity to gold, have been widely used due to their optical and physico-chemical properties.[30–32] Although physical, photochemical and biological methods of synthesis exist, traditional chemical methods remain the most straightforward.[33] In most cases, $AgNO_3$ is reduced ($NaBH_4$) in the presence of a capping or stabilising agent (PVA, PVP, sodium oleate). Among the beneficial properties of AgNPs, are their antibacterial effects against both Gram-negative and Gram-positive bacteria which has been exploited for centuries and are used in clinical dressings today.[34] Silver nanoparticles attach to the bacterial cell membrane disrupting its permeability and affecting the function of the membrane. Interaction of silver nanoparticles with compounds inside bacteria are also reported to contribute to their bactericidal effect. Padilla investigated the bactericidal effect of an AgNP suspension against multidrug resistant Pseudomonas aeruginosa, ampicillin resistant Escherichia coli and erythromycin resistant Streptococcus pyogenes.[35] The silver nanoparticles were shown to inhibit the bacterial growth rate from the time of first contact via a bactericidal mechanism (**Figure 5**).

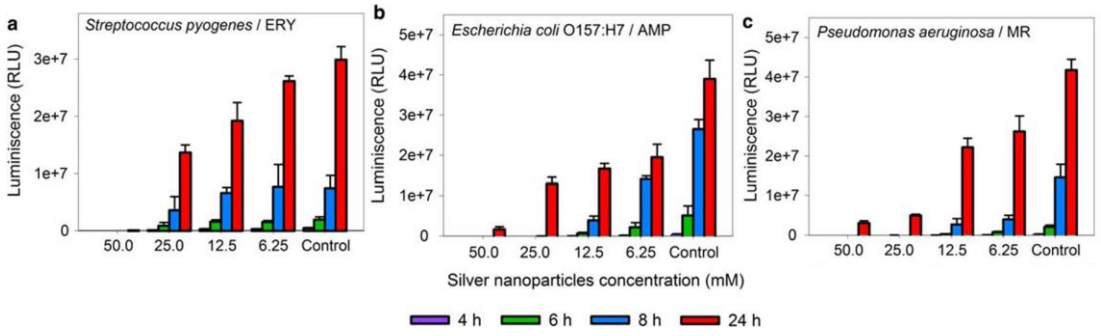

Figure 5: Time-kill assays of drug-resistant bacteria measured using a luciferase-based assay (enhanced luminescence in this assay is proportional to cell death) of (a) erythromycin resistant *S. pyogenes,* (b) ampicillin-resistant *E. coli* O157, and (c) multidrug-resistant *P. aueuginosa*, incubated with media containing different concentrations of silver nanoparticles. Reprinted with permission and adapted from Padilla.[35] Copyright 2009 Springer Science+Business Media B. V.

Magnetic nanoparticles such as those based on iron, nickel and cobalt, or manganese oxide, have applications in imaging, particularly within the field of MRI as contrast agents.[36–39] The most widely studied nanoparticles are iron-based, in part due to the approved medical use of some magnetic iron oxide nanoparticles.[40] Below 128 nm, iron oxide nanoparticles become superparamagnetic,[41] i.e. their magnetism is only exhibited on application of an external magnetic field, thus minimising aggregation of the nanoparticles. In similarity to gold nanoparticles, iron nanoparticles deposited in a tumour released heat when irradiated with an alternating magnetic field. Rabias synthesised maghemite nanoparticles (γ-Fe_2O_3) which showed high absorption of an alternating magnetic field, from ferric chloride and ferrous chloride in the presence of KOH using a coprecipitation method.[42] The nanoparticles were coated with biocompatible dextran which hindered the growth of clusters. Very small quantities of the nanoparticles were demonstrated to be efficient in the heating of small sized tumours reaching temperatures up to 99 °C within 3 min when exposed to a moderate magnetic field (**Figure 6**).

MRI contrast agents based on iron oxide produce strong visual differences between healthy tissue and tumours and overcome the adverse renal effects that more traditional gadolinium compounds can cause.[43] Magnetic nanoparticles functionalised with peptide sequences can target the vascular cell adhesion molecule-1 (VCAM-1), which is involved in the initiation and progression of atherosclerotic plaques. These VCAM-1 internalising nanoparticles were injected into mice and were shown to enhance the MRI signal in the aortic roots (**Figure 7**).[44] The probe was also used to evaluate the therapeutic efficacy of statin treatment of the mice.

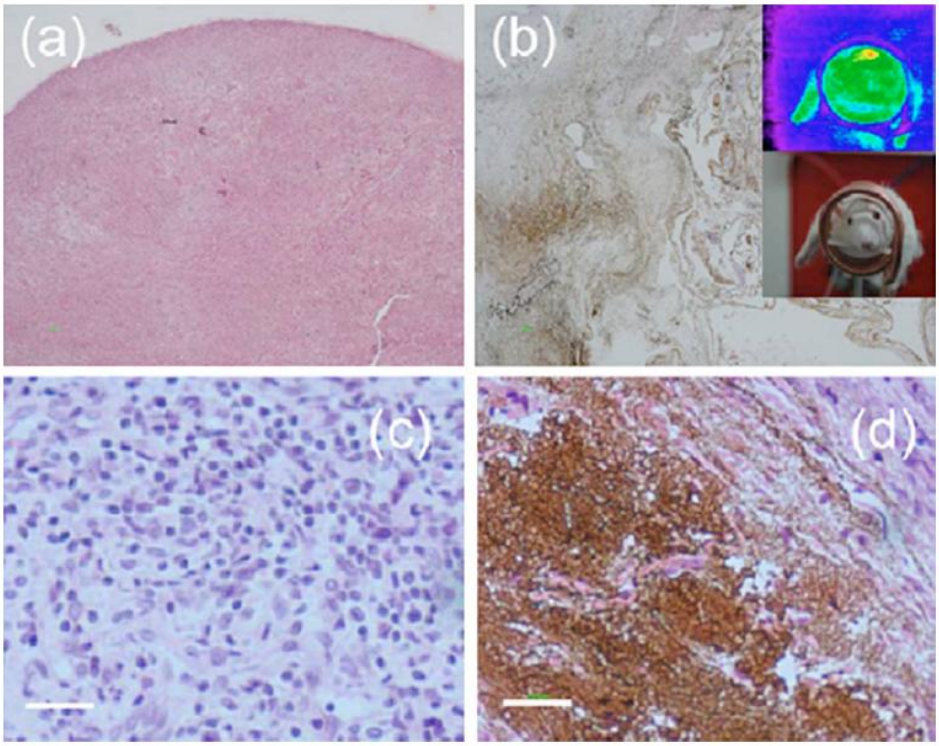

Figure 6: (a) and (c) (low and high magnifications, respectively) show cross sections of control tumour tissue without nanoparticles; (b) and (d) (low and high magnifications, respectively) show damage of the tumour tissue after treatments with iron nanoparticles solution. The upper inset in (b) thermal image showing the ability of the nanoparticles to produce strong localized heating at the tumour site. Reprinted with permission from Rabias.[42] Copyright 2010 AIP Publishing LLC.

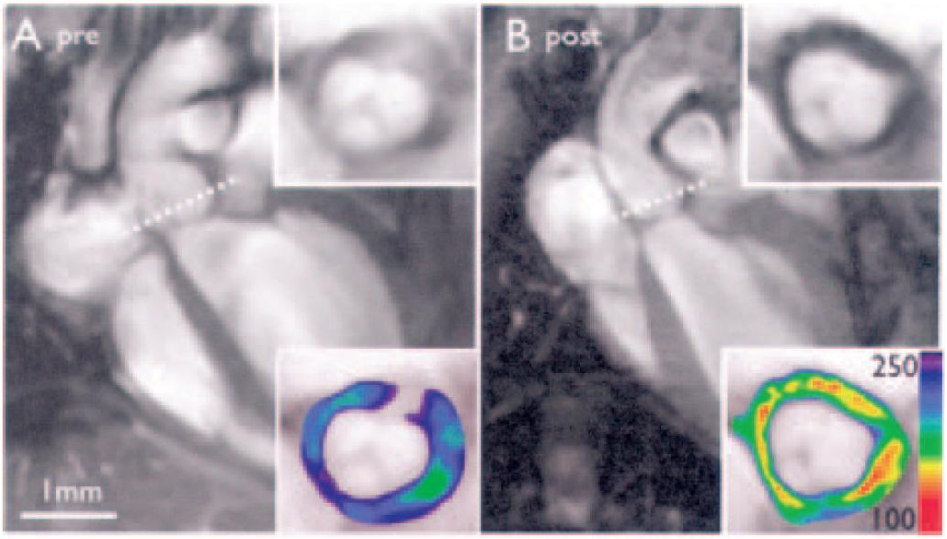

Figure 7: In vivo MRI of VCAM-1 expression. (A) MRI before injection of VCAM-1 nanoparticles (B) same mouse 48 h after injection of VINP-28; (insets are an expansion of the area indicated by the dotted line, lower inset colour coded signal intensity). Adapted and reprinted with permission from Nahrendorf.[44] Copyright 2006 American Heart Association, Inc

Apart from their use as imaging agents, the easy separation of these nanoparticles by the application of a magnetic field has led to their potential in the treatment of contaminated water. Heavy metals chelate with the surface of the functionalised nanoparticles which can quickly be removed from solution. Koehler used polyethylene imine and heavy metal chelators to functionalise iron nanoparticles.[45] These magnetic nanoparticles were shown to extract Pb^{2+}, Cd^{2+} and Cu^{2+} ions from aqueous media to concentrations as low as μg L^{-1}. A scaled up version of the experiment (8 L water and 1 g magnetic nanoparticles) showed 95% of the nanoparticles were recovered on application of a permanent magnet.

Although magnetic nanoparticles have medical applications, the drawbacks associated with these metallic particles include their toxicity,[46,47] even when some polymeric coatings are applied.[48] High local concentrations of nanoparticles can build up inside cells in endosomes.[49] The direct or indirect interaction of metal-based nanoparticles within cells can affect the normal behaviour of the cytoskeleton[50] and disrupt signalling pathways vital for the cell's normal function. Dissolution of the nanoparticle core and leaching of free metal ions into the cytosol has also been shown to induce high levels of apoptosis and inflammation.[51] Particularly associated with magnetic particles, although not exclusively, is the concern around the generation of reactive oxygen species (ROS).[52] Functional groups on the surfaces of nanoparticles, active redox cycling on the surfaces of transition metal nanoparticles and interactions between the particles and the cell are key factors in inducing oxidative stress.[53] Fenton or Haber-Weiss reactions generate ROS with the involvement of transition metals causing reactive OH• to be generated.[54,55] Although a certain level of ROS within the cell is tolerated, nanoparticles can induce levels of ROS within cells that severely disrupt normal function causing apoptosis.[56]

Nanoparticles show many promising applications, however, there are environmental, ethical and toxicological issues to consider before they should be viewed as a panacea. The size of many nanoparticles is important for their advantageous properties but also increases the likelihood of release into waste streams. Public

perception of nanotechnology also remains an issue and a careful balance between scientific progress and regulation must be struck in order for the benefits of these materials to be fully evolved.

1.2 Nanoparticles in Optical Imaging

The incorporation of organic dyes into optically transparent silica nanoparticles has been suggested as an attractive option for optical imaging. By using a fluorescein-labelled aminosilane in the nanoparticle synthesis, Santra was able to synthesise fluorescein-loaded silica nanoparticles.[57] The surface of these nanoparticles was then functionalised with human leukaemia cell specific CD10 monoclonal antibodies with fluorescence microscopy confirming the successful labelling of leukaemia cells. This incorporation method has also been proposed from apatite (calcium phosphate) nanoparticles[58] and inorganic oxide nanocrystals (Y_2O_3, $NaYF_4$).[59] The usefulness of silica nanoparticles lies in the ability to carry cell impermeable fluorescent dyes across the cell membrane.[60] The concentrations of dye within the nanoparticle can be low enough to avoid self-quenching[61] and the versatility of surface functionalisation allows conjugation of a large number of targeting molecules.[62] Silica nanoparticles have been widely used in biological applications. Qian synthesised a ratiometric nanosensor to detect Zn^{2+} and $H_2PO_4^-$ inside living cells.[63] A reference dye was incorporated into the core of a silica nanoparticle and a Zn^{2+} sensitive fluorophore was conjugated to the shell (see **Figure 8**). The scope of silica particles extends beyond dye incorporation and nanoparticles have been used to improve the bioavailability of hydrophobic drugs both via controlled release, and to transport drugs that would not normally be taken up, into cells by endocytosis.[64]

Figure 8: (a) bright field image of HeLa cells incubated with the silica sensor nanoparticles (b) fluorescence image of HeLa cells incubated with the silica sensor nanoparticles (c) fluorescence image of HeLa cells incubated with silica sensor nanoparticles and further incubated with Zn^{2+} (5 x 10^{-5} M) for 30 min. Reprinted with permission from Qian.[63] Copyright 2010 The Royal Society of Chemistry.

Tung developed polymeric nanoparticles based on poly(lysine) with pendent peptide-fluorophore groups.[65] By carefully tuning the peptide-fluorophore ratio, self-quenching of the fluorophores make the probes optically silent. On proteolytic cleavage of the peptide by the enzyme of interest, the fluorophores were released and imaged in vivo (**Figure 9**). Although fluorescent silica nanoparticles and organic nanoparticles have shown promising applications, their optical properties are often still dependent on the incorporation of a small molecule fluorophore rather than intrinsic fluorescence.

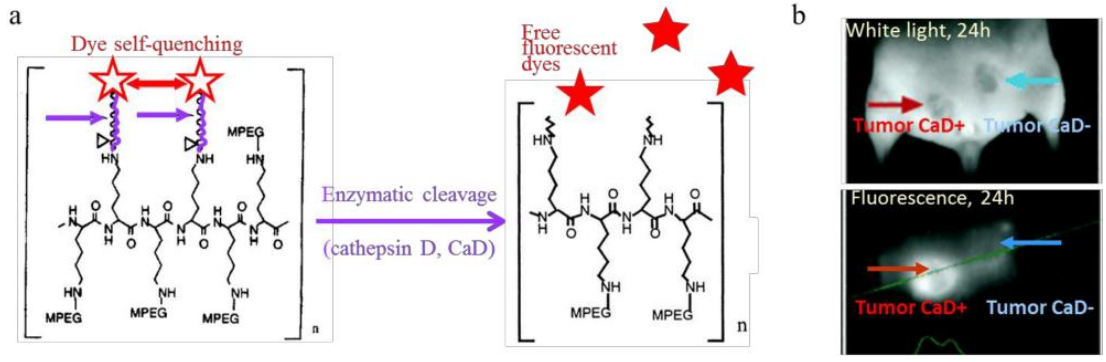

Figure 9: (a) probe structure based on poly(lysine) with pendent peptide-fluorophore moieties is cleaved by the enzyme of interest (in this case, cathepsin D) to release the fluorophores (b) *In vivo* fluorescence images taken 24 h after injection of the probe in mice with cathepsin D positive and negative tumours. Reprinted from Texier *et al,* open access publication.[66] Copyright 2012 Texier *et al.*

1.3 Quantum Dots

The most widely studied photoluminescent nanoparticles are quantum dots, clusters of semiconductor atoms 2–10 nm in diameter. They are predominantly composed of mixtures of elements from groups II and VI (e.g. ZnS, CdSe) or IV and VI (e.g. PbS, PbSe) in an ordered crystal structure.[67] A typical 2 nm quantum dot contains ~100 atoms (10 atom diameter) whereas a 10 nm quantum dot contains ~100,000 atoms (50 atom diameter).[68] Quantum dots were first reported in the early 1980s by Ekimov from molten glass,[69] and Brus from aqueous colloidal solutions of CdS.[70] It was not until 1993, that Murray reported the synthesis of monodisperse colloidal quantum dots with particle size controlled by the temperature of the reaction.[71] The reaction of $CdMe_2$ with PH_3Se, PH_3Te or $(Me_3Si)_2S$ in a coordinating solvent with a high boiling point resulted in luminescent cadmium chalcogenide quantum dots – a turning point in the efficient and controlled production and study of these materials.

The photoluminescence of quantum dots renders them useful in optical imaging and the mechanism of luminescence can be attributed to their size and structural similarity to semiconductors. On absorption of light, electrons in the valence band are excited to electronic levels within the conduction band, leaving behind a positively charged 'hole'. The radiative recombination of the electron hole pair results in the emission of light (**Figure 10**).[72] Larger quantum dots have more energy levels which are more closely spaced meaning less energy is required to promote electrons, i.e. 10 nm quantum dots display red fluorescence whereas 2–3 nm quantum dots display blue fluorescence (**Figure 11**). The fluorescence of carbon dots arises because the energy required to promote an electron from the valence to the conduction band results in the emission of a photon in the visible region of the electromagnetic spectrum.[73]

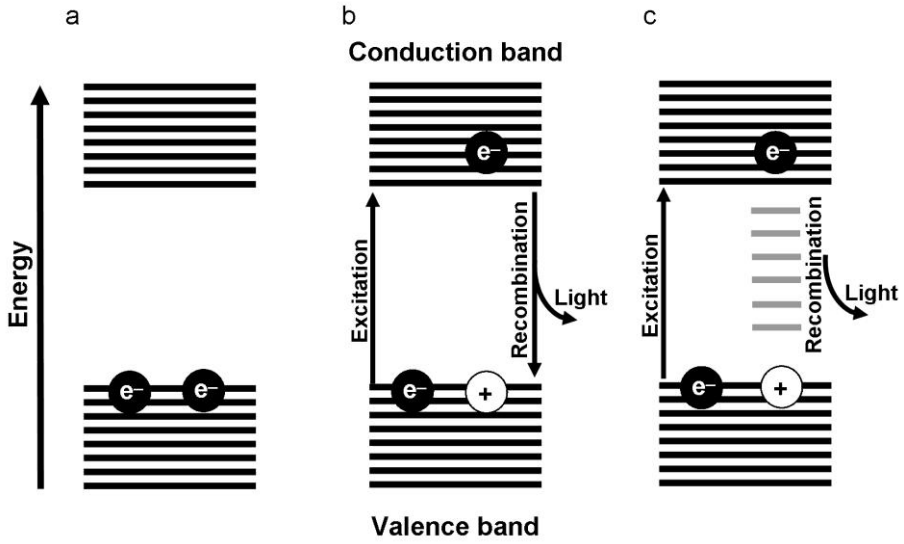

Figure 10: (a) Quantised energy levels in a quantum dot with electrons in the valence band (b) promotion of an electron to the conduction band leaves a positively charged hole in the conduction band, recombination of this electron-hole pair results in emission of light at fluorescence (c) recombination of an electron and hole at surface energy traps (grey lines) results in the emission of light in the form of fluorescence.

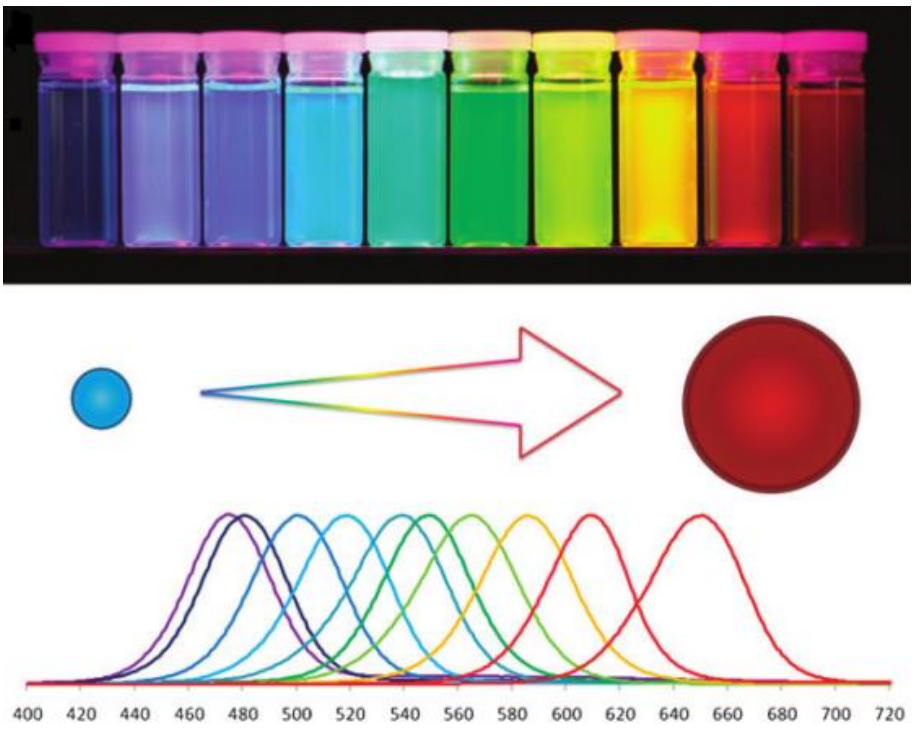

Figure 11: Different sizes of quantum dots display different optical properties; smaller quantum dots with a larger bandgap display blue fluorescence whereas larger quantum dots with a smaller bandgap require less energy to excite electrons, thus appear with red fluorescence. Reprinted with permission from Gao.[73] Copyright 2010 The Royal Society of Chemistry

Key to the photoluminescent properties of the quantum dots is the energy associated with energy traps located on the surface of the dot. The incomplete bonding of atoms at the surface (in comparison to the core material) results in 'dangling' orbitals pointing away from the surface which carry a slight positive or negative charge. If the energy of this orbital is within the bandgap, electrons and holes can be trapped at the crystal surface. Traps for electrons are provided by ‘dangling’ cadmium orbitals, and traps for holes are provided by ‘dangling’ selenium orbitals.[67] Stabilising these traps (passivation) at a specific position with organic molecules increases the chances of radiative recombination of electron-hole pairs at these sites. Early reported quantum yields were in the range of 5–15% for organically passivated quantum dots.[71,74]

It became clear, however, that the majority of ‘naked’ quantum dots or those with organic groups used to passivate the surface gave low photoluminescent quantum yields. Hines remedied this issue by coating the CdSe core with ZnS, an inorganic semiconductor shell with a larger bandgap between the conduction and valence bands.[75] This shell further confines the electron-hole pairs and leads to increased fluorescence intensity. Further coating with a polymeric or water soluble layer enhances biocompatibility and enables cellular uptake (**Figure 12**).[73]

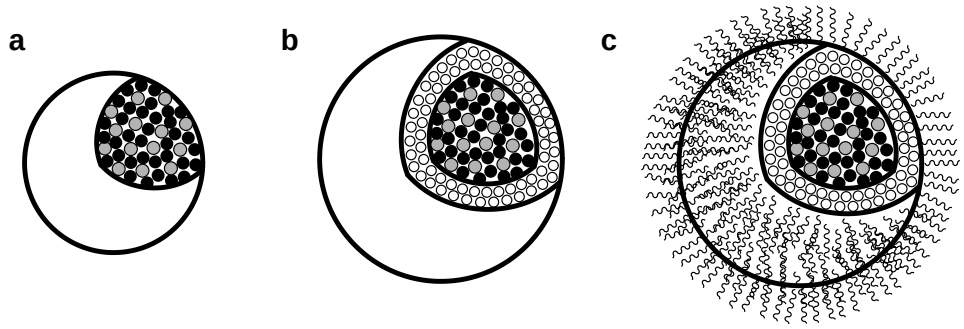

Figure 12: (a) ‘naked’ quantum dots consist of a CdSe core (cut away from spherical dot shown) (b) coating by ZnS further enhances the optical properties (cut away shown) (c) passivation by organic molecules aids biocompatibility and is usually required in ‘top down’ synthesis methods for fluorescence to occur.

One significant advantage of quantum dots over small molecule fluorophores is that they do not undergo photobleaching.[76] This has led to marketing of quantum dots for the long term storage of pathological samples.[77] The quantum size effect of quantum dots allows their emission to be tuneable, i.e. a narrow size distribution of quantum dots gives rise to a sharp emission peak rendering them useful in multi-colour experiments.[78] Emission peaks of quantum dots are symmetric, they have high thermal and photochemical stability and their quantum yields are comparable to those of small molecule fluorophores in the visible region and higher in the NIR region. Quantum dots do, however, suffer from blinking emission caused by the competition between radiative and non-radiative relaxation.[79]

Quantum dots have been used in protein and nucleic acid detection as well as in vivo targeting and imaging.[80,81] The major drawback of cadmium based quantum dots is their toxicity, particularly with 'naked' or uncoated dots.[82] Deterioration of the core lattice and subsequent leaching of Cd^{2+} ions from the structure is known to cause severe hepatic injury.[83] Although coating the cadmium-containing core with the ZnS shell reduces cytotoxicity, it does not eliminate it, hampering applications of these promising materials. Investigation into cadmium free quantum dots based on indium[84] or silicon-based and carbon-based structures at the turn of the 21st century allowed progression of the research into biocompatible photoluminescent nanoparticles.

1.4 Carbon Dots

Carbon dots have provided the next logical step from CdSe quantum dots. Research into these organic nanoparticles has grown rapidly since their first discovery in 2004 with many applications and potential benefits cited.[85] A literature search for the term; "carbon dots" (Web of Knowledge, accessed 23/11/2014) shows the explosion in publications featuring these materials (**Figure 13**).

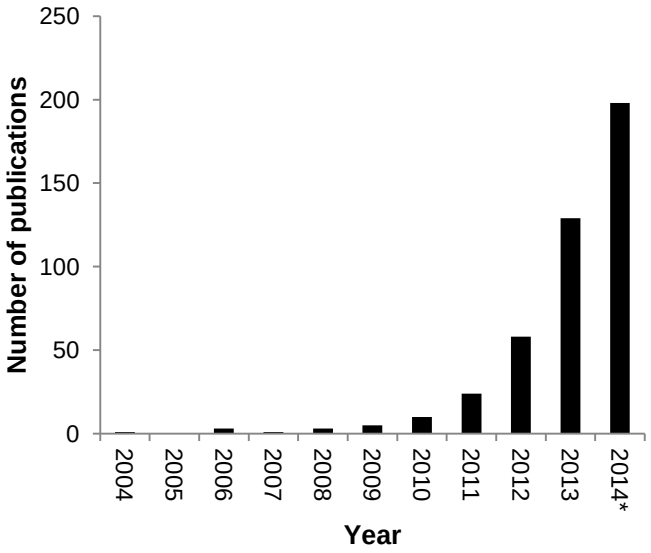

Figure 13: Graph showing the rapid increase in publications that contain the word "carbon dots" since 2004, *data only shows papers up to and including November 2014.

Discovered serendipitously as a by-product of single walled carbon nanotube purification by the Xu group in 2004,[86] carbon dots (also known as carbon quantum dots, carbon nanoparticles or carbon nanodots) have attracted wide interest due to their similarity to quantum dots but with the significant advantage of not containing toxic heavy metals. The dots, which are composed predominantly of carbon, are typically less than 10 nm in diameter and can be produced by breaking down larger

carbon structures (top down approach) or by building from smaller carbon precursors (bottom up approach).

1.4.1 'Top Down' Synthesis

In the gel electrophoresis purification of carbon nanotubes from arc discharge, Xu isolated a fast moving photoluminescent carbonaceous band in addition to the expected bands for the carbon nanotubes and shorter tubular carbon structures (**Figure 14**).

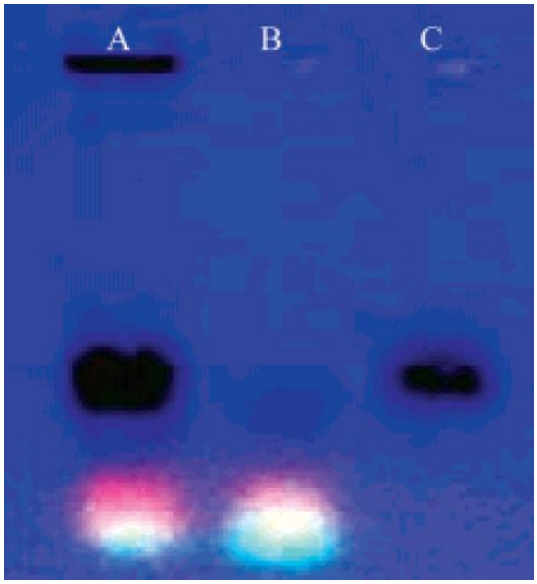

Figure 14: Electrophoresis profile in 1% agarose gel under 365 nm UV light showing (a) crude single walled carbon nanotube suspension; (b) purified fluorescent carbon material; (c) short carbon nanotubes. Reprinted with permission and adapted from Xu.[86] Copyright 2004 The American Chemical Society.

On excitation at 365 nm, three electrophoretic bands were visible; the fastest moving (smallest) exhibited green-blue fluorescence (3–10 kDa), the next displayed yellow fluorescence (10–30 kDa) and the slowest band, orange fluorescence (30–50 kDa). Oxidation of the original arc discharge soot in HNO_3 had introduced carboxylic acid groups to the surface of the carbon dots (confirmed by FTIR), explaining their

migration in the gel. Elemental analysis of the carbon dots formed showed them to be 54% carbon by weight, a characteristic shown later to be shared by carbon dots from other synthetic routes. The quantum yield of the carbon dots in the yellow fluorescent band was determined to be 1.6% and although very low in terms of fluorescence imaging, the material was deemed interesting.

Following the accidental discovery of carbon dots, Sun produced carbon dots by laser ablation, a process which removes material from a solid surface by laser irradiation.[87] A carbon target composed of graphite powder and cement was prepared and mounted in a furnace at 900 °C and 75 kPa with an argon gas flow (**Figure 15b**). A Nd:YAG laser was used to ablate the surface and the carbon material produced was directed to a cooled copper collector. No noticeable fluorescence from the 5 nm particles was seen after the initial ablation, or after oxidation in aqueous concentrated nitric acid for 12 h. Bright luminescence (λ_{ex} 400 nm, λ_{em} 450 nm) was observed, however, after surface passivation with PEG_{1500}. Du proposed a one-step synthesis and passivation of carbon dots by laser ablation through irradiation of dispersed graphite powders in PEG_{200}.[88] The diameter of the carbon dots produced by both methods was 3.2–3.3 nm.

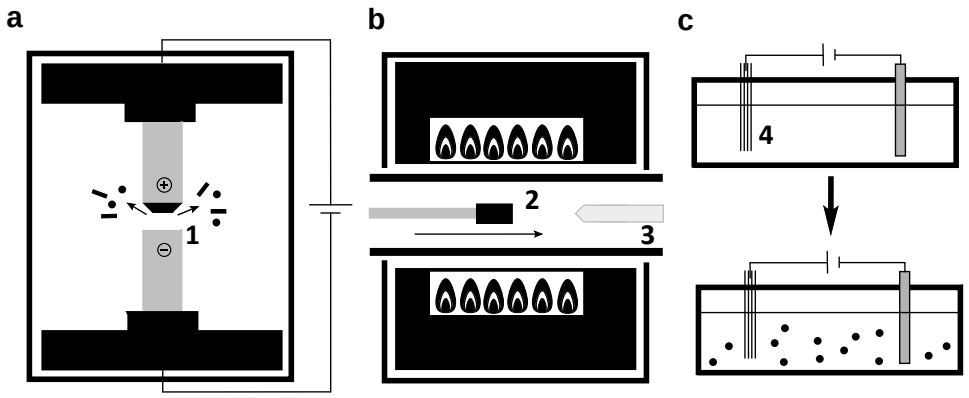

Figure 15: (a) arc discharge electrodes with carbon source (1) at the centre giving rise to carbon dots in addition to previously expected carbon nanotubes; (b) laser ablation of the carbon source (2) in a heated furnace and resulted in carbon dots which were collected on cooled copper (3) and aided by a continuous argon gas flow; (c) chemical exfoliation of carbon dots from MWCNTs (4) being used as an electrode in an electrochemical cell.

The electrochemical exfoliation of carbon dots from multi-walled carbon nanotubes has also proved to be a successful method (**Figure 15c**).[89] Carbon nanotubes were grown on carbon paper, encased in a Teflon jacket designed for electric contact before immersing in a solution containing a supporting electrolyte. The potential was cycled between −2.0 and 2.0 volts at 0.5 Vs^{-1}, and the electrolyte solution turned from yellow to dark brown indicating the formation of carbon dots from the surface of the carbon nanotube electrode. The carbon dots produced were spherical, had diameters of ~3 nm, and exhibited blue fluorescence (λ_{ex} 365 nm, λ_{em} 410 nm). SEM images indicated that the nanotubes had undergone swelling and curling with breaking of the the carbon nanotubes into smaller fragments. In this method, no deliberate passivation was required although it is thought that counter ions effectively passivated the surface thereby making it emissive.

The top down approaches of arc discharge, laser ablation and electrochemical exfoliation dominated early carbon dot research. Bottom up methods focussing on smaller carbon precursors did not appear in the literature until the work of Mao in 2007.[90]

1.4.2 'Bottom Up' Synthesis

The earliest syntheses of carbon dots from smaller carbon rich precursors used thermal combustion.[90] The soot collected on glass plates on top of burning candles was 91% carbon and did not display fluorescence until oxidised with concentrated HNO_3. Separation by gel electrophoresis gave carbon dots <2 nm in diameter with emissions ranging from 415 nm to 615 nm when excited at 315 nm. When H_2O_2/AcOH was used as an oxidant, the carbon dots showed blue fluorescence indicating that the oxidant used may not only break down aggregates and solubilise the particles, but may also influence their optical properties. Purification by gel electrophoresis showed results consistent with carbon dots produced from the earlier

top down methods. Faster moving, smaller nanoparticles displayed green-blue fluorescence whereas slower moving, larger dots displayed orange-red fluorescence. The purified carbon dots were 37% carbon by weight, had low quantum yields (between 0.8% and 1.9%). However no additional surface passivation was required.

Following this approach, the gamut of carbon precursors for nanoparticle fabrication widened, ranging from citric acid and glycerol to substances not usually found in a synthetic chemistry setting, such as orange juice, eggs, honey and instant coffee.[91–95] Giannelis used chemically-defined carbon-based precursors to produce monodisperse carbon dots via a one-step thermal route.[96] Carbonisation of octadecyl ammonium citrate at 300 °C for two hours resulted in "organophilic" nanoparticles of 5–9 nm in diameter, with the authors suggesting the citrate salt acts as the carbon source and the octadecyl unit as the passivation agent. Here, the low melting point of the citrate salts used allowed growth of nanoparticles from the liquid phase rather than solid precursors. The generated carbon dots were dispersible up to 50 mg mL^{-1} in organic solvents, above this concentration, it is expected that aggregation of the dots causes larger particles to be formed. Carbonisation of citric acid alone resulted in an insoluble solid. TEM showed a monodisperse population with an average diameter of 7 nm, and the absorption and emission spectra of the nanoparticles showed similar results to previously functionalised carbon dots.

Solid supported routes for carbon dot synthesis have also gained popularity due to their ability to control the growth of the nanoparticles. Li used SiO_2 microspheres (~120 nm diameter) as a surface on which to 'grow' the carbon dots from smaller molecular weight carbon precursors.[97] The surfaces of the spheres were modified with the polymeric surfactant (F127) and low molecular weight phenol/formaldehyde resins (resols) were adsorbed onto the F127 (**Figure 16**). Stirring at 66 °C for 48 h allowed polymerisation of the resols on the surfactant shell and the resulting composites were isolated by centrifugation. SEM and TEM confirmed the satellite like morphology of the composites which were subsequently calcined at 900 °C for 2 h resulting in the formation of carbon dots on the surface of the silica spheres. The

use of the solid support prevented the aggregation of the nanoparticles usually encountered in high temperature reactions where nanoparticles reduce their high surface energy by forming aggregates. The SiO_2 was etched away using concentrated NaOH to release the carbon dots which were found not to be emissive. Upon oxidation to introduce carboxylic acid groups and passivation with PEG_{1500}, the carbon dots showed blue fluorescence and excitation dependent emission wavelengths.

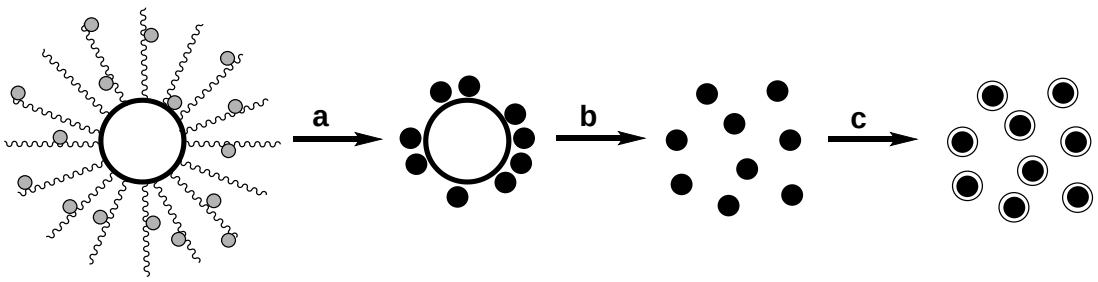

Figure 16: The synthesis of carbon dots using an SiO_2 supported route. SiO_2 spheres modified with surfactant and resols were polymerized, then (a) calcined (b) SiO_2 removal (etching) using NaOH. (c) Passivation of the carbon dots can then proceed as with other methods.

NaY zeolites have also been used as supports for the synthesis of carbon dots.[98] Ion-exchange of the NaY zeolite with 2,4-diaminophenol dihydrochloride followed by thermal oxidation in air at 300 °C decomposed the guest molecules associated with the zeolite (the zeolite itself is left unchanged). The resulting carbon dots, after etching away of the zeolite using HF, were spherical with a diameter of 4–6 nm. Again, the nanoparticles displayed excitation dependent emission properties.

Carbohydrates offer an inexpensive carbon source and have been the most widely used precursor. Yang first reported the microwave synthesis of carbon dots from aqueous solutions of PEG_{200} and glucose.[99] Once again, the carbon dots produced had wavelength dependent emission and had quantum yields of up to 6.1%. When repeated without PEG_{200}, the photoluminescence was drastically reduced, indicating the importance of the one step carbonisation and passivation process.

Carbonisation of glycerol with tiny amounts of phosphate in a domestic microwave oven also generated carbon dots.[100] The synthesised dots (2 nm) displayed fluorescence across a broad range, 430–525 nm, depending on the excitation wavelength, and were stable between pH 4.5–9.0. Although most reported microwave methods produce carbon dots with the desired morphology and optical properties, the use of domestic microwave heating reduces reproducibility.

1.4.3 Other Synthetic Routes

The templated synthesis of carbon dots has been reported.[101] Carbon dots (2–6 nm) were formed by the reduction of CCl_4 inside tetraoctylammonium micelles at room temperature. The micelles formed a 'soft-template' in which the carbon dots could form. The size of the carbon dots was regulated by the hydride used for reduction; stronger reducing agents ($LiAlH_4$) gave smaller carbon dots (1.8 nm) whereas using L-Selectride or $LiBH_4$ gave carbon dots with diameters of 4.5 nm and 5.5 nm, respectively. In another microwave-assisted method, Jiang used histidine in phosphoric acid.[102] The resulting 2 nm carbon dots showed strong photoluminescence (λ_{ex} 360 nm, λ_{em} 440 nm) and high quantum yields (45 %). Other hydrophilic amino acids, arginine, threonine and proline also resulted in photoluminescent nanoparticles, however carbon dots from hydrophobic amino acids (leucine, isoleucine and valine) displayed only weak fluorescence.

1.4.4 Optical Properties

Carbon dots generally show strong absorption in the UV region and weaker absorption in the visible region.[87] Emission in the visible region makes them useful optical tools. Due to their relatively recent discovery, the luminescence mechanism of carbon dots is not fully understood. Of the potential explanations proffered, most have focussed on the radiative recombination of excitons at surface energy traps similar to quantum dots.[87,103,104] The importance of sp2 hybridised carbon atoms as promoters of radiative recombination has also been proposed.[105,106] The requirement for passivation of certain carbon dots also remains unresolved but seems to rely on the method of production.[107] The original laser ablation method by Sun required surface passivation of the carbon dots to render them emissive,[87] whereas those methods incorporating organic passivation agents into the carbonisation reaction generally do not require further passivation, e.g. electrochemical oxidation of graphite.[108]

The emission wavelength of carbon dots relies heavily on the excitation wavelength used (**Figure 17**).[109] As excitation wavelength increases the emission maximum is red shifted. This feature is common to carbon dots produced by most of the synthesis routes described, however, Pang described carbon dots from electrochemical oxidation of graphite which showed size dependent but excitation wavelength independent emissions.[110] The argument that size differences are the sole reason behind the excitation dependent emission is greatly outweighed by the body of evidence indicating the quantum effects or the environment of the surface energy traps also have an effect on the photoluminescent properties.

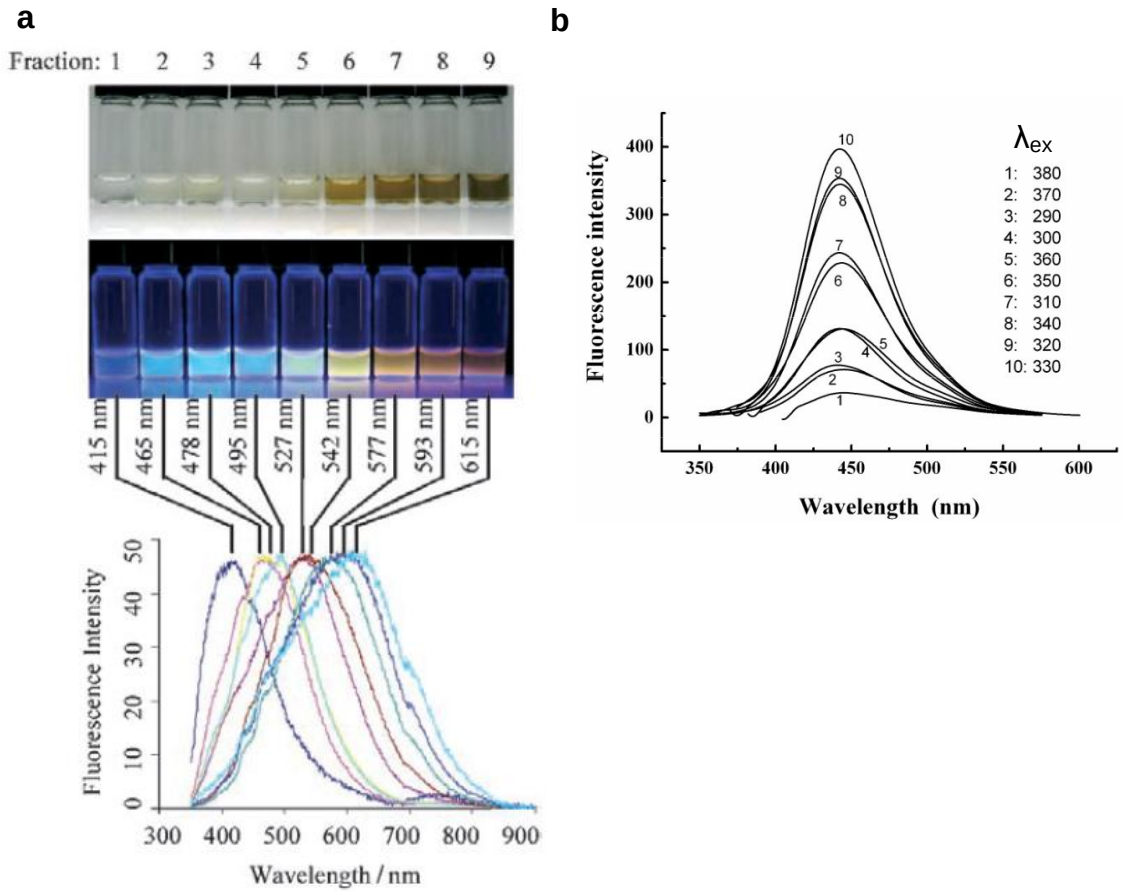

Figure 17: (a) Image of carbon dot fractions separated by gel electrophoresis from candle soot, their fluorescence under UV light and their emission maxima when excited at 325 nm showing the excitation dependent emission properties reported for the majority of carbon dots. Reprinted with permission from Mao.[90] Copyright 2007 Wiley-VCH Verlag GmBH & Co. (b) Data showing the excitation wavelength-independence of carbon dots produced from the electrochemical oxidation of graphite. Reprinted with permission from Pang.[110] Copyright 2008 The Royal Society of Chemistry.

TEM analysis of carbon dots formed from thermal combustion routes tends to support the dehydration and subsequent carbonisation of carbon-based precursors to form graphitic areas.[111] Inspired by the breakup mechanism of graphene sheets and carbon nanotubes, Chen prepared carbon nanoparticles by the thermal decomposition of poly(styrene-co-glycidylmethacrylate) microspheres for 2 h at 200, 300 and 400 °C[112]. The blue, orange and white fluorescent nanoparticles, respectively, had well

resolved lattice spacing of 0.23, 0.27 and 0.34 nm which are close to the (100), (020) and (002) diffraction facets of graphite (**Figure 18**). Theoretical calculations by Kang confirmed the relationship between the size of the graphitic clusters and the photoluminescence.[113] As the size of the graphitic region increases, the band gap between LUMO and HOMO decreases, reaching visible emission with clusters between 1.4–2.2 nm.

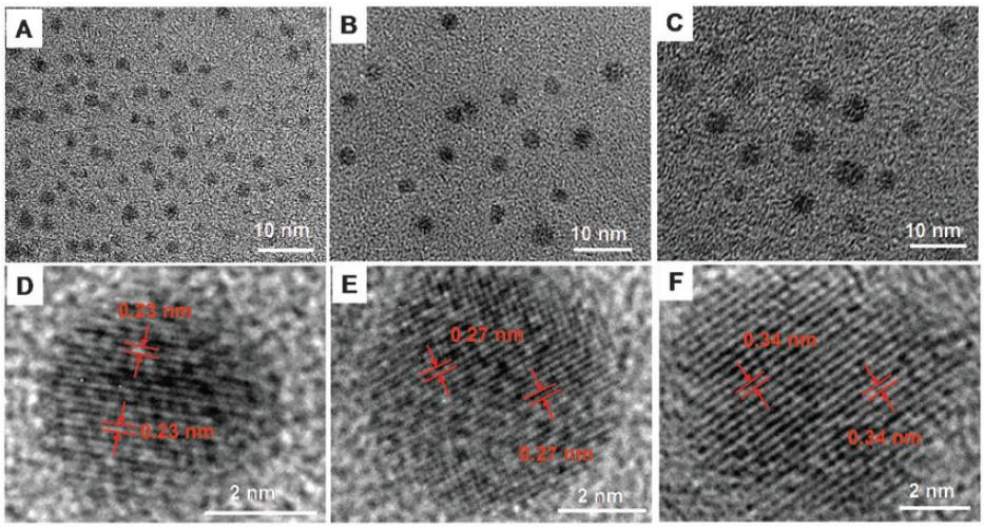

Figure 18: High resolution TEM images of (A) and (D) carbon dots produced at 200 °C, (B) and (E) carbon dots produced at 300 °C, (C) and (F) carbon dots produced at 400 °C. Reprinted with permission from Chen.[112] Copyright 2012 The Royal Society of Chemistry.

1.4.5 Up-conversion?

It has been suggested that carbon dots can 'up-convert' lower wavelength incident light by multi photon excitation (**Figure 19**).[114–116] This phenomenon has been reported in nanoparticles containing lanthanides or some d-block elements and relies on the simultaneous absorbance of two longer wavelength photons.[117,118] Excitation in the visible region penetrates tissue poorly and the up-conversion properties of carbon dots could have beneficial applications *in vivo* as longer wavelength photons penetrate tissue more readily.[119]

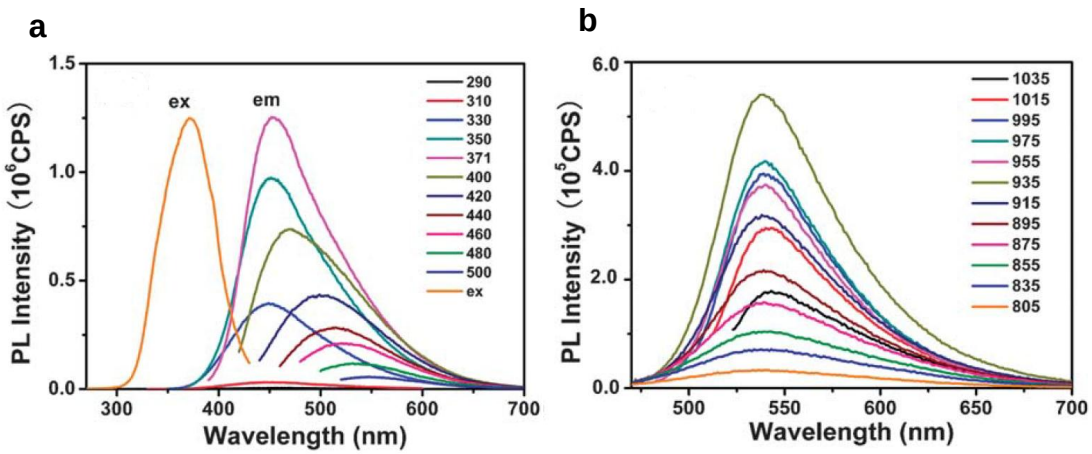

Figure 19: (a) excitation of carbon nanoparticles from 290–500 nm; (b) excitation in the NIR region (805–1035 nm) showing suggested emission in the visible region between 500 – 650 nm. Reprinted with permission from Wang.[115] Copyright 2012 The Royal Society of Chemistry.

Two-photon excitation of carbon dots produced from laser ablation was shown using pulsed infrared laser excitation at 800 nm which showed a quadratic relationship between the excitation laser power and the fluorescence intensity, consistent with two NIR photon excitation.[120] The probability that a molecule will absorb two photons simultaneously (i.e. the average two-photon absorption cross section), was 39,000 ± 5000 GM (1GM = 1×10^{-50} cm^4 s $photon^{-1}$), putting these particles somewhere between CdSe quantum dots (780–10,300 GM)[121] and CdSe/ZnS quantum dots (~50,000 GM).[122] It was suggested that immobilisation of the carbon dots on the glass substrate could have contributed to or affected the optical properties rather than phenomenon being attributed to the carbon dots alone. The emission peak of the two photon excitation was much narrower than that of the one photon excitation in solution suggesting that the immobilisation had an effect on the emission properties. Nevertheless, when these carbon dots were incubated with human breast cancer, MCF7, cells, imaging of the cells was possible using two-photon microscopy.

The incorporation of heteroatoms into the structure of the carbon dot has also been mooted to enhance the optical properties of those carbon dots.[123–125] Nitrogen, sulphur and phosphorus have all been suggested as possible additives to cause the

phenomenon of excitation at longer wavelengths but emission in the visible region or enhanced photoluminescent properties. Niu suggested that defects in the structure created by nitrogen doping accounted for the emission at 675 nm on excitation with near infrared light (980 nm).[126] Xu, in separate work on nitrogen-doped carbon dots, proposed that the nitrogen atoms bonded to carbon distorted the aromatic carbon structures and therefore induces the creation of emissive energy traps.[127]

1.4.6 Quantum Yields

The quantum yield of carbon dots is largely dependent on the synthesis method employed, the nature of the precursors and the passivation method used. Laser ablation carbon dots passivated with poly(propionylethylenimine-co-ethylenimine) had lower quantum yields than those passivated with PEG.[87] When coated with a ZnS shell alone or a combination of zinc coatings with organic passivation agents (e.g. PEG), the quantum yields increased considerably (up to 50%).[128] The incorporation of metals (e.g. Cu, Pd or Ag) to the surface of candle soot carbon dots via ion exchange or coordination to the carboxylic acid groups on the surface of the dots resulted in carbon dot nanocomposites.[111] These nanocomposites showed higher quantum yields (C-Ag, 37%; C-Pd, 33%; C-Cu, 60%) compared to bare carbon dots produced using the same method. Evidence suggests that when the fabrication method used produces dots with carboxyl functionalised surfaces, the quantum yield is generally low but is improved considerably on further passivation with organic molecules such as PEG.[88,90,129] Although many carbon dots have acceptable quantum yields (in general terms 10% is considered acceptable for a fluorophore), the difficulty in controlling the size distribution within a sample broadens the emission profile thereby limiting their use in multicolour analysis.

1.4.7 Applications

Carbon dots added to glycol have been used to print directly on paper, furthermore, a solution of carbon dots with sodium alginate was printed via silk-screen printing.[93] The fluorescence of carbon dots lends them to use in biological systems (**Figure 20**).[130]

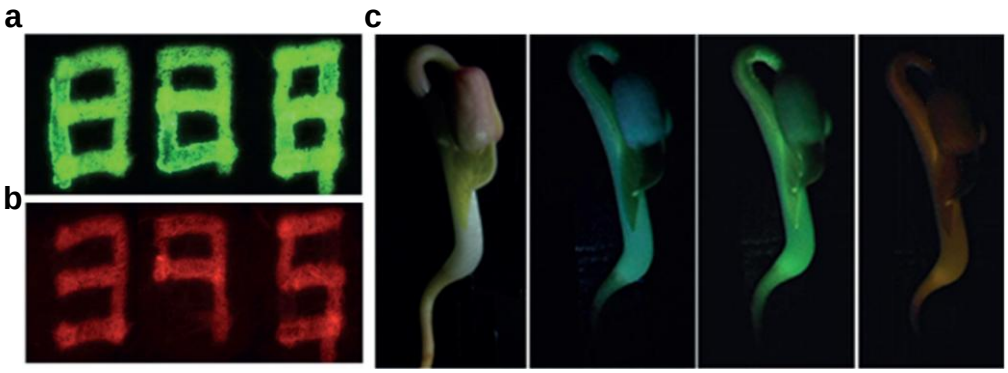

Figure 20: (a) commercially available fluorescent ink illuminated under green-blue light (b) visualisation of three numbers printed with carbon dots visible on excitation with the specific wavelength of the carbon dots (c) fluorescent bean sprouts grown in carbon dot solutions with no apparent differences to bean sprouts grown without carbon dots. Reprinted with permission from Wang.[130] Copyright 2012 Wiley-VCH Verlag GmbH & Co.

Cellular uptake of carbon dots to the cytosol is generally good and evidence highlights pinocytosis as the probable uptake method.[131] Uptake studies with carbon dots in HeLa cells by confocal laser scanning microscopy showed localisation of the nanoparticles in endosomes, multivesicular bodies and lysosomes indicating their uptake via endocytosis. Time-related uptake studies of the same carbon dots showed a rapid increase in carbon dot concentration inside the cell within the first hour of incubation followed by slower uptake in the second hour.[132] Carbon dots have been shown to enter a variety of cell lines, e.g. MCF7, SMMC-7721, HEK293, LLC-PK1, EAC and A549.[133–138] The apparent universality and speed of uptake make carbon dots promising reagents for cell-based studies.

Recently, carbon dots have been used in ratiometric sensing, a domain until now dominated by small molecule fluorophores. Carbon dots were conjugated to the superoxide-sensitive molecule hydroethidine (**Figure 21**).[139] On excitation at 488 nm, the emission at 525 nm was ascribed solely to the carbon dots. After incubation with superoxide, a peak at 610 nm, due to the fluorescence of the hydroethidine appeared. This peak increased with increasing concentrations of superoxide, however the fluorescence of the carbon dots stayed constant (control). Thus, comparing the ratio between the two peaks gave information about the concentration of superoxide present. The low cytotoxicity, stability towards pH, good cell permeability and long term stability enabled the application of this sensor within cells. The ease of conjugation via carboxyl or amine functionalities on the surface of the dots, non-toxicity and characteristics make carbon dots ideal candidates for in vitro and in vivo imaging. Additionally, due to their relative ease of fabrication and optical properties, carbon dots have significant potential in vivo as a credible alternative to small molecule fluorophores.[76]

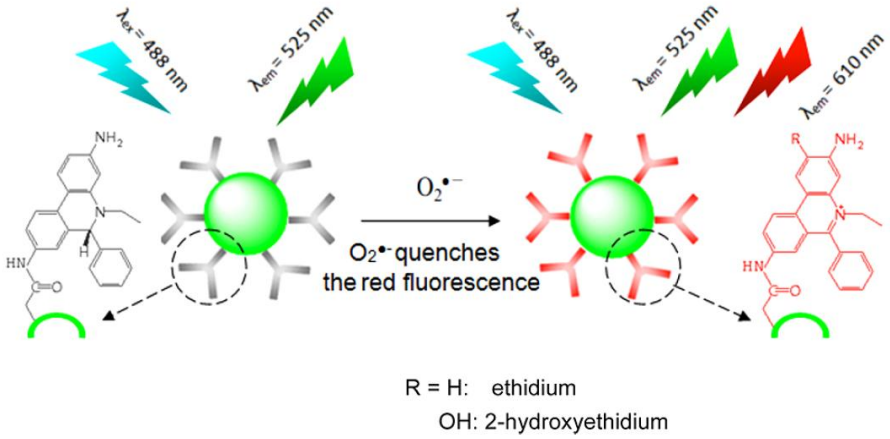

Figure 21: Principle of ratiometric hydroethidine sensing probe. The fluorescence of the carbon dot remains constant with emission at 525 nm, however on addition of superoxide, the fluorescence of the hydroethidine moiety is revealed at 610 nm. Reprinted with permission from Tian.[139] Copyright 2014 American Chemical Society.

1.5 Aims of Thesis

The aim of this work was to synthesise robust, defined and fluorescent carbon nanoparticles in an efficient and robust manner. The structural characteristics and optical properties of these carbon dots were investigated through various spectroscopic and analytical techniques. The possibility of carbon dots' ability to 'up-convert' light of lower energy is discussed. A further aim of the research was to assess the biocompatibility of the synthesised carbon dots and investigate their use as optical imaging agents in vitro. The conjugation of the carbon dots with specific cell targeting cargoes allowing direction to internal and external cell components and visualisation via semi-confocal microscopy is also discussed.

Specifically, the objectives of the work contained in this thesis were:

1. To compare existing carbon dot syntheses based on microwave irradiation and to evaluate whether these methods can be translated to a reproducible format on a large scale.

2. To develop an efficient and reproducible synthesis method for carbon dots from polymeric starting materials.

3. To assess the structural characteristics of the carbon dots using TEM, absorption spectroscopy and XPS.

4. To investigate the optical properties of the synthesised carbon dots by UV/Vis spectroscopy, fluorescence spectroscopy.

5. To investigate the up-conversion properties of the carbon dots.

6. To assess the biocompatibility of the carbon dots and to employ the carbon dots in biological applications to target specific cell components.

Chapter 2:

Thermal and Microwave Assisted Carbon Dot Synthesis

2.1 Introduction and Chapter Aims

The synthesis of carbon dots from a variety of precursors and by a range of methods has widened the scope of this emerging field considerably. Although earlier 'top down' syntheses produced promising results, the bulk of current synthesis is carried out by building up carbon dots from smaller carbon rich precursors ('bottom up' approach). This approach benefits from the enhanced scope of available carbon sources and with equipment readily available in a standard laboratory.

The work in this chapter describes the synthesis of carbon dots from organic precursors using 'traditional' thermal methods and microwave irradiation. Irradiation conditions were investigated and the resulting carbon dots evaluated by dynamic light scattering (DLS) and transmission electron microscopy (TEM). Since DLS is a solution technique, the measurements give a hydrodynamic radius, with solvent molecule associated with the particles, leading to a larger size than that determined by transmission electron microscopy (TEM).

The initial aim of the work contained in this chapter was to fabricate carbon dots in a scalable manner and to evaluate their optical properties. A second aim was to investigate whether carbon dot synthesis methods that use domestic microwave heating could be successfully translated to a monomodal synthesis microwave system, promoting reproducible synthesis. In this work, 'microwave' refers to a monomode microwave reactor unless stated otherwise. The challenges associated with the synthesis and characterisation of carbon dots are discussed.

2.2 Thermal Synthesis of Carbon Dots

2.2.1 Carbon dots from Glycerol, Citric acid and PEG_{1500}

In this method,[140] citric acid acts as the carbon source, and glycerol as the solvent and an additional carbon source. The inclusion of PEG in the reaction mixture provides direct passivation. Glycerol (3 mL) and PEG_{1500} (0.2 g) were sealed in a vial and heated to 270 °C in a heating block before the rapid addition of solid citric acid (0.2 g) and stirring of the reaction continued for 3 h at 270 °C (**Figure 22**) to produce a light brown solution.

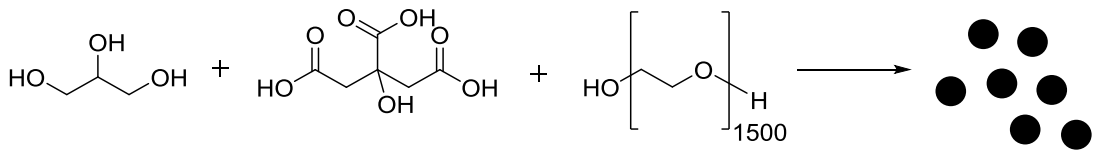

Figure 22: Thermal carbon dot synthesis from glycerol, citric acid and PEG1500 (**thermal CD-CAPEG**)

The reaction mixture was dialysed against water (Molecular Weight Cut Off ≈ 14,000 Da) to remove excess starting material and the size of the particles analysed by DLS (**Figure 23**). This gave a PDI of 0.59 and had an average diameter of 158 nm. This was high compared to carbon dots reported in the literature. However, an aqueous solution of the particles showed green/blue fluorescence under UV light (λ_{ex} 365 nm). TEM analysis of the sample confirmed the presence of particles small enough to be considered carbon dots (**Figure 24b**). Many clusters of carbon dots were visible and were thought to be responsible for the larger particle diameters seen by DLS. The emission spectra of **thermal-CAPEG** showed the excitation wavelength dependence characteristic of carbon dots with a maximum fluorescence intensity when excited at 380 nm (**Figure 24a**).

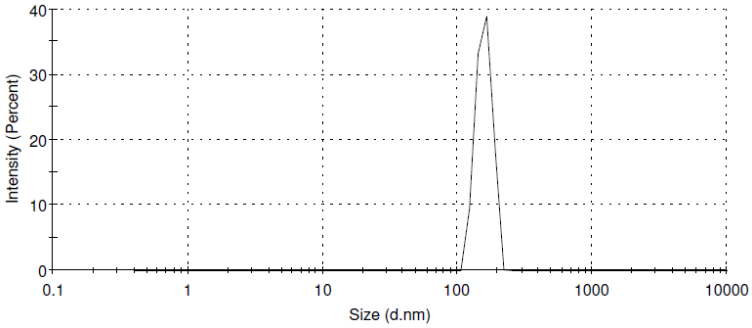

Figure 23: DLS trace of an aqueous solution of carbon dots from the thermal reaction of citric acid, glucose and PEG_{1500} at 270 °C for 3 h (sonicated for 5 min prior to measurement).

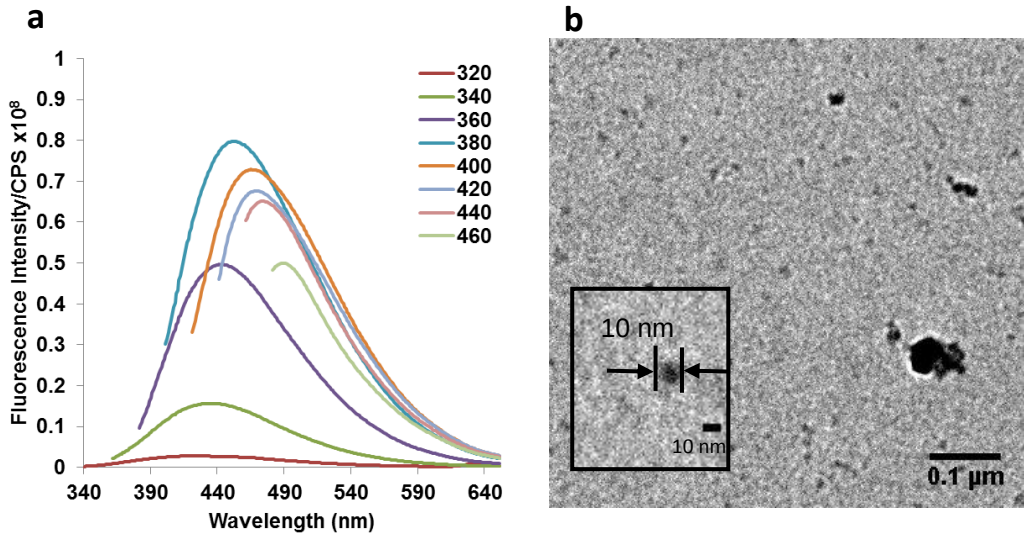

Figure 24: (a) Fluorescence intensities of **CD-CAPEG** at various excitation wavelengths (320 nm – 460 nm); (b) TEM image of **CD-CAPEG** with inset showing an individual carbon dot of ~10 nm diameter.

2.2.2 Carbon dots from P_2O_5 and Acetic Acid

Another literature method,[141] using the heat from an exothermic reaction to form carbon dots in a controlled manner, was attempted (**Figure 25**). In this method, the heat produced from the reaction of P_2O_5 and a small amount of water was sufficient to raise the temperature above the boiling point of the acetic acid used as the carbon precursor. Fang postulated that the acetic acid bubbles act as a template for carbon dot formation and the reaction temperature is kept constant by the insulating effect of the viscous polyphosphoric acid produced by the initial reaction of P_2O_5 and water. Carbonisation of the acetic acid leads to the production of carbon dots and water generated by the reaction reacts with P_2O_5 thus continuing the process until the P_2O_5 is consumed.

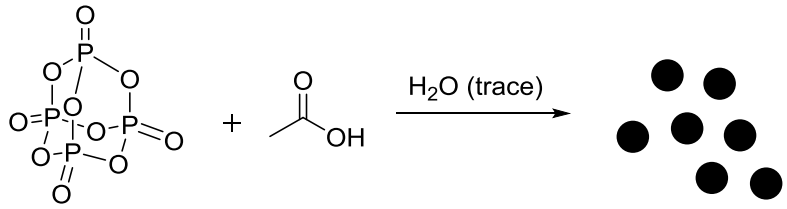

Figure 25: Carbon dot synthesis from P_2O_5 and acetic acid

A mixture of water (80 µL) and acetic acid (1 mL) was added directly to P_2O_5 (2.5 g). The white P_2O_5 quickly changed colour to light brown and the reaction foamed (**Figure 26**). After 10 minutes, the reaction mixture, now dark brown in colour, had ceased foaming and was allowed to cool to room temperature. According to the literature, no purification was required. The crude dark brown product displayed green fluorescence under UV excitation (λ_{ex} 365 nm).

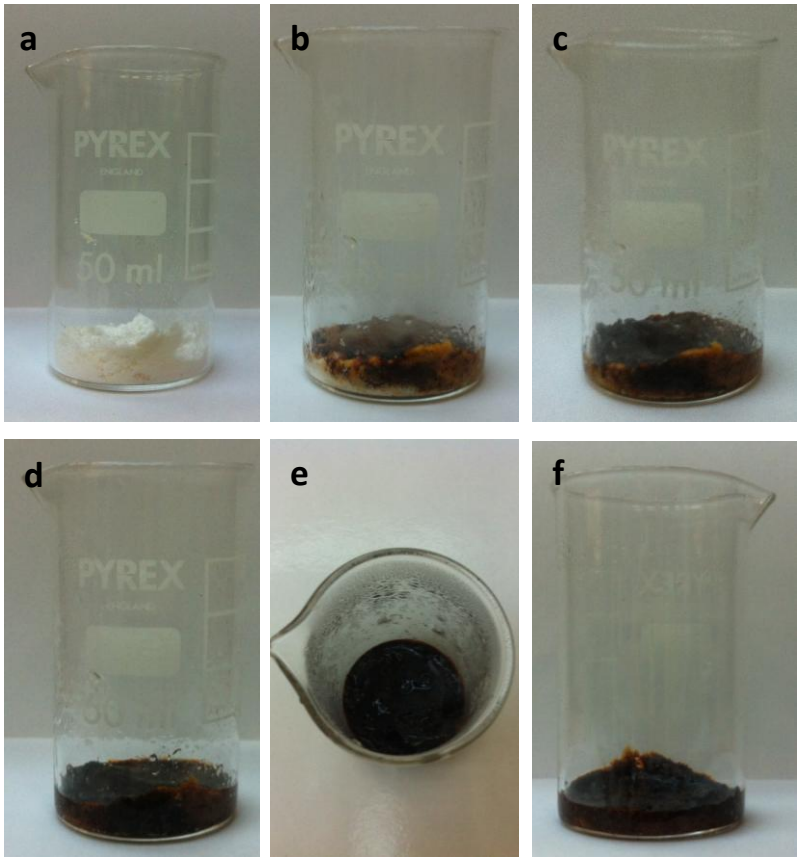

Figure 26: The progress of the reaction between P_2O_5, acetic acid and water at different time points a) before the addition of acetic and water; b) 10 s; c) 20 s; d) and e) 1 min; f) 5 min.

DLS gave a PDI of 0.37 and an average diameter of 193 nm (**Figure 27**). The expected size of the carbon dots was <10 nm (the literature quoted size by TEM as ~5 nm).[141] Fang suggested that the carbon dots aggregate into larger particles thus leading to the large diameter seen with DLS. The particles were thus sonicated for 5 minutes prior to DLS measurements and for 1 minute between each repeat. The sonicated sample gave consistent measurements for average diameter whereas with the unsonicated sample, the average diameter increased with each measurement. TEM was therefore considered the most appropriate method way to size these nanoparticles.

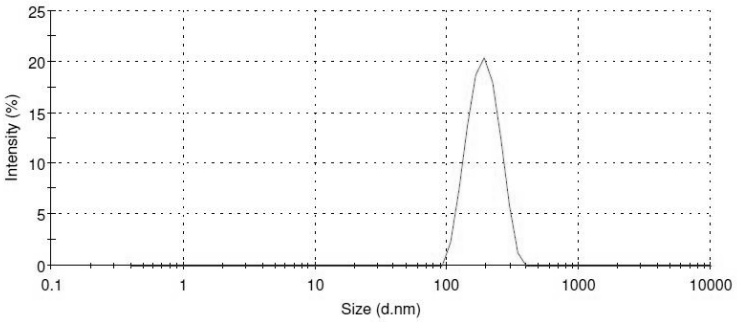

Figure 27: DLS trace of carbon nanoparticles produced from P_2O_5, acetic acid and water sonicated for 5 min (and 1 min between each measurement)

TEM of the carbon dots from P_2O_5 acetic acid and water show the particles to be <10 nm as expected but highly aggregated. In TEM, the carbon dots appeared spherical although aggregation was apparent. Individual carbon dots could be seen on the fringes of these aggregates and their size could be assessed (**Figure 28**).

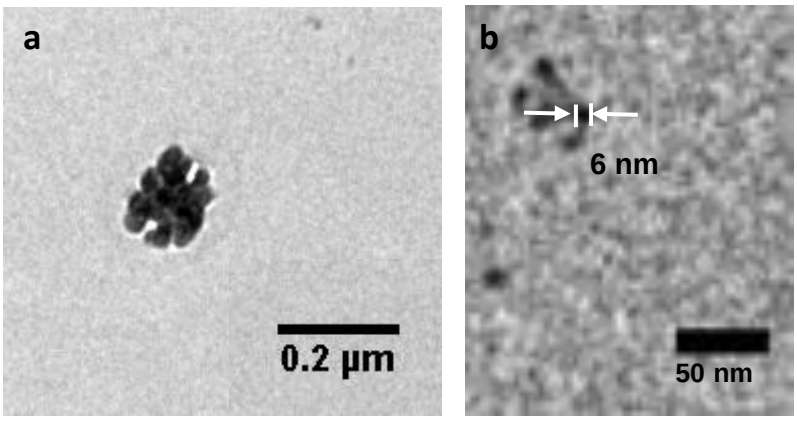

Figure 28: (a) TEM of a cluster of carbon dots from P_2O_5, acetic acid and water ; (b) expansion showing individual carbon dots with a size to be <10 nm.

Absorbance measurements (in water) showed peaks at 246 nm and 296 nm indicative of $\pi - \pi^*$ and $n - \pi^*$ transitions respectively. Strong absorption in the UV range tailed off in the visible region with almost no absorption above 500 nm (**Figure 29**).

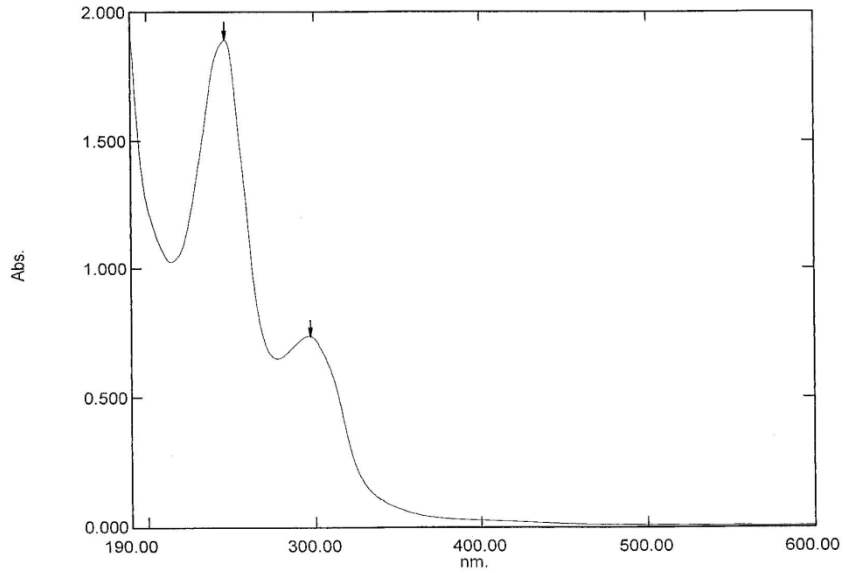

Figure 29: Absorbance of carbon dots from P_2O_5, acetic acid and water showing two peaks at 246 nm and 296 nm and a tail off over 400 nm.

The optical properties of the carbon dots were analysed by fluorescence spectroscopy. An aqueous sample of the carbon dots was excited from 350–400 nm in 10 nm increments (**Figure 30**). The carbon dots showed excitation dependent emission in the visible region which increased on increasing excitation wavelength from 475 nm (λ_{ex} 350 nm) to 488 nm (λ_{ex} 400 nm). The Stokes shift decreased as excitation wavelength increased (i.e. red shifting) from 125 nm (λ_{ex} 350 nm) to 88 nm (λ_{ex} 400 nm). The emission peak was broad denoting the range of sizes within the sample and the aggregates. An aqueous solution of carbon dots was analysed by fluorescence microscopy whereupon water droplets containing dots displayed red, green and blue fluorescence (**Figure 31**). The range is consistent with their large emission profile across the visible region.

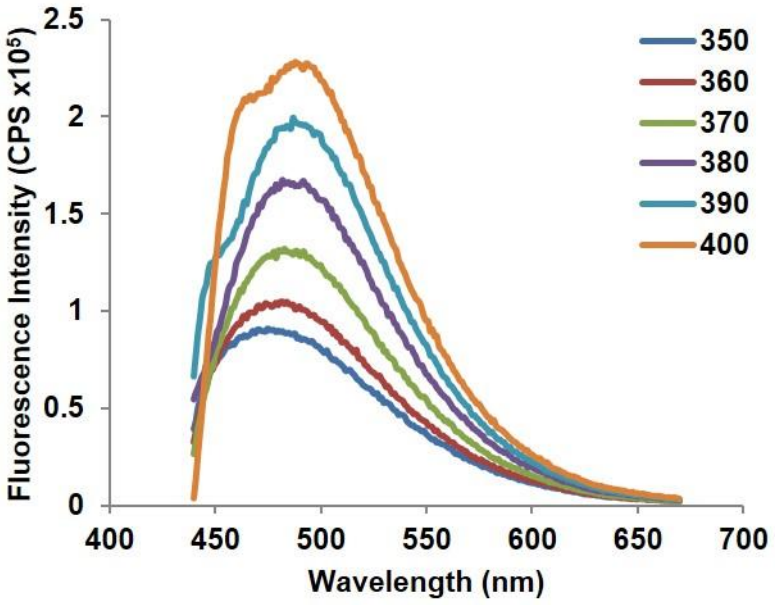

Figure 30: Emission spectra of an aqueous solution of fluorescent carbon dots synthesised from P_2O_5, acetic acid and water excited from 350–400 nm in 10 nm increments.

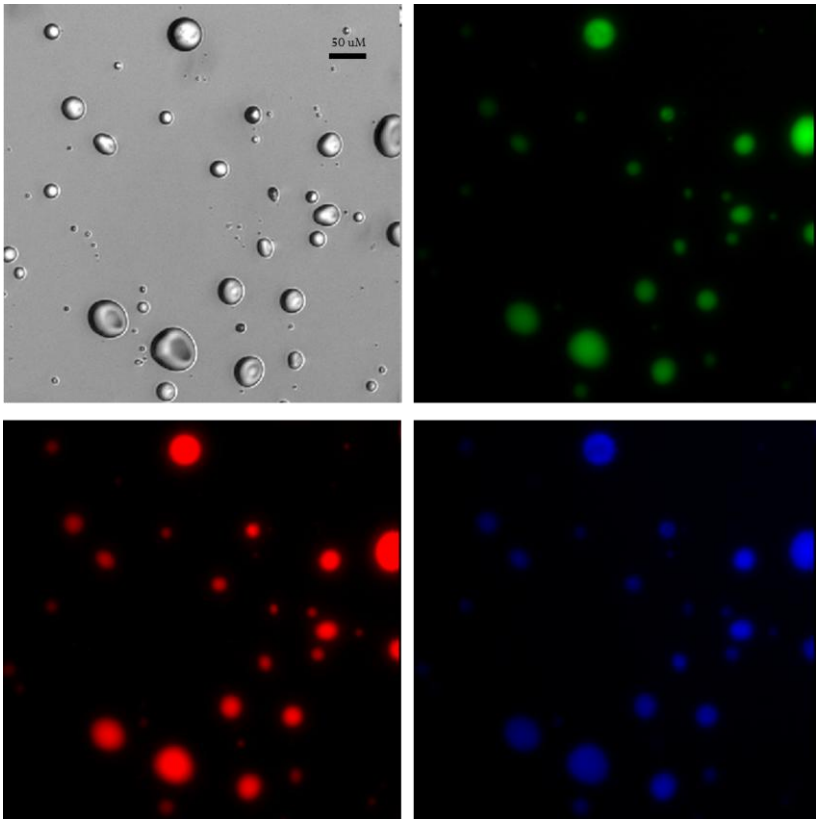

Figure 31: Fluorescence microscopy images of droplets containing carbon dots showing green, red and blue fluorescence (bandpass filters λ_{ex} 447–494, 527–563 and 340–395 nm respectively). Scale bar = 50 µm.

2.3 Microwave Assisted Synthesis of Carbon Dots

2.3.1 Introduction

A widely used approach to carbon dot synthesis involves microwave irradiation which has gained considerable interest in the carbon dot community.[142–144] The use of microwaves in chemistry is a relatively modern idea, first being used in the 1950s[145] but gaining wider acceptance in the mid-1980s and 1990s.[146,147] Microwave irradiation causes polar molecules to 'try' to rotate in "time" with the oscillating electromagnetic field. This causes them to oscillate back and forth as they cannot orientate themselves rapidly enough, thus generating heat due to 'molecular friction' (**Figure 32**). Compared to conventional heating, which heats the vessel with the heat percolating into the sample by conduction, microwaves heat all regions of the sample directly and hence more uniformly.[148]

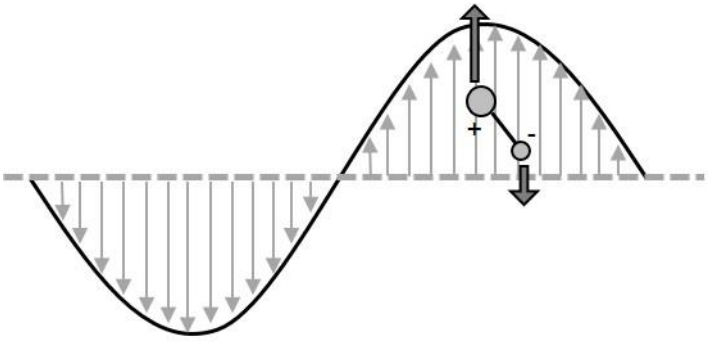

Figure 32: Representation of a diatomic molecule in the presence of a microwave. The electromagnetic field exerts a torque on molecules with an electric dipole moment causing them to rotate.

Following the original microwave methods of making carbon dots by Yang,[99] sugars and other small molecule organic compounds, e.g. citric acid[149] have been primarily used as the carbon source. The use of domestic microwaves, however, reduces the reproducibility of these syntheses due to differences in the way the radiation reaches the sample. Domestic (kitchen) microwave ovens are multimode instruments with the majority of the electromagnetic radiation that enters the reaction cavity being reflected by the walls of the cavity (**Figure 33a**). In contrast, in the monomode

systems currently used for chemical synthesis, the radiation is directed at the sample from a fixed distance with the sample in a defined position in the standing wave (**Figure 33b**).

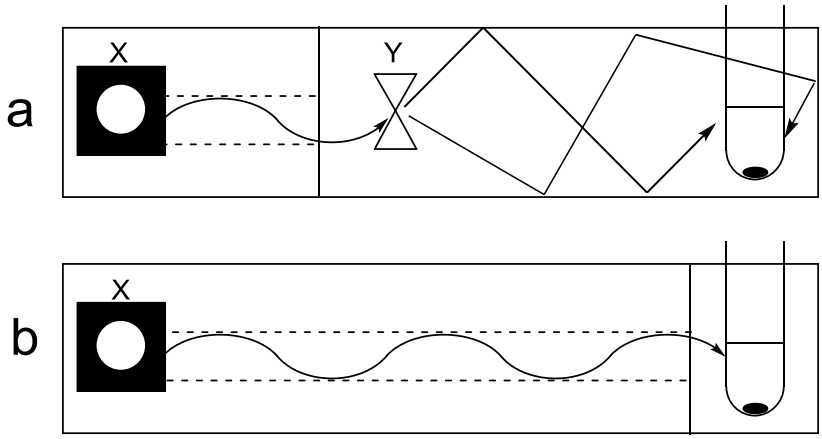

Figure 33: (a) representation of a multimode microwave. The electromagnetic radiation generated by the magnetron (X) is guided to a rotator (Y) which causes the waves to disperse around the chamber before reaching the reaction vessel (or more normally food); (b) representation of a monomode microwave where a wave-guide channels the electromagnetic wave to the reaction vessel, thus keeping the distance travelled by the wave constant.

Of the three experimental variables in microwave chemistry (irradiation time, power and temperature), the time (user controlled) and power (defined by the apparatus and unfocussed by nature) can be controlled when using a domestic microwave. In a monomode microwave reactor, it is possible to control all three variables however the safety features of these reactors can restrict very high temperature or pressure reactions. The lack of reproducibility and potential safety hazards associated with domestic microwave ovens has led to a decline in their use in chemical laboratories and acceptance by the scientific community.[150] Thus, the investigation of carbon dot synthesis in monomode microwave reactors is an important extension of the work already carried out in the field.

2.3.2 Carbon dots from Glycerol, Citric acid and PEG_{1500}

To investigate whether carbon dots successfully produced from traditional thermal methods could be translated to a monomode microwave, the reaction of glycerol, citric acid and PEG_{1500} (see Chapter 2.2.1) was used. PEG_{1500} (0.2 g) was dissolved in glycerol (3 mL) in a microwave vial and solid citric acid (0.2 g) added. The mixture was microwave irradiated at the maximum temperature allowed by the apparatus (250 °C) for 1 h at a time for a total of 3 h. The resulting straw coloured solution was similar to that obtained from the thermal version of the experiment. The solution was dialysed extensively against water (MWCO = 14,000) to remove excess starting material and the fluorescence intensity of the resulting clear solution was obtained (**Figure 34**).

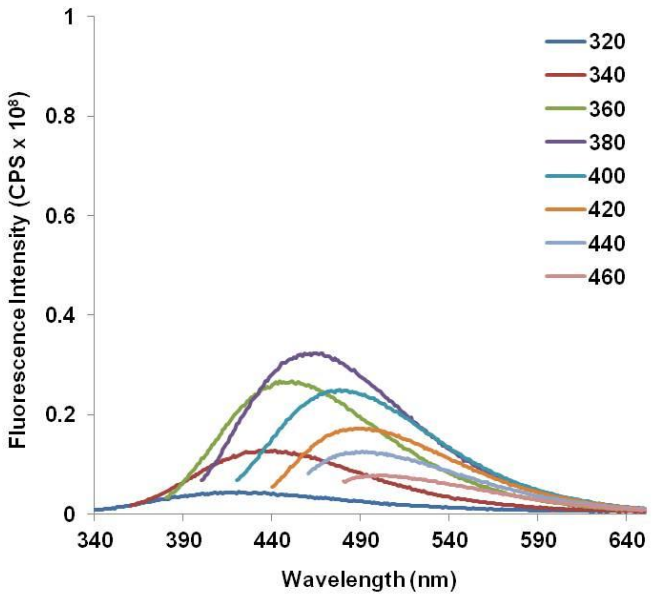

Figure 34: Emission spectra of nanoparticles from the μW reaction of PEG_{1500}, citric acid and glycerol (λ_{ex} 320–460).

The fluorescence intensity of the product from the microwave reaction showed similarities to **CD-CAPEG** (synthesised thermally), with a maximum fluorescence intensity two fold lower than the thermal synthesis when excited at 380 nm. The fluorescence intensities when excited at other wavelengths showed a similar pattern

to the thermal synthesis with negligible fluorescence when excited at 320 nm. The fluorescence intensities for the microwave synthesis were consistently lower than the thermal method. The emission is excitation wavelength dependent (similar to the thermal synthesis) with a maximum fluorescence intensity when excited at 380 nm. The DLS measurements of the microwave method (**Figure 35**) was compared to the thermal method. The average diameter (109 nm) was less than that of the thermal method (158 nm) however the PDI (1.00) was higher than the thermal method (0.59). Both samples were fluorescent on UV excitation (λ_{ex} 365 nm) and the similar fluorescence intensities of both thermal and microwave methods suggested that in this case, the method of heating did not affect the resulting nanoparticles.

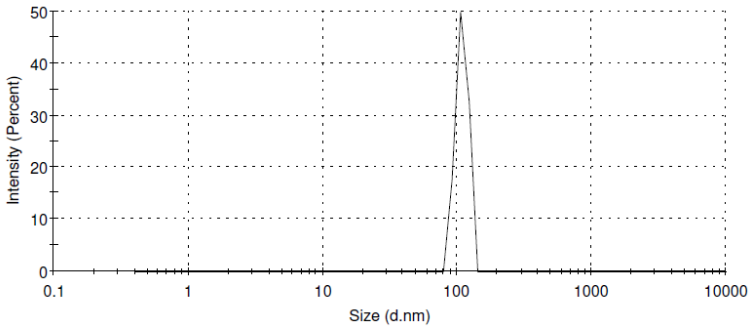

Figure 35: DLS trace of carbon nanoparticles produced from the microwave irradiation of citric acid, PEG_{1500} and glycerol sonicated for 5 min (and 1 min between each measurement)

2.3.3 Carbon dots from Glucose and PEG

Using Yang's procedure,[99] glucose (2 g) was dissolved in water and PEG_{400} (10 mL) added and the clear liquid microwave irradiated for a total of 80 min at varying temperatures (3 × 10 min at 120 °C then 2 × 15 min at 150 °C then 1 × 20 min at 150 °C) to give a dark brown solution (**Figure 36**).

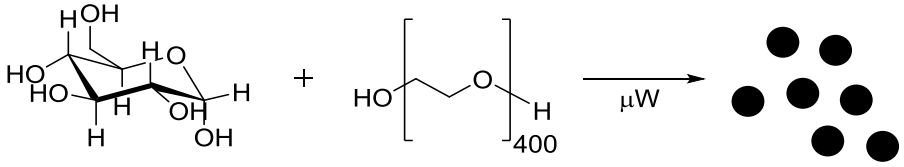

Figure 36: Microwave reaction of polyethylene glycol (average molecular weight = 400) and glucose to produce carbon dots (**CD-GPEG**).

The time taken for the solution to attain the dark brown appearance suggested in the experimental detail was eight times longer than the 10 minutes quoted for the reaction in a 500 W domestic microwave. The resulting brown solution was dialysed against deionised water for 36 h, then MeOH for 3 h, to remove unreacted starting materials. Size separation of the carbon nanoparticles was attempted by centrifugation in a mixture of solvents. Some carbon dots have been reported to be 'soluble' in water and EtOH but not in $CHCl_3$[137] therefore an aqueous solution of the carbon dots was added to water/EtOH/$CHCl_3$ (1:3:1). The solution was centrifuged for 10 minutes at 4,000, 5,000, 6,000, 8,000 and 16,000 rpm, sequentially, the brown solid material which collected at the bottom being removed each time. At lower speeds heavier particles are expected to leave the water/EtOH layer and fall to the bottom of the $CHCl_3$ layer. After the filtrate was removed from this solid material it was centrifuged again at successively higher speeds leading to a separation of the sizes. There was no solid material after centrifugation at 16,000 rpm indicating that any particles present in the solution were small enough to remain 'solvated'. After removal of the solvents, the dark brown solid material was redispersed in water and analysed by DLS (1 µg mL^{-1} solution of **CD-GPEG**) (**Figure 37**). The uniformity in size (polydispersity) (0.92) and average diameter of the nanoparticles (121 nm and 156 nm) were larger than those quoted from the domestic microwave method (3.6 nm). Again, TEM showed them to be smaller than first anticipated by the DLS measurements but the mixture was very heterogeneous (**Figure 38**).

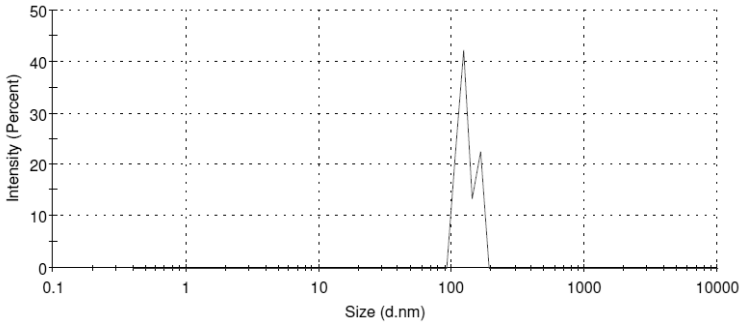

Figure 37: DLS trace of carbon nanomaterial from the microwave irradiation of glucose and PEG_{400} with two populations around 121 nm and 156 nm.

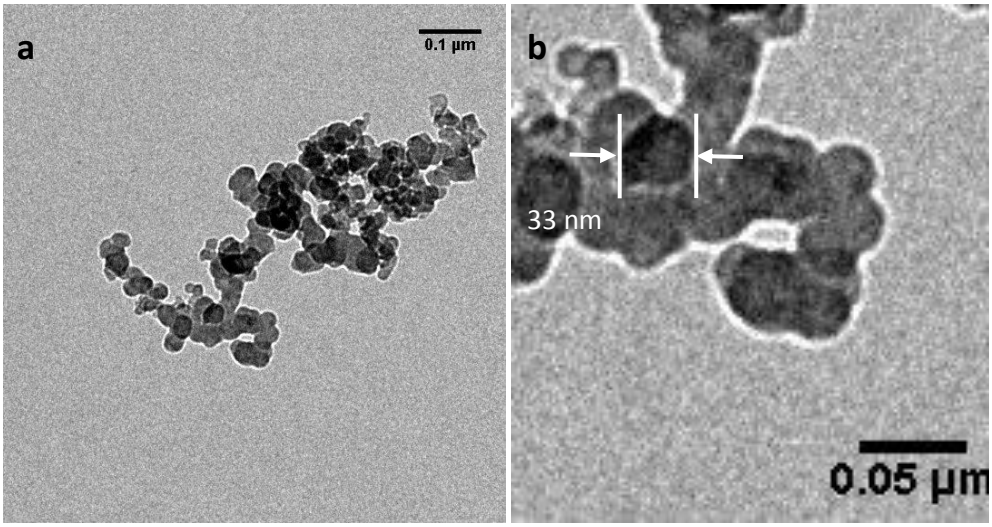

Figure 38: (a) TEM image of carbon material from the microwave irradiation of PEG_{400} and glucose for 80 min at 120 °C–150 °C (b) expansion of a cluster of nanoparticles showing one to be 33 nm in diameter.

TEM analysis of the sample indicated that the nanoparticles were considerably smaller than the DLS results suggested, due to aggregation. TEM images indicated a range of sizes of the material of varying shapes. Clusters of particles were visible and the material did not display noticeable fluorescence under UV light (λ_{ex} 365 nm). Fluorescence spectroscopy of **CD-GPEG** confirmed the particles to be weakly fluorescent over a range of excitation wavelengths (λ_{ex} 320–460 nm) (**Figure 39**).

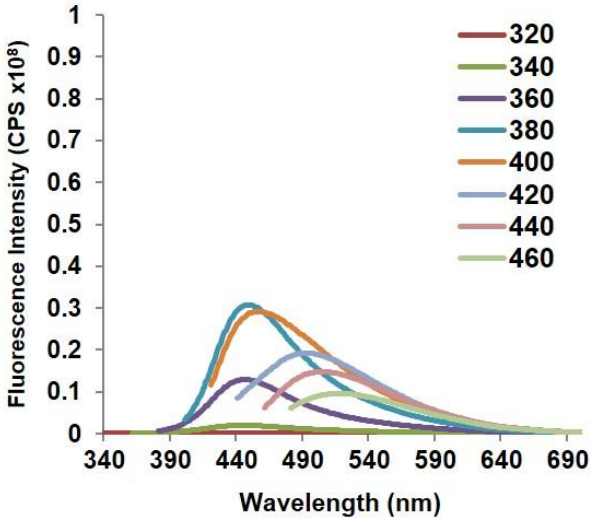

Figure 39: Graph showing the weak fluorescence properties of CD-GPEG in aqueous solution (1 mg mL^{-1}) over a range of excitation wavelengths (λ_{ex} 320 nm–460 nm)

2.3.4 Carbon dots from Sucrose and Phosphoric Acid

Although the glucose/PEG method produced nanoparticles, none were of the desired size, thus a different method based on another sugar was employed. A synthesis method using sucrose as the carbon precursor was attempted to investigate the impact of the irradiation time on the formation of carbon dots and their size. Sucrose, an inexpensive disaccharide, was used as the carbon source and H_3PO_4 used as the solvent. In the reported synthesis by Chandra,[151] the carboxylate and hydroxyl functionalised carbon dots also featured phosphate groups on the surface. However, use of a domestic microwave oven limited the reproducibility of the synthesis and thus a translation to a more reliable microwave method was attempted.

Sucrose (0.75 g) was dissolved in a minimum volume of water and H_3PO_4 acid added. The reaction mixture was sealed inside a microwave vial and microwave irradiated at 100 W for 165 s (**Figure 40**). In this case, the power of the microwave was adjusted to reflect that of the domestic microwave and the temperature was uncontrolled, thus reflecting the conditions in the original experiment as closely as possible. The temperature of the reaction increased as the reaction progressed (to ~150 °C) but did not reach the 250 °C limit allowed by the microwave reactor.

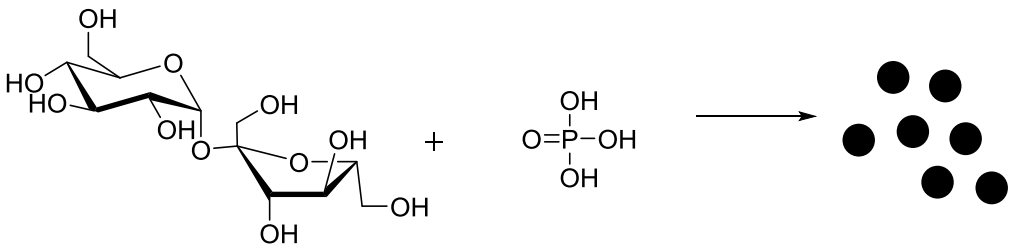

Figure 40: Microwave reaction of sucrose and phosphoric acid to produce carbon dots.

The colour of the solution changed from clear to dark brown associated with the formation of carbonaceous material. After dilution with water, the brown solid material was removed after centrifugation (4,000 rpm, 10 min) and the supernatant

dialysed against water to remove the phosphoric acid. The resulting brown solution did not show any noticeable fluorescence under UV light (λ_{ex} 365 nm).

To investigate the effects of irradiation time on the synthesis of the carbon dots, the same ratio of monomers was irradiated for various times at a constant temperature (100 °C for 75 s, 90 s, 105 s and 120 s). The colour of each solution changed from clear to brown or dark brown. Any larger carbonaceous material was removed by filtration and after addition of water, the supernatant was dialysed against water and the size analysed by DLS (**Table 1**). The PDIs ranged from 0.85 (90 s) to 1.00 (75 s and 120 s) with average diameters of 157 nm (75 s), 209 nm (90s), 196 nm (105 s) and 153 nm (120 s). There was no noticeable trend with respect to the size or polydispersity on increasing irradiation time.

TEM analysis of **CD-SPA** showed that particles produced were spherical and with 75 and 90 s heating ~250 nm in diameter (**Figure 41a** and **b**). Smaller particles were visible from irradiation for 105 s although larger particles (not shown in **Figure 41c**) were also present. Particles from irradiation for 120 s showed similar sizes to that of 75 and 90s (~200–400 nm) however they were less clustered. Similar results were found when the irradiation time was kept constant (90 s) and the temperature was varied from 75 °C to 150 °C in 25 °C increments. Irradiation at 100 °C, 125 °C and 150 °C produced carbon material that, although of a spherical morphology, was too large for carbon dots. On TEM analysis, carbon material of the correct morphology and size for carbon dots was visible although larger material was the predominant feature of the samples. Irradiation at 75 °C showed particles of ~10 nm diameter, however, a range of sizes was visible. In all samples, small crystalline fragments, assumed to be unreacted sucrose, were visible in the TEM images indicating that not all the starting material had been consumed in the reaction or removed via dialysis.

Table 1: PDIs and diameters of carbon nanoparticles produced from sucrose and H_3PO_4 with differing irradiation times (n = 3)

Time (s)	PDI[a]	Diameter (nm)	DLS trace
75	1.00	157	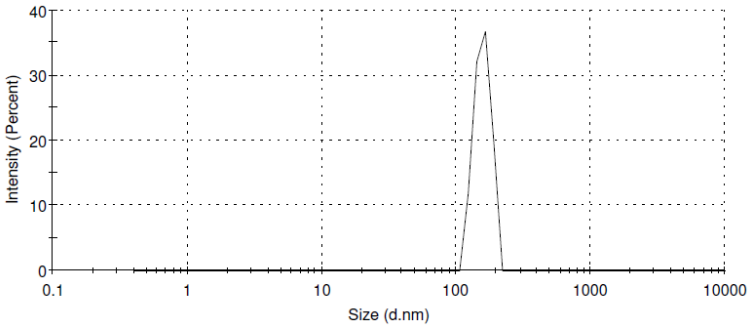
90	0.84	209	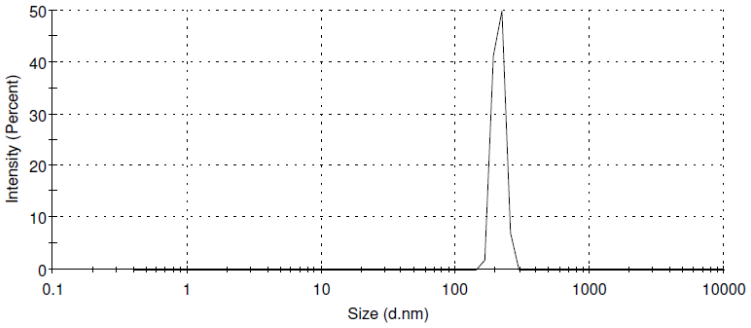
105	0.85	196	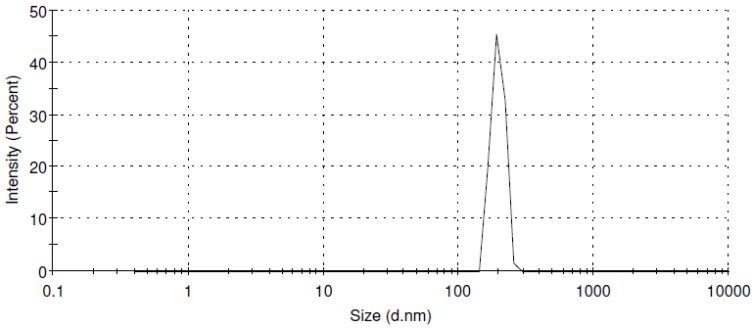
120	1.00	153	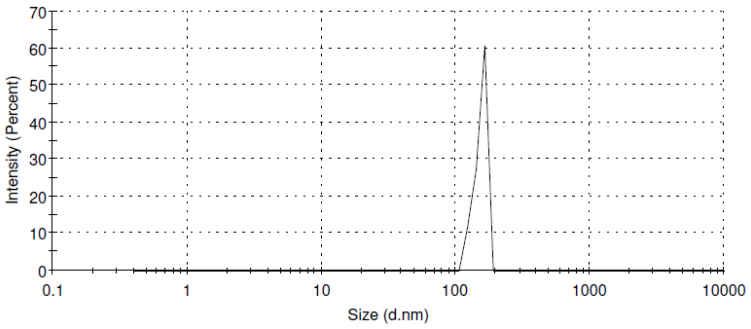

[a] measure of the uniformity of size and shape of particles within a sample from 0 (monodisperse) to 1 (most polydisperse)

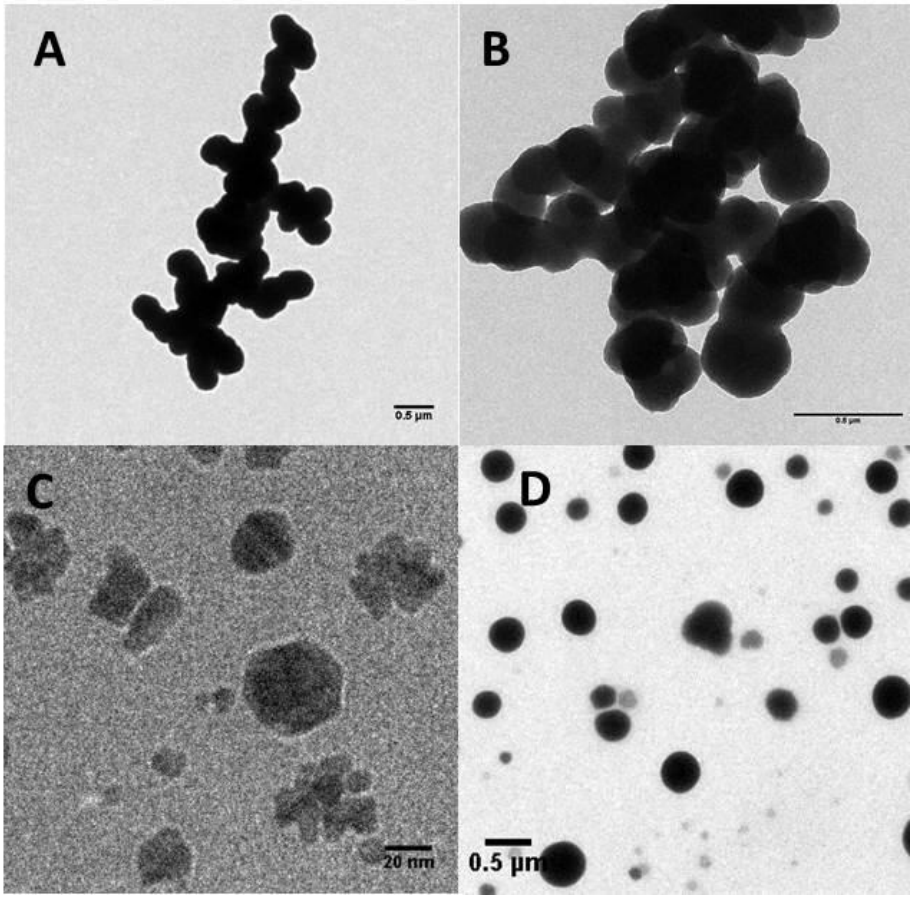

Figure 41: TEM images of carbon nanomaterial from the microwave irradiation of sucrose and H_3PO_4 for (a) 75 s; (b) 90 s; (c) 105 s; (d) 120 s.

DLS measurements of **CD-SPA** irradiated at different temperatures showed consistently large particles; 258 nm (100 °C), 232 nm (125 °C), 247 nm (150 °C) and smaller particles at 75 °C (165 nm) (

Table 2). Of the two microwave methods attempted, neither appeared to provide results consistent with the reported domestic microwave experiments. The uneven heating provided by a multimode microwave may have a beneficial effect on the production of carbon nanoparticles through localised ‘hot-spots’. Additionally, the temperature in a domestic microwave oven synthesis is not controlled which could influence the rate of carbon dot synthesis.

Table 2: PDIs and diameters of carbon nanoparticles produced from sucrose and H_3PO_4 with differing irradiation temperatures (n = 3)

Temp (°C)	PDI	Diameter (nm)	DLS trace
75	0.80	165	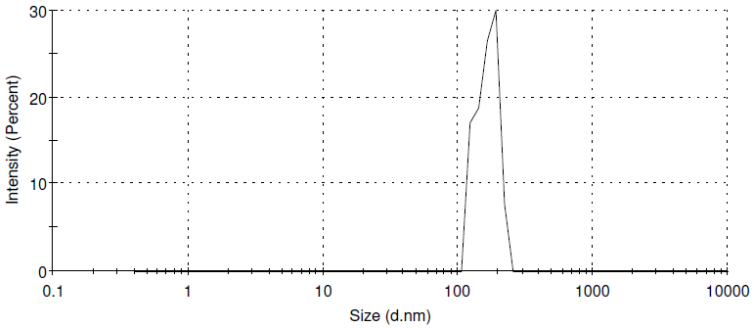
100	1.00	258	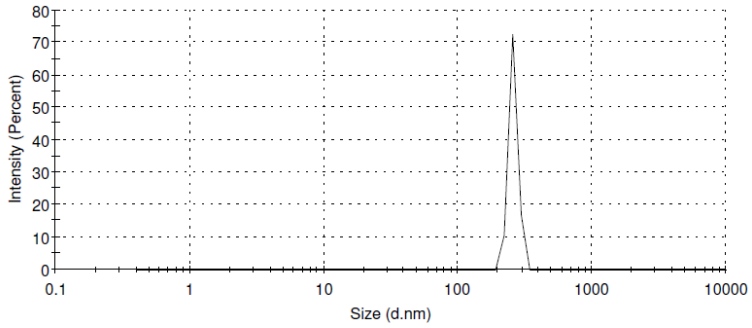
125	0.83	232	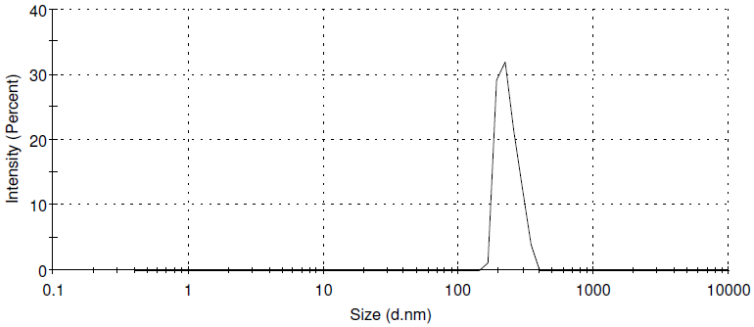
150	0.85	247	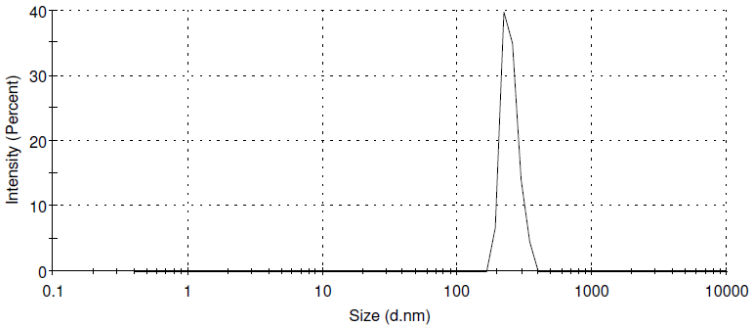

One further investigation of the translation of microwave methods was attempted based on the previous method proposed by Yang. The original experiment was performed in a domestic microwave oven and translation to a monomode reactor did not produce carbon dots of the desired size, therefore, a thermal method based on the starting materials (glucose and PEG_{400}) was trialled. Glucose (2 g) was dissolved in water and PEG_{400} (10 mL) added. The clear liquid was heated on a hotplate at 200 °C with stirring for 3 h to give a dark brown solution. The solution was dialysed (MWCO = 14,000) against water, the emission spectra obtained (**Figure 42**).

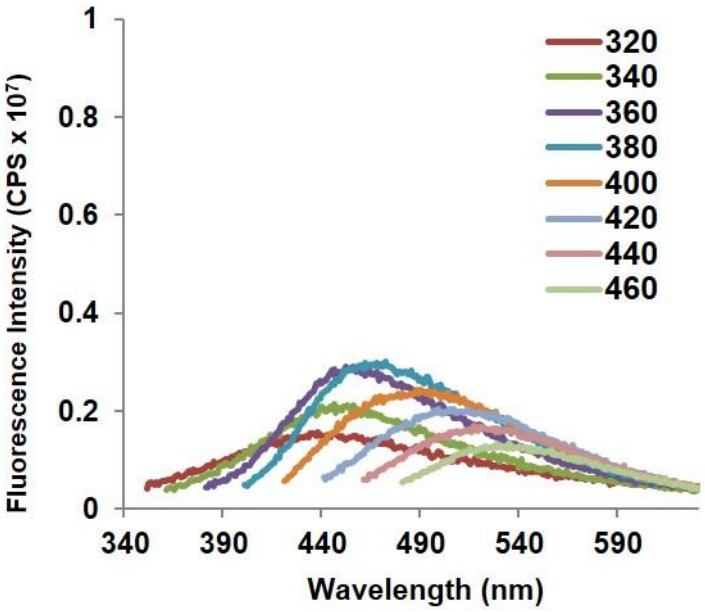

Figure 42: Emission spectra of carbon material from the microwave irradiated reaction of PEG_{400} and glucose (λ_{ex} 320-460 in 20 nm increments).

Although the emission spectra showed similar characteristics to those expected of carbon dots (excitation wavelength dependent emission), the fluorescence was ~10 fold lower than when produced via microwave irradiation and was not visible when viewed under a UV lamp (λ_{ex} 345 nm).

2.4 Conclusions

The desired aim of translating the synthesis of carbon dots from a domestic to a monomode microwave resulted in a new set of questions regarding the mode of synthesis of carbon nanoparticles. The uneven heating of a domestic microwave may enhance the formation of carbon dots whereas a constant temperature monomode microwave does not appear to promote carbon dot formation in these methods. Although carbon dots of the desired size could not be produced, the change in colour of the reaction mixture suggested the formation of carbon material. Traditional thermal routes, although not appearing to produce carbon dots of the desired size, resulted in fluorescent material with interesting optical properties characteristic of carbon dots. Interestingly, carbon material from PEG_{1500}, glyercol and citric acid yielded fluorescent material from microwave and thermal methods (although thermal methods gave higher fluorescence) but there was negligible fluorescence from PEG_{400} and glucose via thermal methods (compared to weak fluorescence from microwave methods). This anomaly indicates that the choice of carbon source is important when choosing the method for carbon dot synthesis.

The reliance on DLS for size analysis gave inconsistent results due to aggregation of the carbon dots over short periods of time, interference caused by the fluorescence of the samples as well as the vast differences in size within a single sample. Purification methods which remove larger particles as well as further dialysis to remove the lower molecular weight starting materials would be necessary for future syntheses via either microwave or thermal methods. The size analysis of carbon dots would benefit from a ‘dry’ method, i.e. transmission electron microscopy (TEM) to verify the true diameter of the particles. The need for robust, reproducible and larger-scale methods for carbon dot fabrication still remains a key focus.

Chapter 3:

Synthesis and Properties of Carbon Dots from 1,4-Addition Polymers

Parts of this chapter were previously published as: Jiang, Z., Nolan, A., Walton, J. G. A., Lilienkampf, A., Zhang, R., and Bradley, M., Photoluminescent Carbon Dots from 1,4-Addition Polymers, Chemistry A European Journal 2014, 20, 10926–10931. The author of this thesis was joint first author.

3.1 Introduction

Since their discovery, the scope of precursors for carbon dot synthesis has widened considerably, however, ambiguity in the nature of the starting materials has led to a lack of reproducibility. Thus, there is a need for synthetic methods using chemically defined starting materials to produce carbon dots in a robust and reproducible manner. In this work, defined addition polymers were synthesised and investigated as precursors for carbon dots. The heteroatom content of the precursors and their relationship to the optical properties of the resulting carbon dots was investigated.

3.1.1 1,4-Addition Polymerisation

The 1,4-addition of a nucleophile to an activated alkene (usually an α,β-unsaturated carbonyl compound) is a useful route for the formation of carbon-carbon bonds (**Figure 43**). In a Michael addition, the nucleophile is typically derived from the deprotonation of the α-carbon of aldehydes, ketones, nitriles and β-dicarbonyl compounds.[152] The activated alkene can vary widely in structure with a variety of electron withdrawing groups possible.

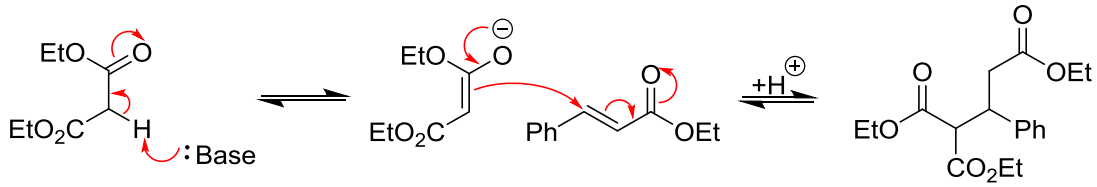

Figure 43: The Michael addition of a malonate anion onto the double bond of ethyl cinnamate

Research into a variety of 1,4-addition polymerisations was pioneered by Ferutti with the synthesis of various poly(amidoamine)s from bisacrylamines and amines (**Figure 44a**) at moderate temperatures (15–60 °C) in protic or aprotic solvents.[153–155] The rate of polymerisation is higher in protic solvents such as water where the reaction proceeds to higher molecular weight polymers. The rate of polymerisation is also dependent on the nucleophilicity of the secondary diamine used and the steric hindrance of the amine.[156] An interesting example of a poly(amidoamine) polymer is the copolymerisation of amino acids with bisacrylamides (**Figure 44b**).[157] Bisacrylamides can be replaced by divinylsulfones or diacrylates as monomers, thus widening the range of polymers.

Poly(aminoester)s are synthesised using diamines and diacrylates instead of bisacrylamides (**Figure 45a**). Their low cytotoxicity and the degradation into low toxicity products has led to their use as gene transfection agents.[158] Another example of 1,4-addition polymers include those based on quinones, which have found use in anti-corrosion coatings[159] and water-resistant adhesives (**Figure 45b**).[160] The wide range of diamines and diacrylates make this class of 1,4-addition polymers versatile. The use of secondary amines in polymerisation ensures linear step growth of the polymer chain rather. If a primary amine is used, a double addition at the amine takes place which can result in a branched like structure depending on the concentration of the starting material.

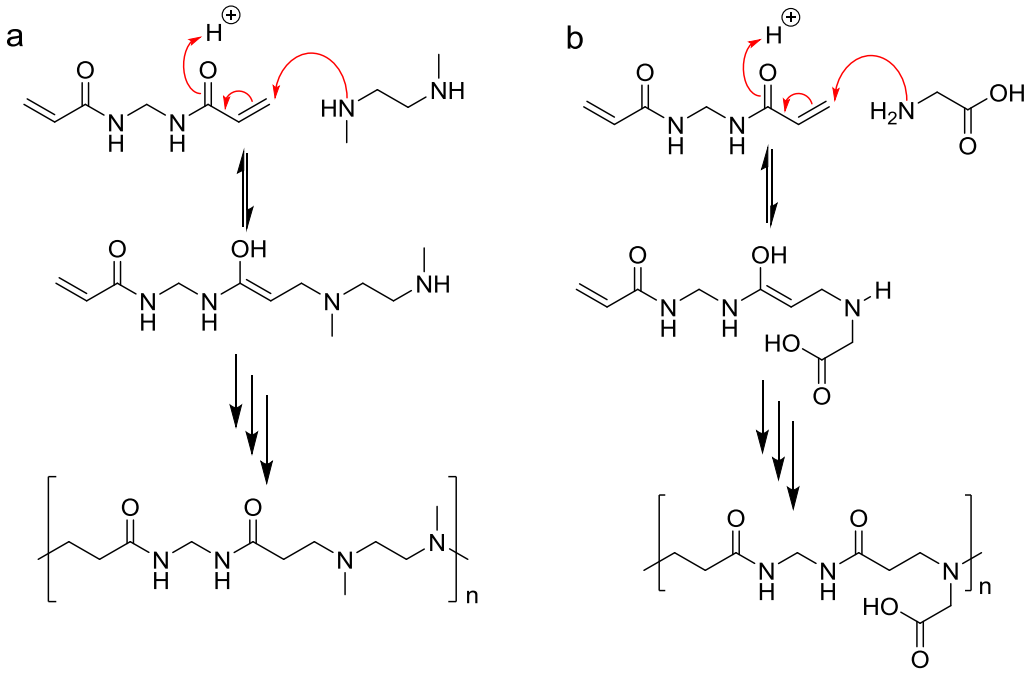

Figure 44: (a) poly(amidoamine) synthesis from methylene bisacrylamide and *N*,*N*'-dimethylethylenediamine; (b) a poly(amidoamine) from methylene bisacrylamide and glycine.

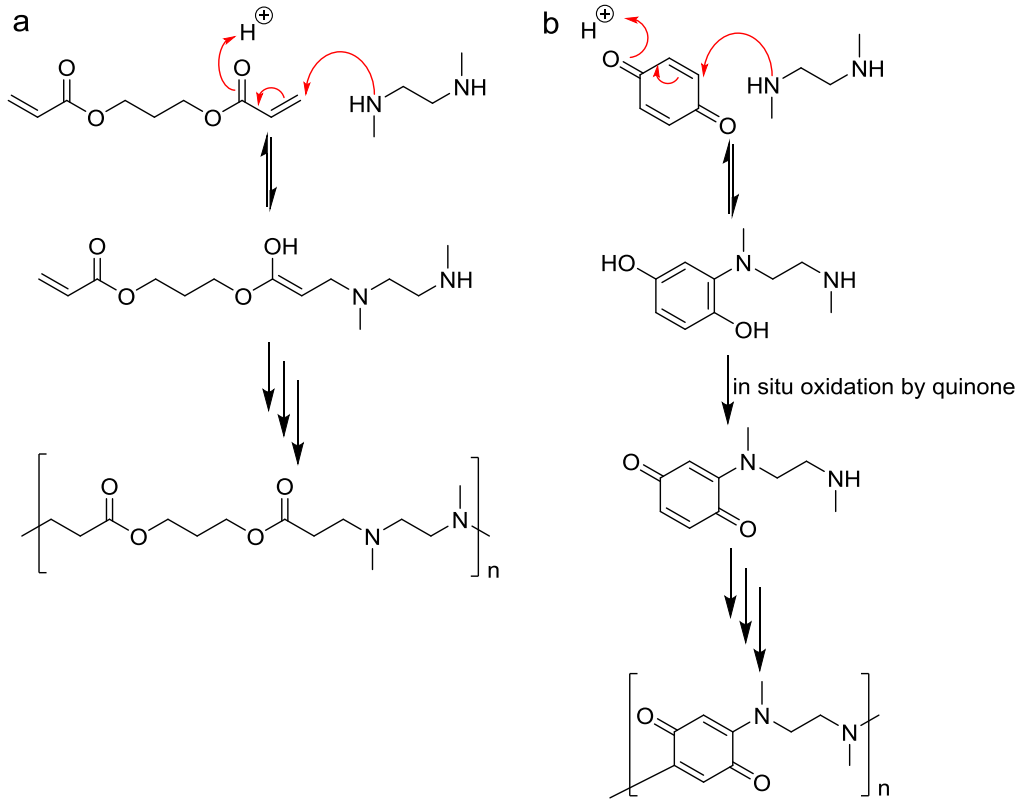

Figure 45: (a) structure of a poly(aminoester) synthesised from a diacrylate and secondary diamine; (b) structure of a poly(aminoquinone)

3.2 Choice of Monomers and Polymer Synthesis

In this work, 1,4-addition polymerisation was considered an attractive route to obtain polymers for the synthesis of carbon dots. Diamines, dithiols and diacrylates are readily available, inexpensive, starting materials. The 1,4-reaction of these monomers can proceed in water, at relatively low temperatures, and the work up to obtain the desired polymer is usually simple and efficient.

The monomers chosen for the addition polymer synthesis are shown in **Table 3**. The use of diamine or dithiols as monomers removes the need to introduce a base to catalyse the reaction. In a previous study, Ferruti showed base promoted polymerisation rates increased in the order: DIPEA < *N*,*N'*-dimethylethylenediamine < 2-methyl piperazine < piperazine, (pKa 10.5, 10.2, 9.6 and 9.7, respectively), i.e. reaction rates increased with decreasing basicity and lower steric hindrance.[161] To control the polymerisation, the use of a secondary amine ensured that chain growth was linear (and not branched as with a primary amine). In order to investigate the effects of heteroatoms on the properties of the carbon dots, dithiothreitol (DTT), was also chosen as a monomer. One nitrogen-containing diacrylate, methylene bisacrylamide (MBA) and one diacrylate without nitrogen, tetraethylene glycol diacrylate (TEGDA), were chosen as the diacrylates. The combinations of these monomers allowed a set of polymers with nitrogen and sulphur to be produced. Additionally, *bis*-(2-hydroxyethyl) ethylenediamine (BHEDA), was used to probe whether a polymer with free hydroxyl groups had an effect on the characteristics of the resulting carbon dots, and give rise to self-passivation or the generation of a chemical handle. The monomers were chosen to yield polymers with varying levels of heteroatoms to investigate whether heteroatom content had an effect on the photoluminescent properties of the resulting carbon dots.

Table 3: Structures of monomers used for 1,4-addition polymerisation

Acrylates	Diamines/Dithiols
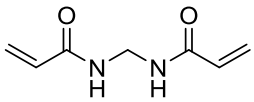 Methylene bisacrylamide (MBA)	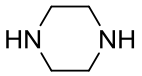 Piperazine
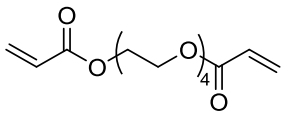 Tetraethylene glycol bisacrylamide (TEGDA)	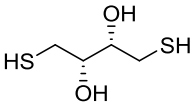 Dithiothreitol (DTT)
	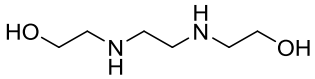 Bis-(2-hydroxyethyl)ethylenediamine (BHEDA)

Equimolar ratios of the diamines, dithiols and the diacrylates were used to give addition polymers of varying molecular weights and polydispersities (**Table 4**). Monomers for **P1**, **P4** and **P5** are solid at room temperature and were dissolved in water before polymerisation, whereas TEGDA was used neat. All monomer mixtures were degassed with N_2 for 30 min and polymerised overnight in an oven at 40 °C.

Table 4: Monomers and the molar ratios used in the synthesis of the addition polymers and the resulting polymer characterisation

	Monomer A	Monomer B	Monomer C	Molar Ratio[a]	Mn[b]	Mw[c]	Đ[d]
P1	MBA	Piperazine	BHEDA	2:1:1	8500	17300	2.0
	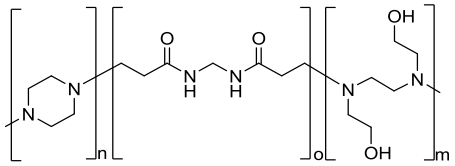						
P2	TEGDA	DTT	-	1:1	10300	21700	2.1
	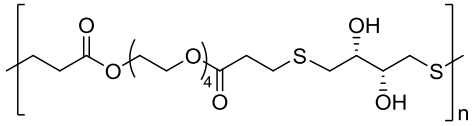						
P3	TEGDA	Piperazine	-	1:1	5000	8500	1.7
	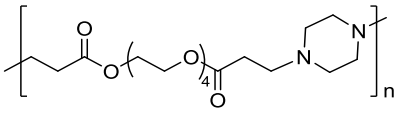						
P4	MBA	DTT	-	1:1	5600	10400	1.9
	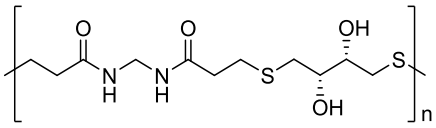						
P5	MBA	Piperazine		1:1	12500	18000	1.4
	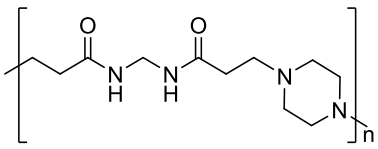						

[a] Molar ratio of monomers used in synthesis of each polymer. Reaction carried out on 10mmol scale
[b] Number average molecular weight
[c] Weight average molecular weight
[d] $Đ = M_w/M_n$

The polymers were dissolved in chloroform, and precipitated by the addition of hexane, collected by centrifugation, and dried overnight. On a 10 mmol scale, the yield by mass of each polymer were broadly constant; **P1** (2.58 g, 66%), **P2** (2.12 g, 47%), **P3** (3.17 g, 82%), **P4** (2.83 g, 92%) and **P5** (2.16 g, 90%). Polymers containing MBA were obtained as off-white solids whereas **P2** formed a sticky gel and **P3** a viscous oil. The polymers were dissolved in NMP and analysed by gel permeation chromatography (GPC) (**Table 4**) showing Mn's between 8500–21700 Da and polydispersities between 1.4 and 2.1. Synthetic addition polymers can have PDIs >10 but the equimolar ratios of the monomers used for the 1,4-addition polymers resulted in polymers with relatively narrow PDIs.

3.3 Carbon Dot Synthesis

Carbon dots were synthesised by thermopyrolysis of **P1**–**P5**. Each polymer (0.1 g) was sealed inside a 5 mL glass microwave vial and purged with N_2 for 30 minutes. The sealed tube was heated in a stainless steel heating block on a hotplate at 250 °C for 2 hours. Over this time, the reactions changed from colourless to brown and then to black. The crude products were suspended in water and centrifuged (14,000 rpm, 30 min) to remove the visible solid material. The light brown supernatant was collected and filtered by ultrafiltration through a regenerated cellulose membrane (MWCO 50,000, 14,000 rpm, 15 min). Dialysis of the filtrate through a cellulose membrane (MWCO = 14,000) in large volumes of water ensured any unreacted monomers were removed. The water was removed by evaporation overnight in an oven at 125 °C to give the carbon dots as a dark brown solid in ~10% yield. The synthesis was scaled up by a factor of 10 with no noticeable differences in the resulting carbon dots obtained, (1 g of **P1** gave ~100 mg of carbon dots). The carbon dots dispersed well in water or DMF, however they were found not to disperse in acetone or hexane.

3.4 Structural Properties

Confirmation of the successful synthesis of carbon dots was achieved by structural analysis and comparison to carbon dots synthesised by other methods. Elemental analysis of the carbon dots showed weight percentages of carbon consistent with the literature of other carbon dots by thermal routes (**Table 5**).[162] As expected, the weight percentage of nitrogen in the carbon dots increased with increasing nitrogen content in the monomer precursors reaching a maximum of 17% in **CD-P1** and **CD-P5** in which all monomers contained nitrogen. **CD-P3** and **CD-P4**, which possessed only one nitrogen containing monomer, showed 7.3 and 10.1% of nitrogen, respectively and **CD-P2**, which was not formed from nitrogen containing monomers, contained no nitrogen. The oxygen content of the two TEGDA containing monomers (**CD-P2** 31.7% and **CD-P3** 28.2%) was expectedly higher than those containing MBA. The elemental analysis of the carbon dots correlated well with the feed ratio of the monomers (**Table 5**). The size and shape of nanoparticles are important as they influence the optical properties as well as their behaviour and uptake in biological systems.

Table 5: Elemental analysis of **CD-P1** to **CD-P5**. **CD-PX** denotes the carbon dots derived from polymer X in Table 4 (n = 3)[a].

Carbon dot	Elemental Analysis (% weight) (feed ratio of starting polymer in brackets)				
	C	H	N	O	S
CD-P1	57.7 (53)	8.0 (9)	17.0 (22)	18.3 (16)	0.0 (0)
CD-P2	53.2 (47)	7.4 (7)	0.0 (0)	31.7 (32)	7.0 (14)
CD-P3	57.5 (56)	8.0 (8)	7.3 (7)	28.2 (29)	0.0 (0)
CD-P4	58.6 (43)	5.2 (6)	10.1 (9)	10.4 (21)	14.1 (21)
CD-P5	56.8 (55)	7.4 (9)	17.1 (23)	16.4 (13)	0.0 (0)

[a] Average of 3 elemental analyses

Table 6: PDIs and diameters of **CD-P1** to **CD-P5** measured by DLS in water after 5 min sonication and 1 min sonication between each measurement

CD	PDI	Diameter (nm)	DLS trace
CD-P1	0.83	55	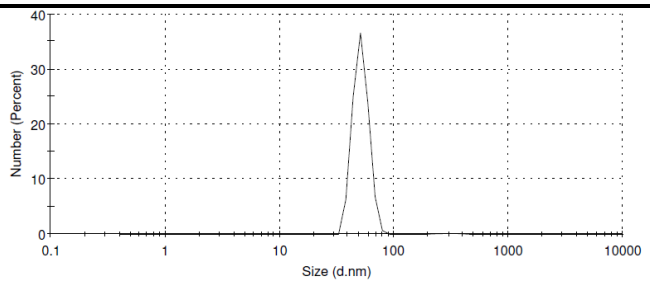
CD-P2	0.67	259	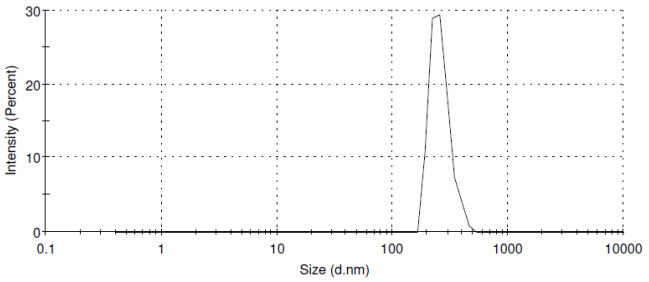
CD-P3	0.93	157	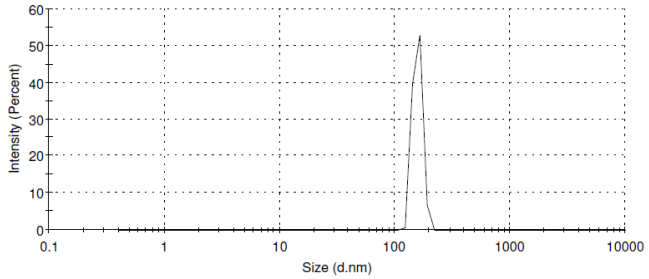
CD-P4	0.78	165	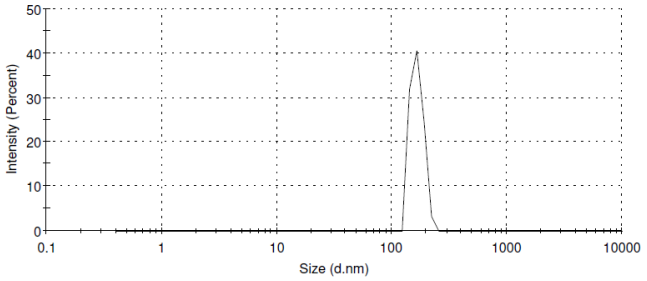
CD-P5	0.95	182	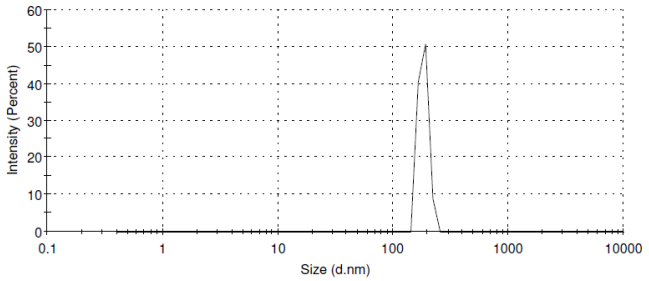

As discussed in Chapter 2, DLS measurements were found to give diameters much larger than those expected for carbon dots and need be used in conjunction with other imaging techniques to give the true, rather than hydrodynamic, diameter of the nanoparticles. By DLS, the measured diameters of **CD-P1** to **CD-P5** in aqueous solution (1 µg mL^{-1}) were between 55–325 nm and all carbon dots had high PDIs; 0.83 (**CD-P1**), 0.67 (**CD-P2**), 0.93 (**CD-P3**), 0.78 (**CD-P4**) and 0.95 (**CD-P5**) (**Table 6**). In the case of **CD-P1**, the size by number of particles is shown, giving an average diameter of 55 nm. For **CD-P2** to **CD-P5** the size by intensity is given as these did not differ from the size by number. Each sample was sonicated prior to measurements and between each of the three repeats, aggregates or clusters of the nanoparticles in aqueous solution were assumed to contribute to the larger diameters. The diameters of **CD-P1–P5** were measured by DLS in albumin and a surfactant (Tween) was used in order to disaggregate the nanoparticles. The DLS traces produced for each sample gave a peak around 8–9 nm however the control solution of Tween also gave an identical peak (**Figure 46**). The peak around 8–9 nm was therefore attributed to the albumin.

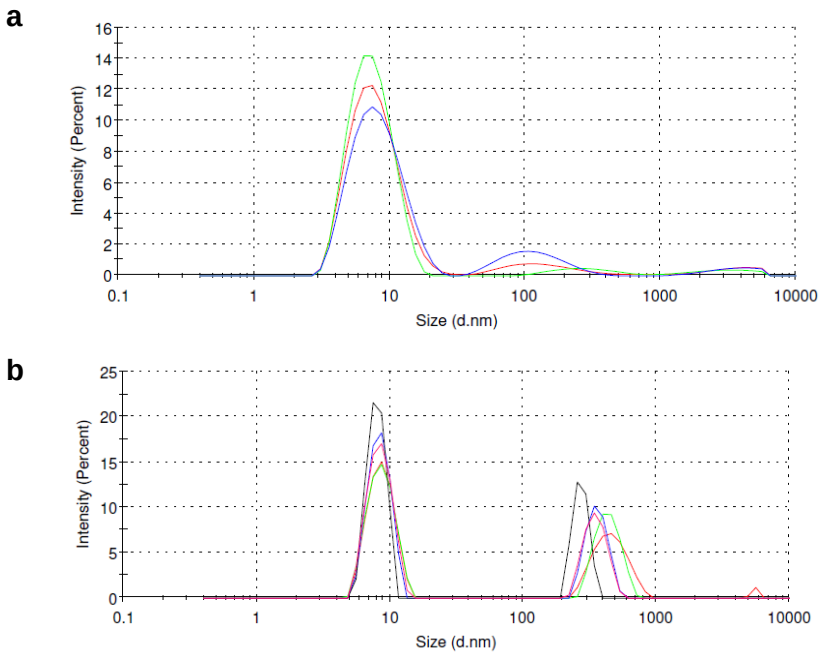

Figure 46: (a) DLS trace of albumin control solution (blue), **CD-P1** (red) and **CD-P2** (green), (b) DLS trace of **CD-P1** (red), **CD-P2** (green),**CD-P3** (blue),**CD-P4** (black) and **CD-P5** (pink) with the peak at 8–9 nm remaining unchanged.

Electron microscopy gives a clear image of the dry diameter of nanoparticles. Scanning electron microscopy (SEM) is generally used for particles >200 nm, whereas transmission electron microscopy is used for particles <200 nm. For TEM analysis, samples of the nanoparticles were dispersed in acetone, deposited on to a copper-coated formvar grid and dried in air. A 400 keV microscope was used to image the carbon dots which showed the dots to be spherical and of the desired size, i.e. <10 nm. High magnification TEM of **CD-P1** showed the nanoparticles to be broadly consistent in morphology, monodisperse and ~5 nm in diameter (**Figure 47**). The lattice spacing within an individual carbon dot was determined to be 0.21 nm (lattice spacing measurements give the distance between atomic planes with 0.21 nm consistent with the (100) diffraction planes of nano-crystalline graphite).[163]

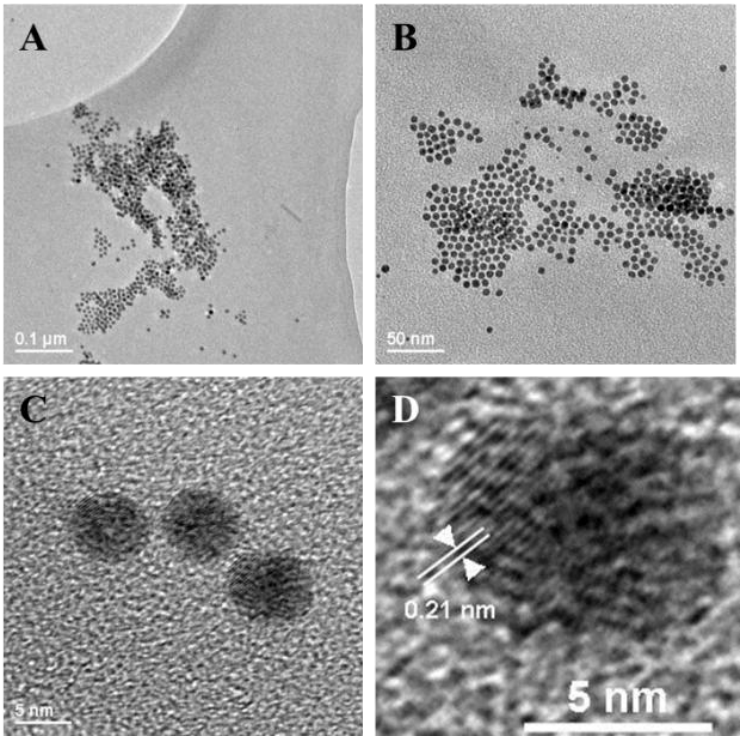

Figure 47: TEM images of **CD-P1** at (a) ×10,000, (b) ×40,000 and (c) ×200,000 magnification (d) high-resolution TEM image of an individual carbon dot.

TEM was carried out on **CD-P2** to **CD-P5** using a 100 keV microscope. Although aggregates of the carbon dots made identification of individual carbon dots difficult under the lower resolution, images of **CD-P2** to **CD-P5** showed the carbon dots to be spherical and ~5 nm in diameter (**Figure 48**).

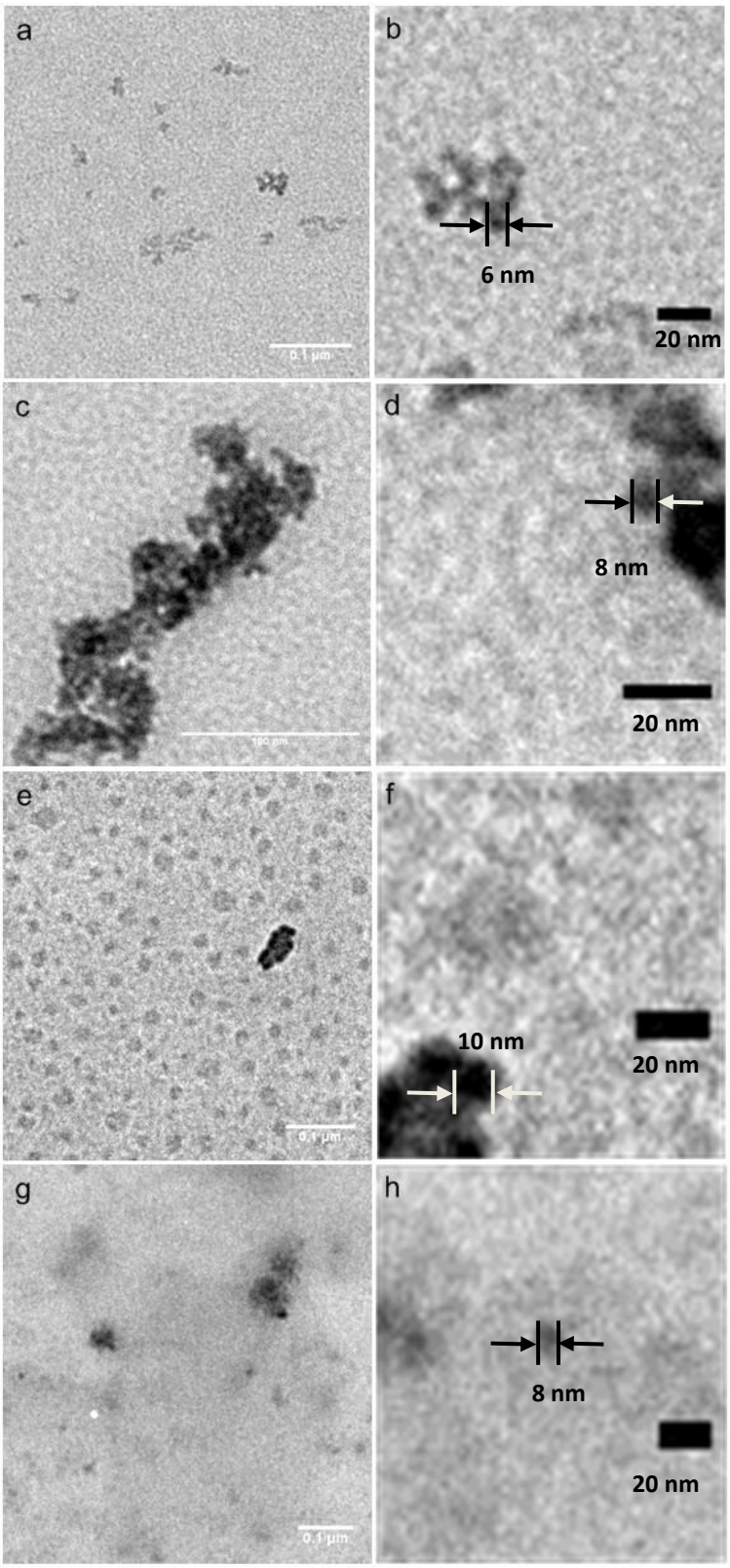

Figure 48: Low and high magnification TEM images of (a and b) **CD-P2**, (c and d) **CD-P3**, (e and f**) CD-P4**, (g and h) **CD-P5**, respectively. Arrows indicate an individual carbon dot in each sample.

X-ray photoelectron spectroscopy (XPS) gives information about the nature of the atoms on the surface of particles. After X-ray irradiation of a sample, the number and energy of the electrons that escape from the top 10 nm can be analysed.[164] Because the sizes of carbon dots are <10 nm, XPS can give information about the environments of the atoms within the sample and give an indication of the relationship between the polymeric starting materials and the carbon dot products. A full XPS survey was obtained for each of the five carbon dot samples and a higher resolution scan carried out on the major peaks. The full XPS survey of **CD-P1** (**Figure 49**) showed the presence of carbon, nitrogen and oxygen, corroborating the presence of these elements in the polymer. **CD-P1** C1s peaks at 284.6 eV, 285.4 eV and 287.6 eV were attributed to sp2 hybridised carbon, amine (C-N or C-NH) bonds, and ether or amide bonds, respectively. Common features of the precursor polymers for **CD-P2**–**CD-P5** were shown through similar peak positions in the XPS spectra of **CD- P2**–**CD-P5**. The C1s spectra of **CD-P2**–**CD-P5** showed a C-C sp2 peak around 284.1 eV–284.8 eV (**Figure 50** – **Figure 53**).

Carbon dots synthesised using TEGDA-containing polymers (**CD-P2** and **CD-P3**) gave peaks attributable to the C1s carboxylate peaks at the characteristic higher binding energy of 288.7 eV–288.9 eV. The high degree of overlap between C1s peaks indicative of amino, ether, hydroxy and thioether groups render absolute identification difficult, however, peaks around 286.09 eV–286.18 eV in **CD-P2**, **CD-P3** and **CD-P4** were assigned to C-S, hydroxyl or ether carbons.

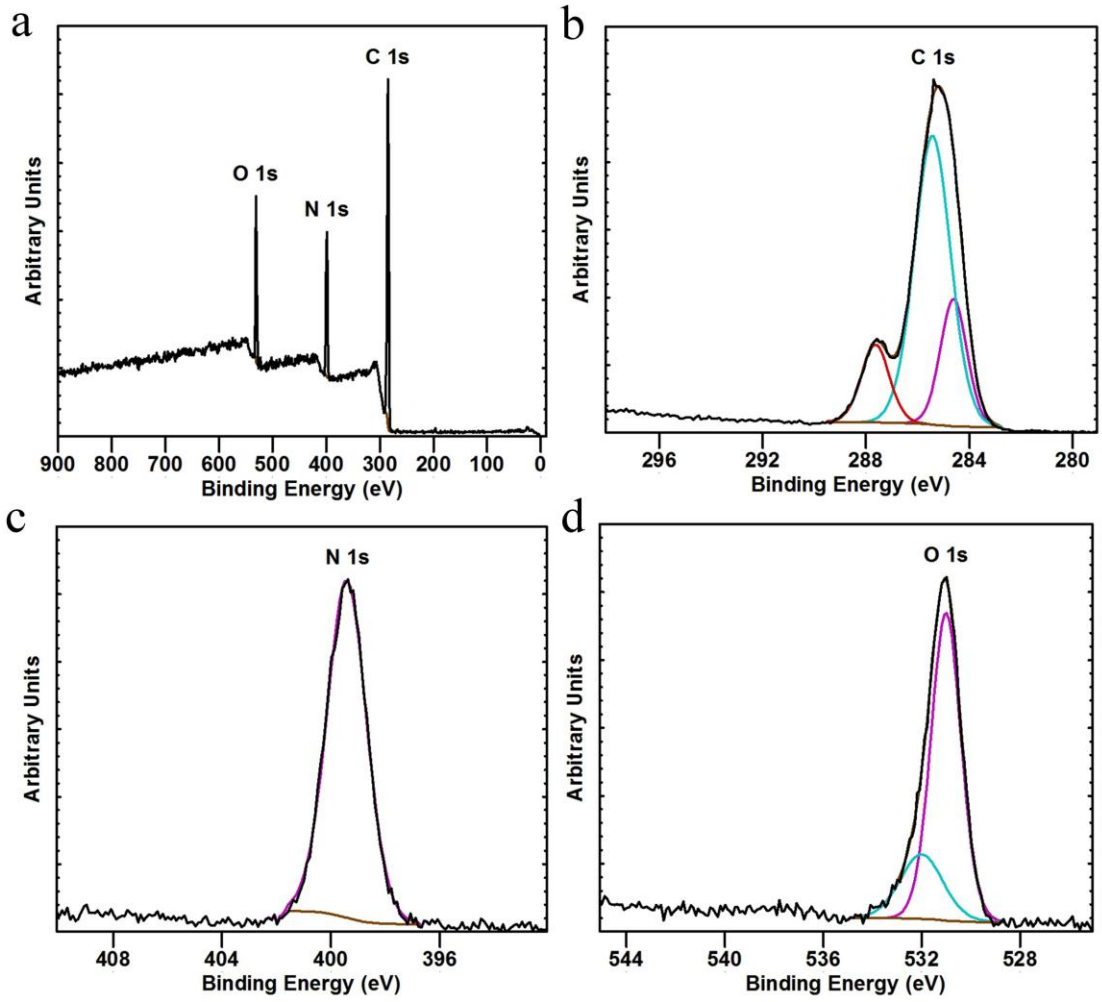

Figure 49: (a) XPS of **CD-P1** showing characteristic C1s, N1s and O1s peaks at 292, 400 and 525 eV respectively; (b) analysis of the high resolution scan of the C1s region (282 – 289 eV) showing sp2 hybridised carbon (284.6 eV), amine bonds (285.4 eV) and ether or amide functionalities (287.6 eV) (c) analysis of the high resolution scan of the N1s region showing amine environments (d) analysis of the high resolution scan of the O1s region indicating the presence of C=O double bonds present in esters or amides.

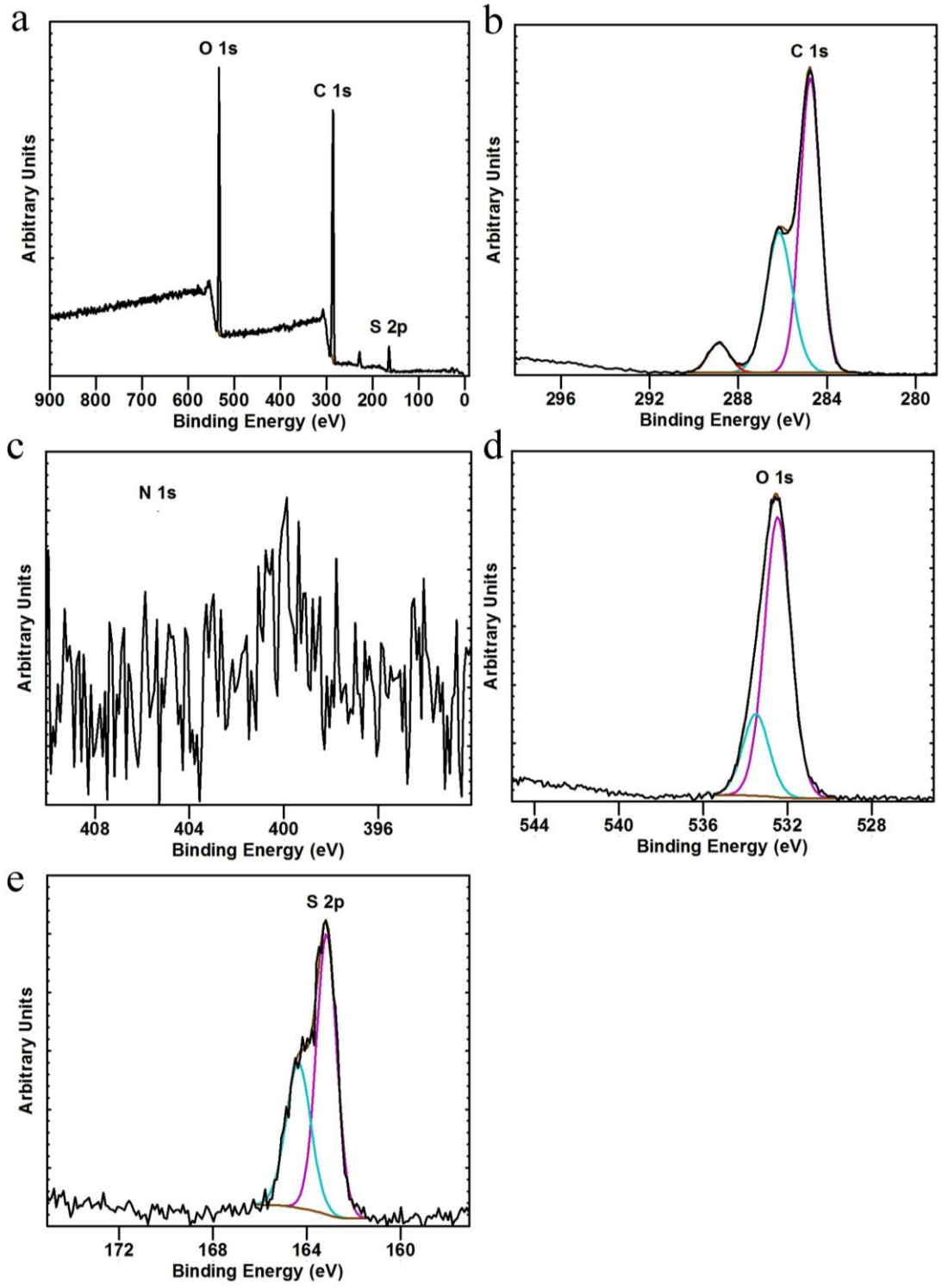

Figure 50: (a) XPS of **CD-P2** showing characteristic S2p, C1s and O1s peaks at 165/228, 292, and 525 eV respectively; (b) analysis of the high resolution scan of the C1s region indicating C-S bonds, carboxylate groups (288.7 eV–288.9 eV) (c) high resolution scan of the N1s region showing no nitrogen functional groups present (d) high resolution scan of the O1s region indicating the presence of C=O double bonds present in esters or amides (e) analysis of the high resolution scan of the S2p region showing the presence of sulphur (C-S bonds).

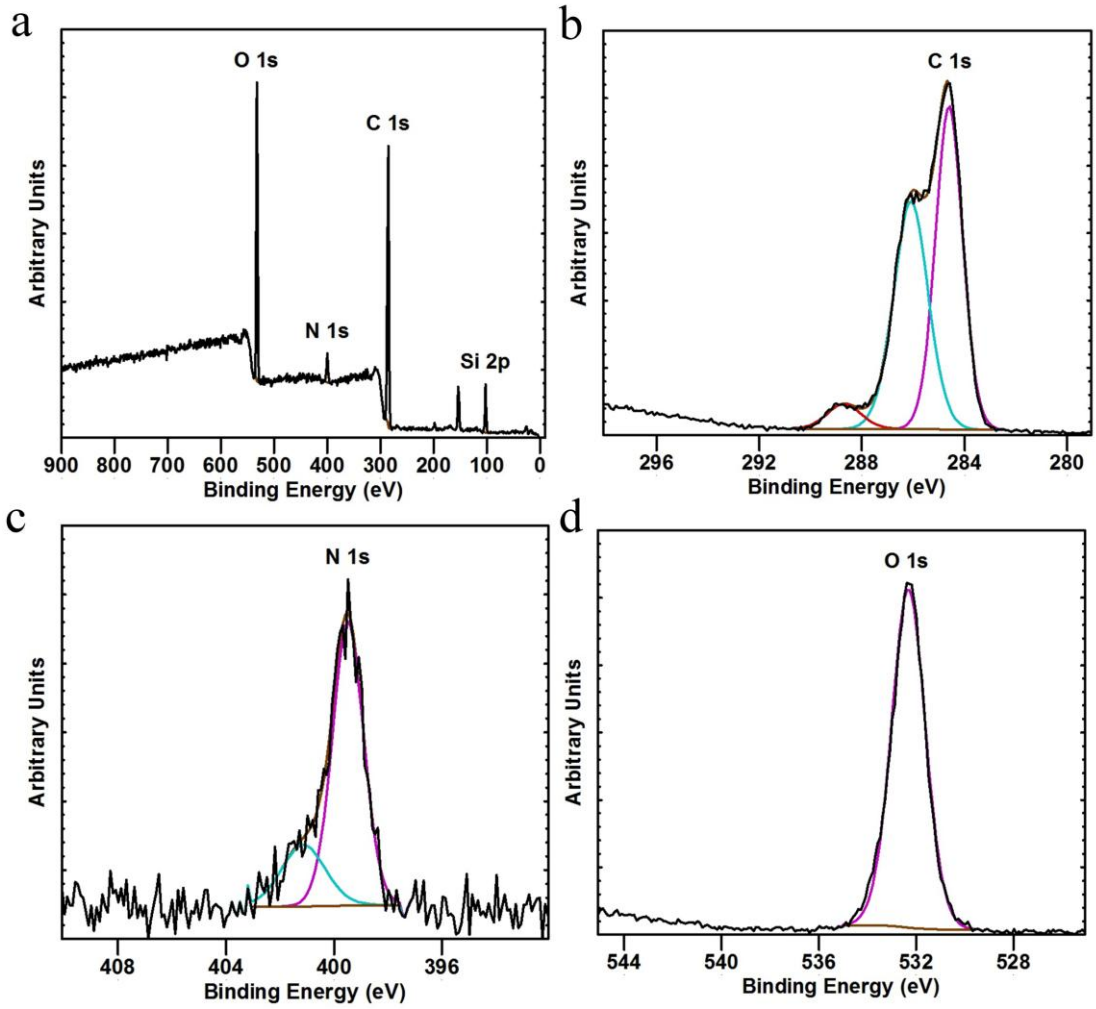

Figure 51: (a) XPS of **CD-P3** showing characteristic C1s, N1s and O1s peaks at 292, 400 and 525 eV respectively; (b) analysis of the high resolution scan of the C1s region showing sp2 hybridised carbon, carboxylate groups (288.7 eV–288.9 eV) (c) high resolution scan of the N1s region showing amine functionality (d) high resolution scan of the O1s region indicating the presence of esters

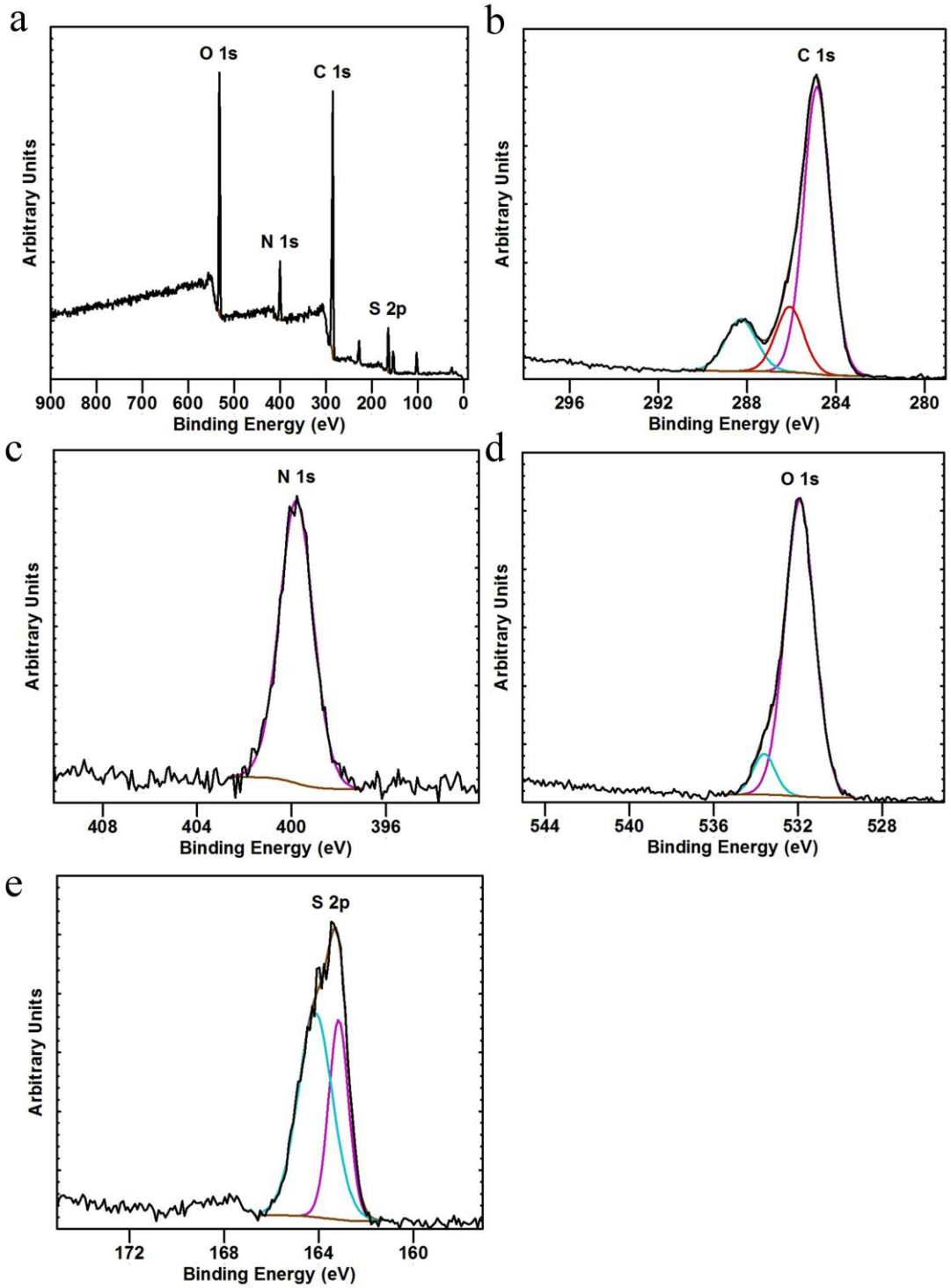

Figure 52: (a) XPS of **CD-P4** showing characteristic S2p, C1s, N1s and O1s peaks at 165/228, 292, 400 and 525 eV respectively; (b) analysis of the high resolution scan of the C1s region showing sp2 hybridised carbon, C-OH and amide groups (c) high resolution scan of the N1s region showing amine functionality (d) high resolution scan of the O1s region indicating the presence of amides and hydroxyl groups (e) high resolution scan of the S2p region indicating C-S bonds

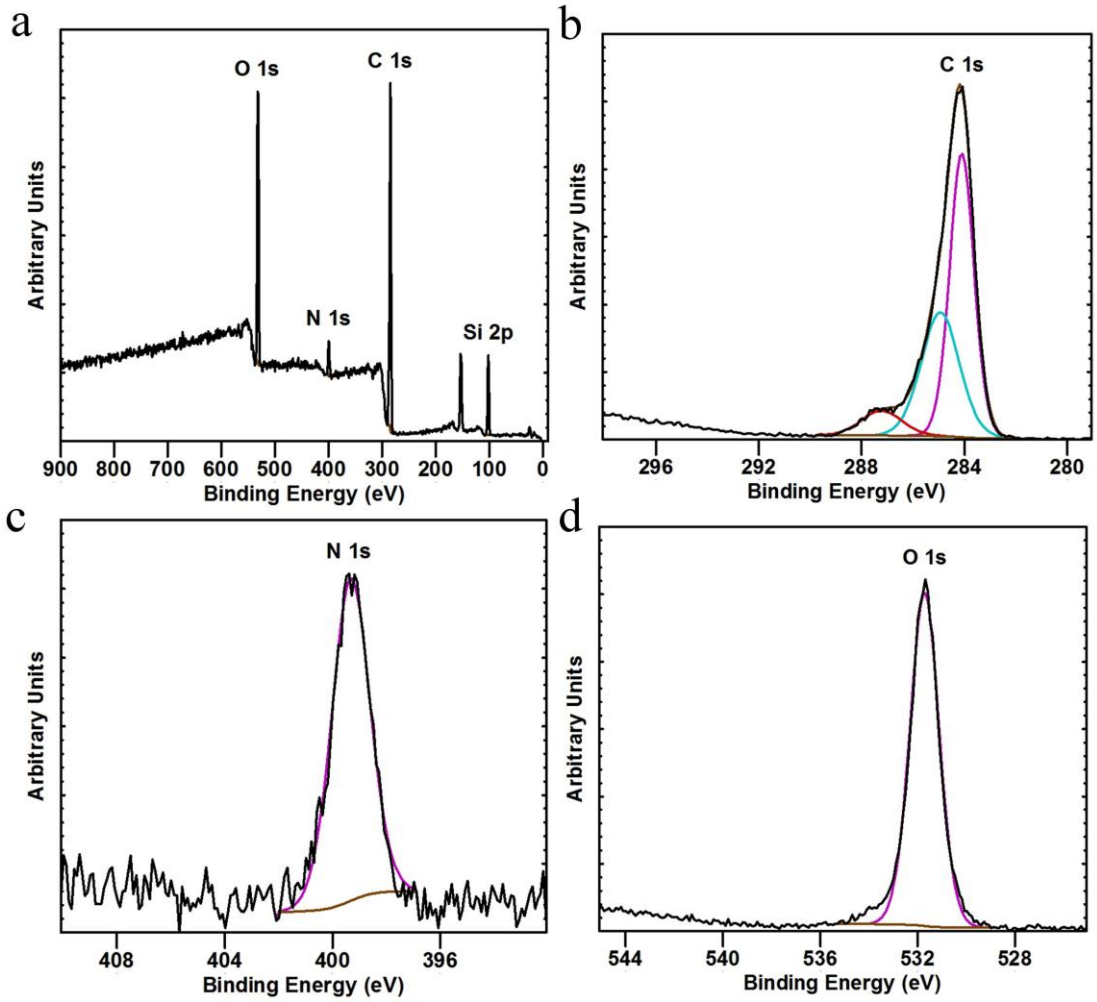

Figure 53: (a) XPS of **CD-P5** showing characteristic C1s, N1s and O1s peaks at 292, 400 and 525 eV respectively; (b) analysis of the high resolution scan of the C1s region showing sp2 hybridised carbon, amide groups (287-288 eV) (c) high resolution scan of the N1s region showing amine/amide functionality (d) high resolution scan of the O1s region indicating the presence of amides

The amide carbon present in MBA still gave a characteristic peak between 287.23 eV –288.28 eV in **CD-P1**, **CD-P4** and **CD-P5** suggesting that the temperature used for pyrolysis did not completely decompose the polymers. High resolution N1s scans showed typical amine and/or amide peaks in **CD-P1**, **CD-P3**, **CD-P4** and **CD-P5**. The absence of an N1s peak in the scan for **CD-P2** was consistent with the elemental composition of the polymer used. O1s peaks confirmed the presence of oxygen in every sample with energies attributable to the predominance of C=O double bonds (either ester or amide). The characteristic peaks of C-S S2s (~228 eV) and S2p (~164

eV) were evident in **CD-P2** and **CD-P4** with a high resolution scan of the S2p peak showing the asymmetry associated with spin-orbit splitting ($S2p_{1/2}$ and $S2p_{3/2}$) particularly evident in **CD-P2**. Si2p peaks present in **CD-P3**, **CD-P4** and **CD-P5** were thought to be contaminants and not an integral part of the carbon dot surface.

3.5 Optical Properties

The optical properties of carbon dots are of interest, especially considering their use as alternatives to CdSe-based quantum dots and small molecule fluorophores. Encouragingly, aqueous solutions of the carbon dots displayed varying degrees of blue fluorescence under UV irradiation (λ_{ex} 365 nm). On visible inspection, **CD-P1** displayed the highest fluorescence whereas **CD-P2** showed negligible fluorescence (see **Figure 54**).

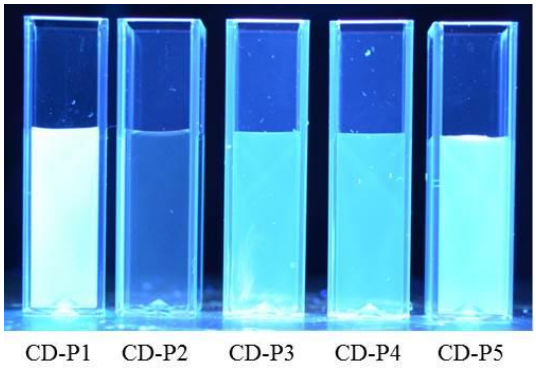

Figure 54: Aqueous solutions of carbon dots **CD-P1**–**CD-P5** (0.1% w/v) excited at 365 nm

Quantification of the optical properties of the carbon dots was carried out by measurements of the absorbance, excitation and emission spectra, and quantum yields and compared to other carbon dots produced by thermal routes.

3.5.1 Absorption and Emission Spectra

To quantify the optical properties of the carbon dots produced, the absorption of each of the samples was measured in water at a concentration of 0.1% (w/v) (**Figure 55**). Absorption was seen in the 220–500 nm region which tailed-off beyond ~530 nm.

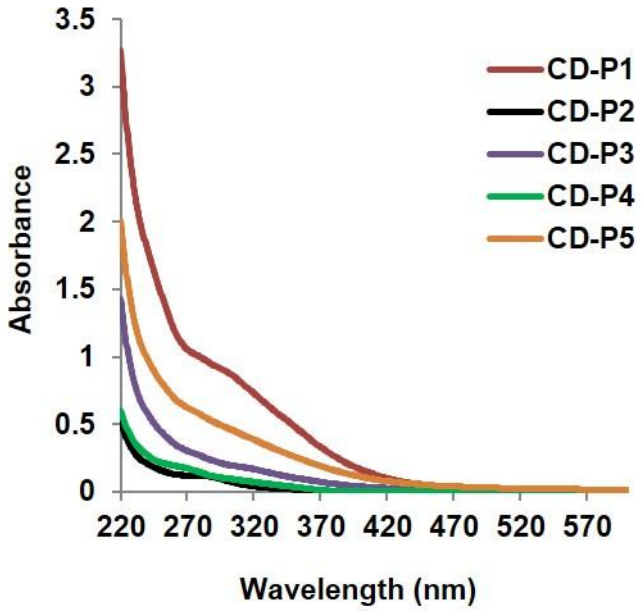

Figure 55: Absorption profile of aqueous solutions of **CD-P1**–**CD-P5** (0.1% w/v) from 220 – 570 nm.

Elemental carbon, carbon-black (up to ~97% carbon by weight) and other carbonaceous material with significant carbon content all absorb radiation strongly, particularly in the UV region.[165] Soot and the organic compound containing "brown carbon" comprise ~60% carbon with hydrogen, oxygen, nitrogen and sulphur making up the remaining 40%. Brown carbon has strong absorption-wavelength dependence and absorbs more strongly towards shorter wavelengths (near UV), generally due to π - π^* transitions in the organic elements.[166–168] **CD-P1** to **CD-P5** are ~60% carbon by weight with varying amounts of the accessory elements and due to the similar levels of composition to brown carbon, it is likely that the UV absorption is similar. It is generally accepted that light absorption by aromatic compounds shifts towards longer wavelengths as the graphitic cluster size grows.[105] The presence of a range of different sized graphitic clusters within the carbon dots could contribute to the

absorption properties, particularly in the UV region. The shape of the absorption profile was consistent with carbon dots produced from thermal methods with a tail off around 500 nm. A shoulder at ~300 nm can be attributed to n-π* transition of carbon-oxygen double bonds within the carbon dots in agreement with the XPS data. The broad nature of the absorption can be attributed to the complicated band structure of the carbon dots due to their random composition and subsequently the varying numbers and sizes of graphitic clusters.

For emission analysis, **CD-P1** to **CD-P5** in deionised water (0.1% w/v) (**Figure 56**), emission of **CD-P1** to **CD-P5** showed excitation wavelength dependence consistent with other reported carbon dots. The broad nature of the emission spectra, and therefore multi-colour emission is attributable to the small differences in the size of carbon dots within each sample and is a common feature of many carbon dot containing samples.

The carbon dots displayed maximum emission between 419 nm (**CD-P4**) and 446 nm (**CD-P2**) when excited at 380 nm. Even though the excitation profile in **CD-P3** and **CD-P5** appeared at higher wavelengths, the maximum emissions occurred when excited at 380 nm (443 nm and 433 nm, respectively). Maximum emission with 380 nm excitation was also seen with **CD-P1** (437 nm). Analysis of **CD-P2** showed poor fluorescence visible under UV excitation, nevertheless these particles still showed excitation dependent emission, reaching a maximum of 442 nm when excited at 360 nm. The excitation maxima of **CD-P1**, **CD-P2**, **CD-P3** and **CD-P5** were all within 10 nm of each other. A feature shared by some carbon dots is the blue-shifting of their emission spectra at increasing excitation wavelengths, i.e. a decrease in Stokes shift. The normalised emission spectra of **CD-P1**–**CD-P5** show increased spacing as higher excitation wavelengths are used (**Figure 57**).

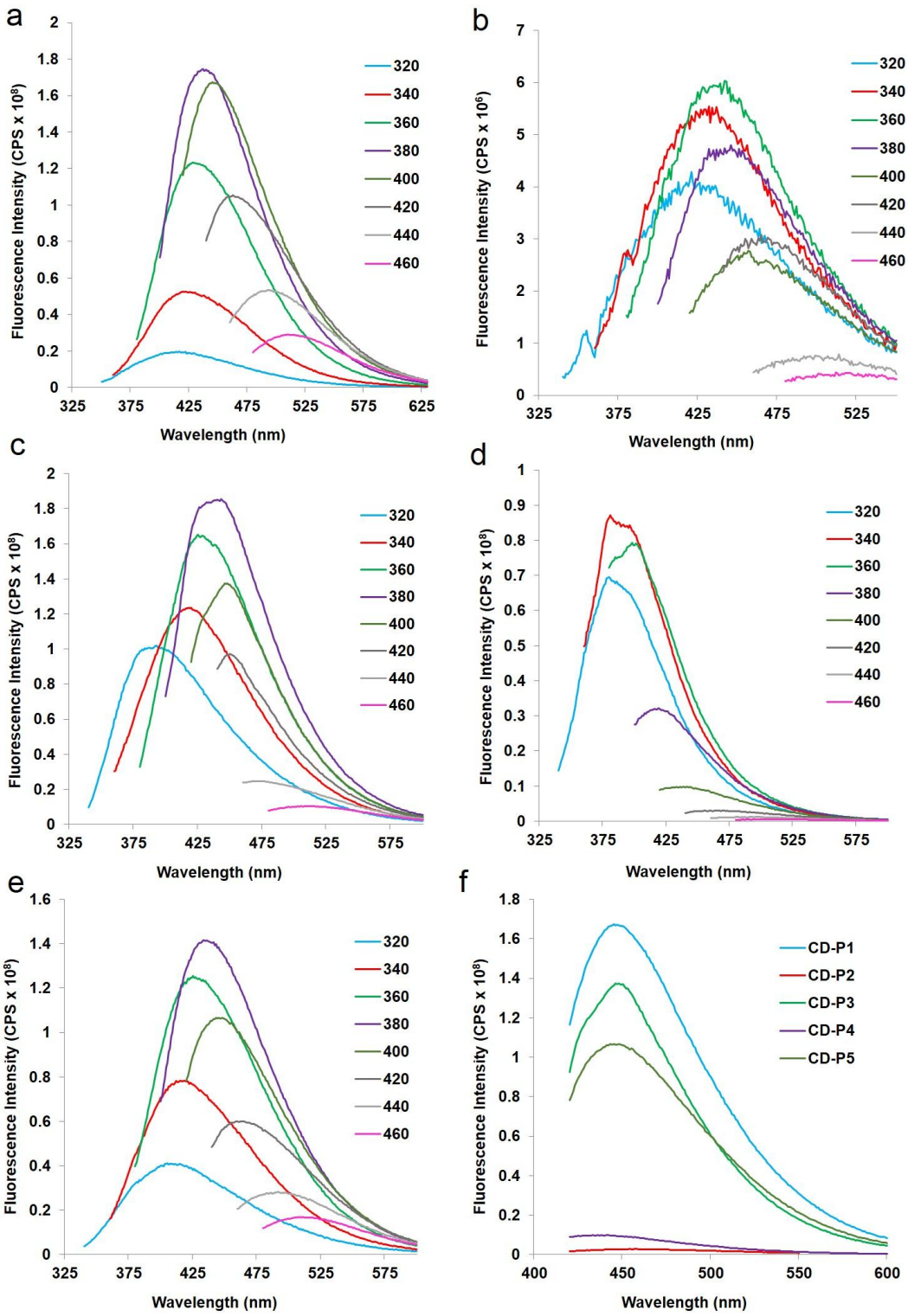

Figure 56: Emission spectra of (a) **CD-P1**, (b) **CD-P2**, (c) **CD-P3**, (d) **CD-P4**, (e) **CD-P5** excited from 320 nm–460 nm in 20 nm increments (f) emission spectra of **CD-P1–CD-P5** excited at 360 nm (n = 3)

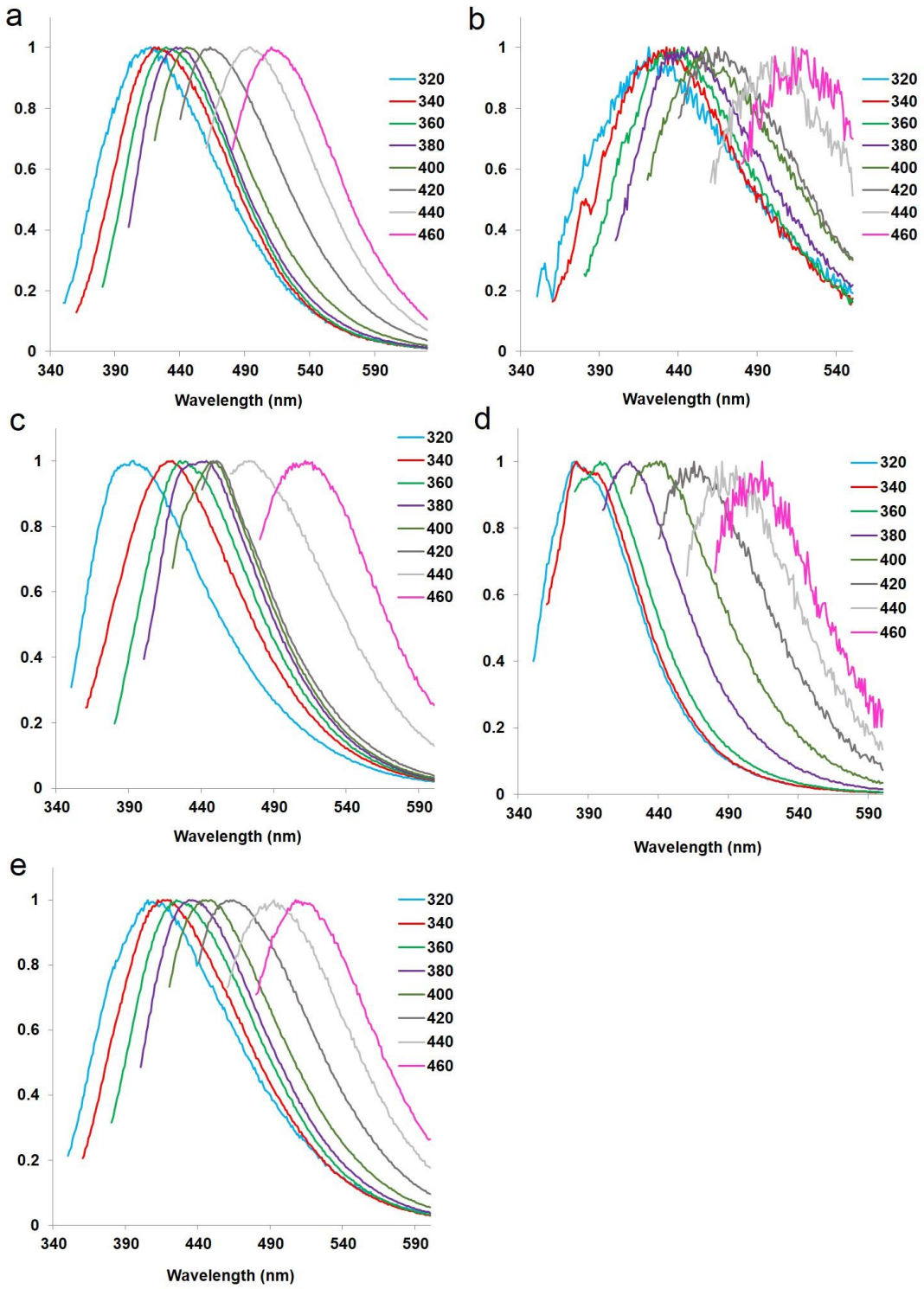

Figure 57: Normalised emission spectra of (a) **CD-P1**, (b) **CD-P2**, (c) **CD-P3**, (d) **CD-P4**, (e) **CD-P5** excited from 320 nm–460 nm in 20 nm increments (n = 3)

The Stokes shift versus the excitation wavelength shows a good correlation for **CD-P1**, **CD-P2**, **CD-P3** and **CD-P5** at wavelengths up and including 440 nm (**Table 7** and **Figure 58**). At wavelengths >440 nm the trend is not so clear, however, this may be attributed to the weakness of the fluorescence at higher wavelengths. **CD-P4** showed a constant Stokes shift (**Figure 58**).

Table 7: Maximum emission wavelength of **CD-P1** to **CD-P5** on excitation between 320–460 nm and corresponding Stokes shift (nm).

λ_{ex}	**CD-P1**		**CD-P2**		**CD-P3**		**CD-P4**		**CD-P5**	
nm	λ_{em}	Shift	λ_{em}	Shift	λ_{em}	Shift	λ_{em}	Shift	λ_{em}	Shift
320	417	97	421	101	393	73	380	60	85	85
340	420	80	432	92	420	80	381	41	75	75
360	429	69	442	82	425	65	398	38	65	65
380	437	57	446	66	443	63	419	39	53	53
400	445	45	457	57	448	48	442	42	43	43
420	463	43	465	45	450	30	465	45	42	42
440	494	54	514	74	474	34	485	45	52	52
460	510	50	512	52	511	51	514	54	47	47

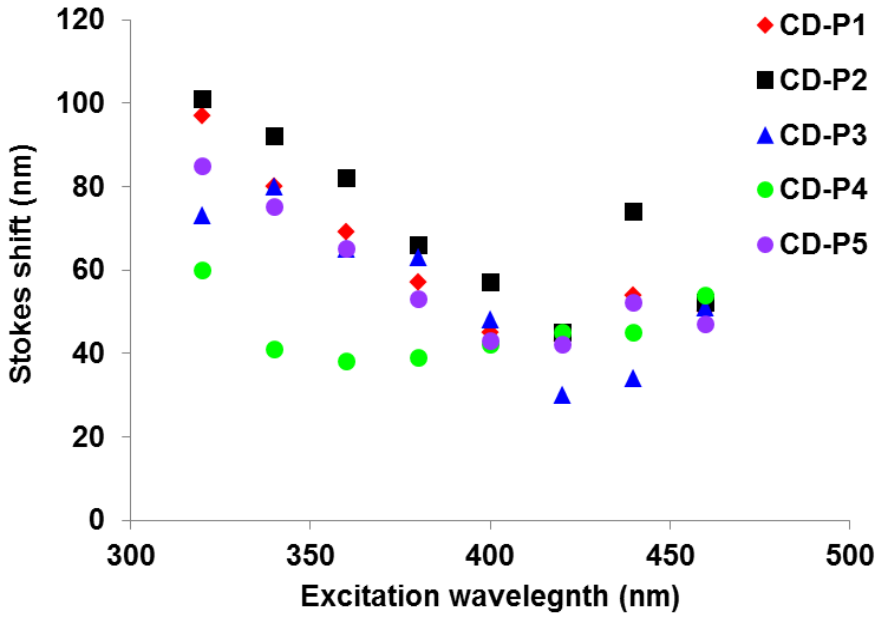

Figure 58: The relationship between increasing excitation wavelength and decreasing Stokes shift of **CD-P1** to **CD-P5**

Interestingly, the emission intensity of the carbon dots increased with increasing nitrogen content of the precursor polymers. **CD-P2**, which contained no nitrogen showed negligible fluorescence, **CD-P3** and **CD-P4** (from polymers with one nitrogen containing monomer) displayed increased fluorescence but **CD-P1** and **CD-P5** (in which all the monomers contained nitrogen) showed the highest fluorescence. When the elemental composition of the dots was compared with the fluorescence intensities, no noticeable trend was seen with the levels of oxygen or sulphur. Increasing nitrogen content did not appear to have any effect on the maximum emission wavelength.

The fluorescence of aqueous solutions of the carbon dots (λ_{ex} 380 nm) remained stable over a pH range of 4.0 to 9.0 with only very minor variations observed (**Figure 59**).

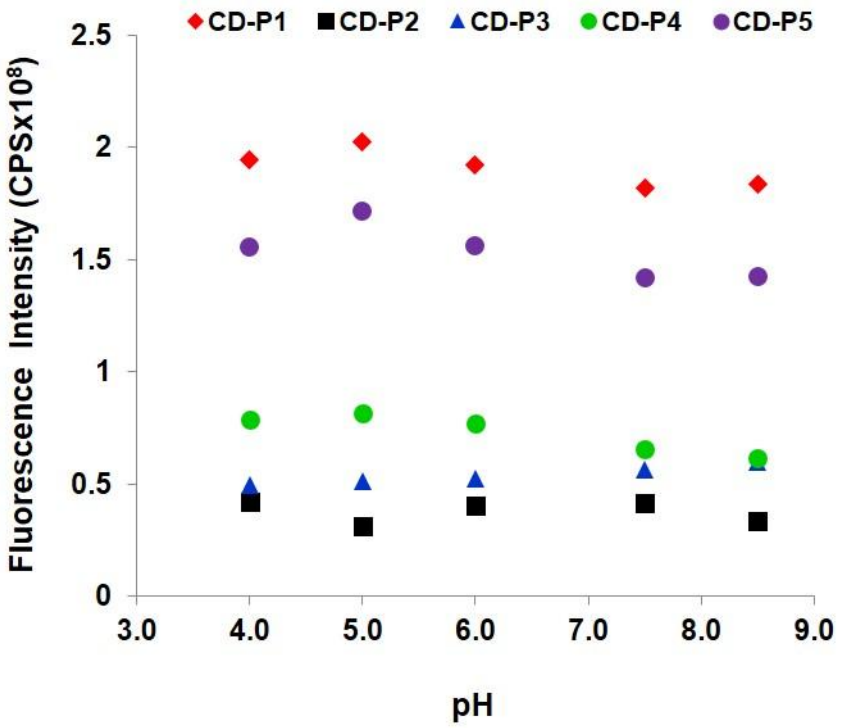

Figure 59: Fluorescence intensity of **CD-P1** to **CD-P5** in aqueous solutions (0.1 % w/v) at pH 4.0–9.0 (λ_{ex} 380 nm)

3.5.2 Quantum Yields

In order to evaluate the carbon dots as tracking agents, the quantum yields of **CD-P1** to **CD-P5** were calculated. The quantum yield (Φ) of a fluorophore is an important consideration and can be described as the ratio between the number of photons emitted and the number of photons absorbed. The maximum quantum yield of 1.0 (100%), i.e. every photon absorbed is consequently emitted, is hardly ever achieved, however, some small molecule fluorophores come close to this; fluorescein in ethanol has a quantum yield of 0.91 ± 0.05 (in 1 M NaOH)[169] and sulforhodamine 101 in ethanol is 0.93 ± 0.02.[170] A molecule is still deemed as appreciably fluorescent with a quantum yield of 0.1.

Initially, quantum yields were calculated using the absorbance and fluorescence readings taken from a platereader in parallel. The absorbance and fluorescence

intensities of samples in a 0.001% w/v aqueous solution were measured with 4',6-diamidino-2-phenylindole (DAPI) in water used as a standard. The calculated quantum yields, although within the expected range, did not correlate well with the observed fluorescence intensities of the aqueous carbon dot solutions under UV light (λ_{ex} 385 nm). Similar quantum yields were obtained for **CD-P2** and **CD-P3**, but did not match with the marked differences in fluorescence on visual inspection.

In order to measure the quantum yields of the five carbon dot samples effectively, the absorbance and fluorescence of a range of concentrations was measured individually and compared against a standard. An aqueous solution of **CD-P1** was excited at different wavelengths with varying slit widths to verify that the specified excitation wavelength produced a full peak, that the signal was not saturated, that the absorption was adequate and that it was compatible with the DAPI standard in DMSO. DAPI is more fluorescent in DMSO than water and the ability to correct for the refractive index of the solvents allowed for a solvent other than water to be used. Following this, five concentrations (1, 2.5, 5, 7.5 and 10 μg mL^{-1}) of each of the carbon dot samples were made up in water using a 0.1 % (1 mg mL^{-1}) stock solution and five concentrations of DAPI in DMSO were made up to be used as standards. The fluorescence spectrum of each sample was measured between 350 nm and 650 nm (λ_{ex} 330 nm, slit widths 3.5 mm, n = 3). The area under the integrated curve of the fully corrected spectrum was then recorded and plotted against the absorbance for the same sample (**Figure 60**).

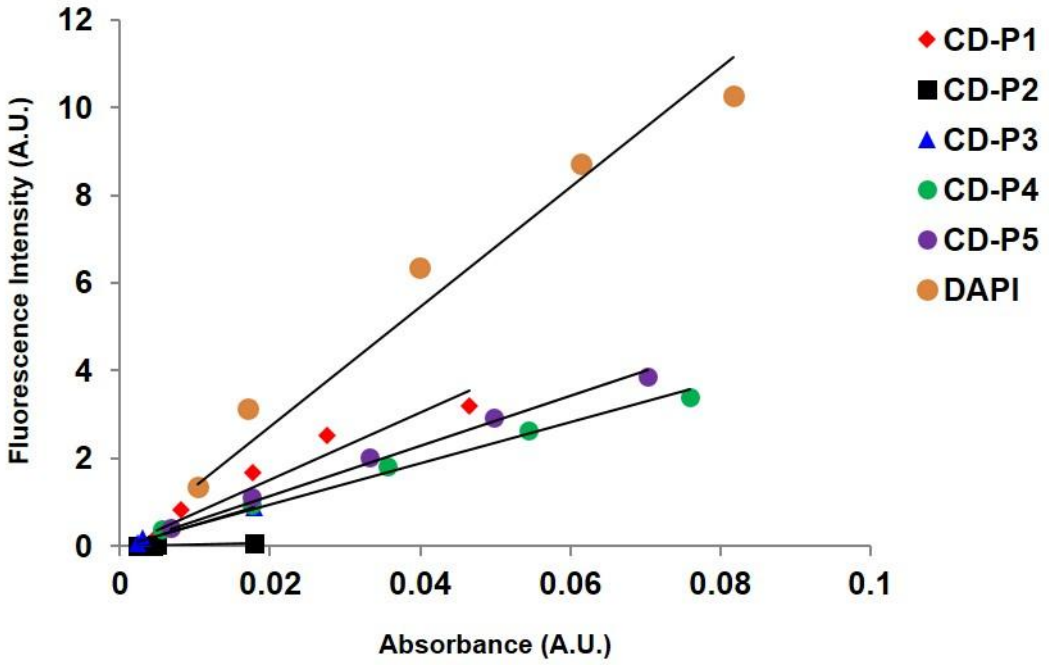

Figure 60: Graph of the absorbance of five concentrations of **CD-P1**–**CD-P5** (n = 3) versus the integrated area of the fluorescence intensity of each sample (n = 3)

Using the gradient of each line and taking into account the dispersity index of the solvents used and the quantum yield of the reference sample, the quantum yield was calculated using the following formula[171]:

$$\Phi_X = \Phi_{ST}\left(\frac{Grad_X}{Grad_{ST}}\right)\left(\frac{\eta_X^2}{\eta_{ST}^2}\right)$$

Where the ST and X subscripts denote the standard and test, respectively, Φ is the quantum yield, Grad is the gradient from the straight line graph of integrated fluorescence *vs* absorbance, and η the refractive index of the solvent.

The quantum yields of the carbon dots matched the observed fluorescence intensities (**CD-P1** 26%; **CD-P2** 2%; **CD-P3** 13%; **CD-P4** 16%; **CD-P5** 20%). The quantum yields of **CD-P1** and **CD-P5** gave a better representation of the observed fluorescence intensities and were comparable to previously published syntheses from thermal methods. **CD-P1**, as the most fluorescent and possessing the highest quantum yield (26%), was selected for further study and biological experiments.

3.5.3 Up-conversion Studies

Up-conversion of near infrared light (lower energy) with emission in the visible (higher energy) region via a two or multi-photon process is a suggested property of carbon dots. The potential benefits offered by two-photon excitation of carbon dots has led to claims of two-photon microscopy with carbon dots being possible, however, there is growing doubt that the phenomenon exists in carbon dots[172] (with the exception of carbon dots incorporating f-block metals which are known to promote two-photon excitation).[117] To investigate the ability of carbon dots from 1,4-addition polymers to display up-converting properties, aqueous solutions of **CD-P1** (0.1% w/v) were excited with light in the near infrared region (650–900 nm in 50 nm increments). **CD-P1** appeared to show excitation dependent emission in the visible region on excitation with NIR light (**Figure 61a**).

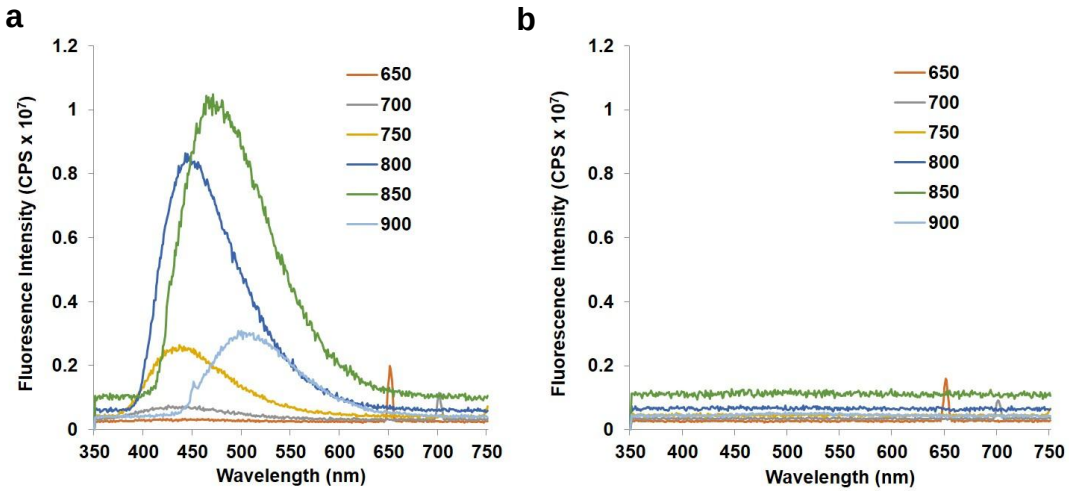

Figure 61: (a) emission spectra of **CD-P1** excited between 650–900 nm in 50 nm increments without long pass filter (b) identical spectra of **CD-P1** with 455 nm long pass filter.

The fluorescence intensity increased from negligible at 650 nm to a maximum of 476 nm (λ_{ex} 850 nm) before decreasing at higher wavelengths. One comparison of the probabilities of one and two-photon excitation suggests that in bright sunlight, a good one- or two-photon absorber will absorb one-photon every second but only once per ten million years in a two-photon process.[173] On continuous wave excitation, 100–1000 times more average power than pulsed excitation is required to yield the same

rate of two-photon excitation.[174] The fluorescence intensity of the carbon dots on two-photon excitation is expected, therefore, to be only a fraction of that of one-photon excitation. The maximum measured fluorescence intensity of **CD-P1** is 1.8 x 10^8 CPS (λ_{ex} 380 nm) whereas the maximum when excited at near-infrared wavelengths is 1 x 10^{-7} CPS (λ_{ex} 850 nm). This represents an 18-fold decrease in fluorescence intensity whereas based on the maximum rate of two-photon absorption at least a 100-fold decrease would be expected. In order to assess the likelihood that **CD-P1** undergoes two-photon excitation, the excitation spectra were re-measured with a 455 nm long pass filter (optical setup described in **Figure 62**). A long-pass filter prevents light below a certain wavelength from passing through the lens, in this case <455 nm. Thus, the effects of second order diffraction could be assessed.

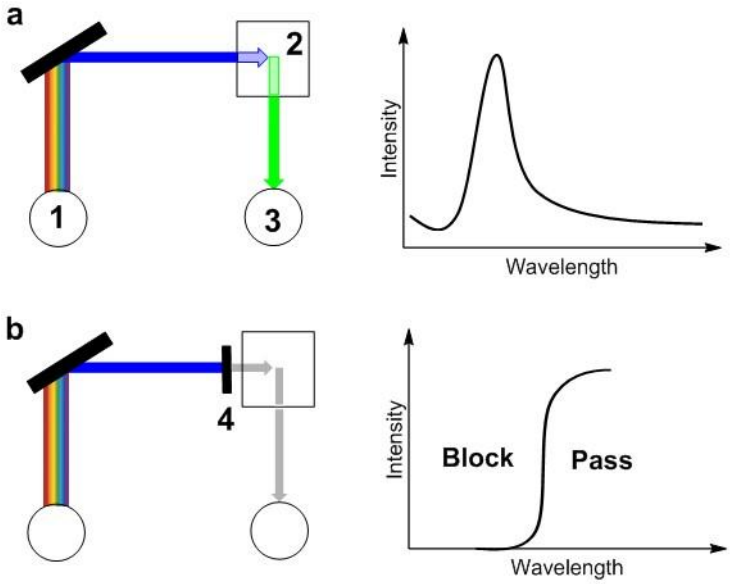

Figure 62: Top view representation of experimental setup for fluorescence intensity measurements (left) without long pass filter (right) with long pass filter. Full spectrum light is generated by the light source (1) and light of the specified wavelength is diffracted by the diffraction grating before exciting the sample (2). The fluorescence intensity measured at each wavelength of the specified scan is measured (3). A long pass filter (4) is placed in front of the sample chamber to prevent light below a certain wavelength for passing through the sample.

On NIR excitation (650–900 nm in 50 nm increments), no emission was observed in the visible region, confirming that the emission in the absence of the filter arose not from up-conversion but as a result of second order diffraction of light (i.e. light of half the excitation wavelength) (**Figure 61b**). This study adds weight to the doubt surrounding two-photon excitation although does not rule it out for all carbon dots.

3.6 Cellular Studies

The ability of certain carbon dots to be taken up by cells and their lack of cytotoxicity is well documented[175,176] and is crucial if using the carbon dots in biological applications. It is presumed that carbon dots enter cells by pinocytosis due to their small size. In order to assess the biocompatibility of the carbon dots from 1,4-addition polymers, the cytotoxicity of all the carbon dots was evaluated and the uptake of **CD-P1**, the most fluorescent particles investigated.

3.6.1 Cytotoxicity

The cytotoxicity of carbon dots differs somewhat from the cytotoxicity of other predominantly carbon-containing materials. The toxicity of carbon nanotubes can be attributed to their fibre like structure when aggregated[177] whereas there is a wealth of evidence showing carbon dots are not cytotoxic.[178] Of the more visual cytotoxicity experiments, Wang showed the growth of beansprouts was not hindered by an aqueous carbon dot solution of 1.5 mg mL^{-1}. The resulting sprouts exhibited excitation dependent fluorescence emission. An aqueous carbon dot solution (0.7 mg mL^{-1}) given orally to mice showed no adverse effect. Interestingly, while the urine of the mice showed excitation dependent fluorescence, a blood sample did not. After time, the fluorescence in the urine of the carbon dot fed mice disappeared suggesting renal clearance.[130]

To evaluate the toxicity of the carbon dots to cells an MTT assay was applied. This colorimetric assay indirectly provides a determination of the acute toxicity of a material of interest to a particular cell line.[179] After incubation of a compound within cells, a tetrazolium dye (3-(4,5-dimethylthiazol-2-yl)-2,5-diphenyltetrazolium bromide) is added. In healthy, metabolically active cells oxidoreductases reduce the tetrazolium to an insoluble formazan, producing purple crystals on the cell surface. The amount of formazan can be 'quantified' by solubilising the crystals and measuring the absorbance at 540 nm (in comparison to a control sample of healthy cells) thereby giving an indication of the number of viable cells.

Prostate cancer (PC3) cells were chosen as a robust cell line. These cells are easy to handle and culture and are widely used for cell toxicity and cell uptake studies. **CD-P1** to **CD-P5** were incubated with cells and the % viability of the cells after incubation determined. The PC3 cells were incubated with three different carbon dot solutions (2, 1 and 0.1 mg mL^{-1}) for 5 h after which, visualisation of the cells under a microscope showed high levels of formazan crystals. The crystals were solubilised and the absorbance of the solutions at 540 nm recorded.

CD-P1 did not show any cytotoxicity on PC3 cells up to 2 mg mL^{-1} (**Figure 63**). Similarly, **CD-P2**, **CD-P3** and **CD-P5** did not show notable cytotoxicity for all concentrations (cell viability > 90% when incubated with 2 mg mL^{-1}). While **CD-P4** did not show noticeable cytotoxicity at 0.1 and 1 mg mL^{-1}, there was minor cytotoxicity (70% cell viability) at 2 mg mL^{-1}. **CD-P4** did not disperse as well as the other carbon dots in the stock solution which could have led to the slight cytotoxicity observed at higher concentrations.

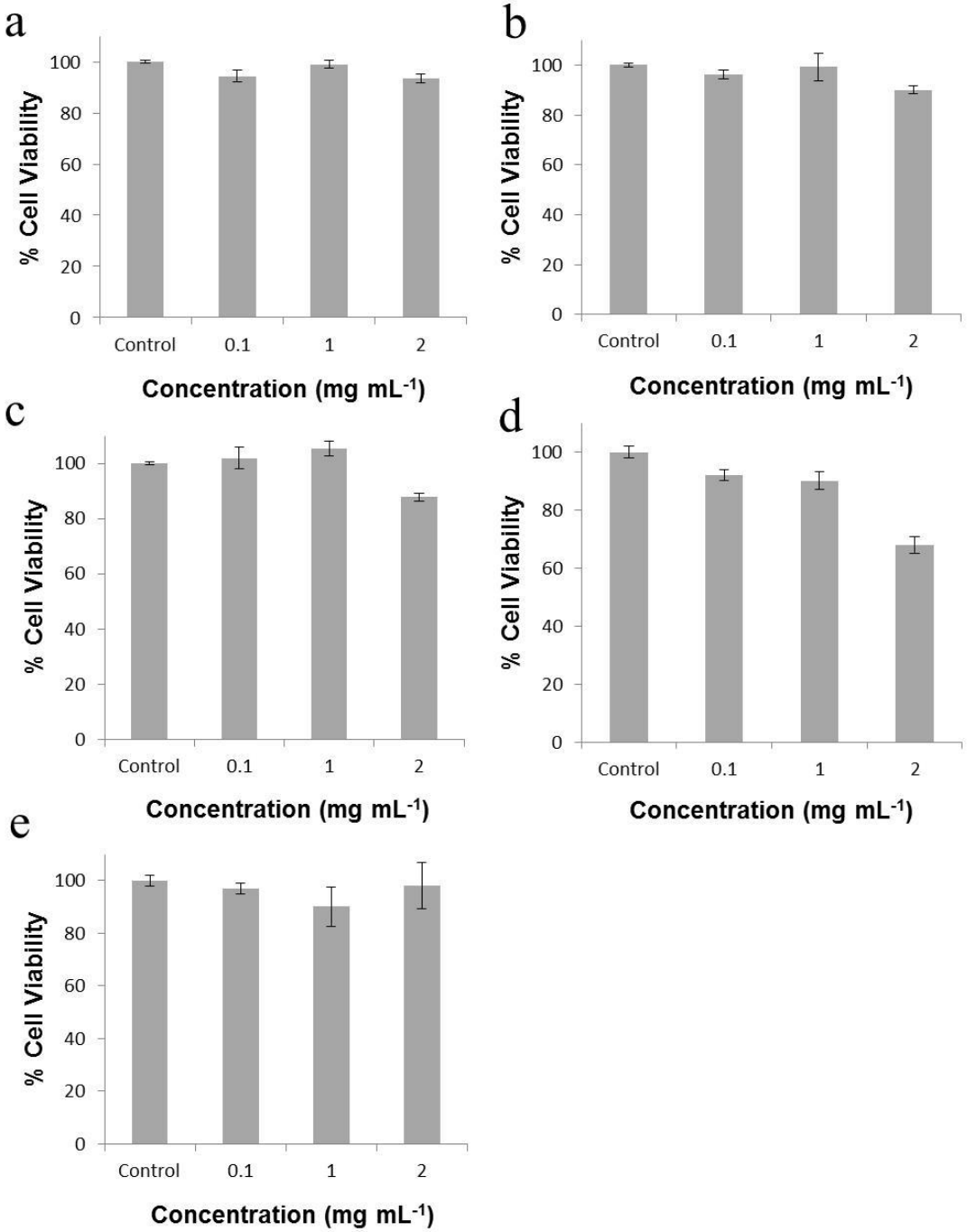

Figure 63: Cell viabilities after incubation of PC3 cells with three different concentrations of (a) **CD-P1**, (b) **CD-P2**, (c) **CD-P3**, (d) **CD-P4** and (e) **CD-P5**; (n = 5)

3.6.2 Cellular Uptake

Cellular uptake studies of the carbon dots were carried on PC3, breast cancer cells (MCF7) and macrophages (RAW). Cells were seeded at ~100,000 cells per well and cultured overnight. The media was changed and **CD-P1** was added at 1 mg mL^{-1}. After incubation for 5 hours, the cells were washed with PBS and imaged using fluorescent microscopy (λ_{ex} 340–395 nm, λ_{em} 430–505 nm). (**Figure 64**).

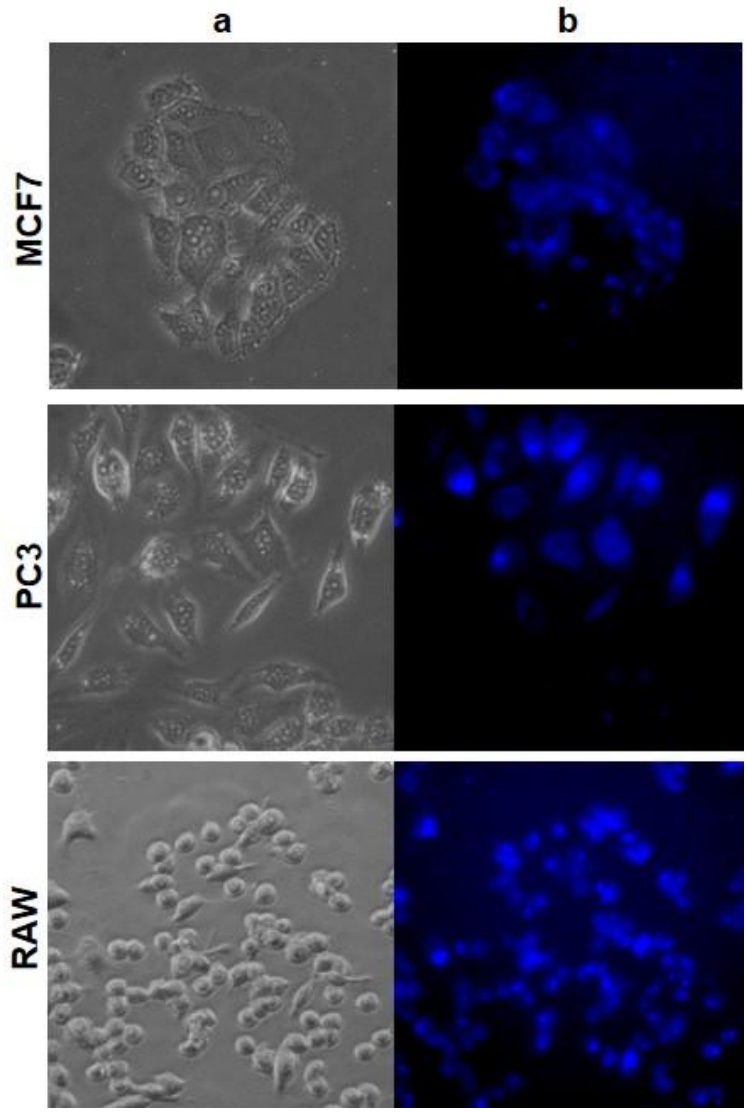

Figure 64: Fluorescence microscopy images of a 0.1% aqueous solution of **CD-P1** incubated with MCF7, PC3 and RAW cells (× 40 magnification) after 5 h incubation (a) bright field image (b) band-pass filter λ_{ex} 340–395 nm

Visualisation of the cells by semi-confocal microscopy clearly showed cellular uptake of the particles into the three different cell lines. These results were verified by flow cytometry. PC3 cells were incubated with **CD-P1** at 2, 1 and 0.1 mg mL^{-1}, and the cells cultured overnight. After washing and trypsination, uptake was evaluated by flow cytometry (λ_{ex} 355 nm and a 450–490 nm filter) and analysed using the FlowJo software (**Figure 65**).

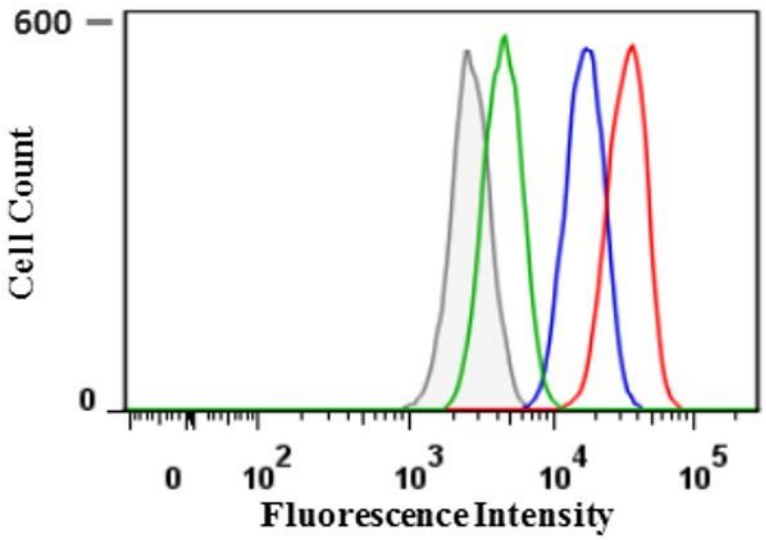

Figure 65: Flow cytometry analysis (λ_{ex} 355 nm) of PC3 cells incubated with **CD-P1** at 0.1 mg mL^{-1} (green), 1 mg mL^{-1} (blue) and 2 mg mL^{-1} (red). Untreated cells were used as a control (grey)

The cellular uptake of **CD-P1** was identified by an increase in fluorescence intensity following incubation with the carbon dots in a concentration dependent manner. On incubation with 1 mg mL^{-1} **CD-P1**, the whole population was **CD-P1** positive indicating take up of the carbon dots into 100% of the cells.

3.7 Conclusions

Five 1,4-addition polymers with varying heteroatoms were synthesised and characterised. These five polymers were pyrolysed directly to synthesise carbon dots in a robust and reproducible manner. Investigation of the structural properties showed them to be spherical and of the desired size (<10 nm). The optical properties of the carbon dots were dependent on the amount of nitrogen incorporated. **CD-P2** with no nitrogen containing monomers was poorly fluorescent whereas **CD-P1** and **CD-P5**, with the most nitrogen, displayed the highest fluorescent intensity. All carbon dots produced showed excitation dependent emission and the optical properties showed commonalities with carbon dots produced from other thermal methods. The reported up-conversion property of the carbon dots was investigated with **CD-P1** but experiments showed the suggested up-conversion phenomenon were in fact a result of second order light diffraction.

The herein synthesised carbon dots can be synthesised efficiently on an appreciable scale. The initial monomers are commercially available and inexpensive and no specialist equipment is required for the synthesis of the carbon dots. This method is reproducible and the route to the carbon dots and is robust and efficient. These particles are dispersible in water and stable over a physiological pH range, thus they can be applied to fluorescence imaging in cells. Amines from the polymers may be accessible on the surface of the carbon dot.

Chapter 4:

Biological Applications of Carbon Dots

4.1 Introduction and Aims

The non-cytotoxic nature, cell uptake properties and stability of carbon dots at a range of pHs make them candidates for biological imaging. Carbon dots have previously been conjugated to biomolecules, such as tumour targeting molecules and dyes.[180–182] The aim of the work in this chapter was to investigate conjugation of biomolecules to the carbon dots that had been prepared and to apply them in a number of cell targeting environments, namely to the nucleus and mitochondria. In addition an innovative tool for a protease assay using IR was explored.

The nucleus contains genetic material and is responsible for DNA synthesis.[183] It is separated from the other cell components by a nuclear envelope membrane. Transport across this double lipid bilayer is tightly regulated and certain molecules must pass through in order to maintain key cell processes.[184–186] Small molecules may enter the nucleus by diffusion through the nuclear pore complexes (NPCs)[187] whereas larger molecules such as proteins gain entry to the nucleus usually via recognition of a nuclear localisation sequence (NLS). The NLS is recognised by importin-α (Impα) and subsequently importin-β (Impβ) which together facilitate the transport of the cargo across the double membrane. The Ran protein regulates the direction of the transport by binding to GDP (within the cytoplasm) or GTP (within the nucleus) (**Figure 66**). A seven amino acid sequence (PKKKRKV) from the SV40 Large T-antigen was the first NLS discovered[188] and due to its widespread use in nuclear localisation of proteins and ease of synthesis, it was chosen to conjugate to carbon dots.

Imaging of the nucleus can be used to localise cells within tissues and can provide a way of following changes in the nucleus through processes such as mitosis. For live cell applications, it is important that anything used to identify the nucleus does not adversely affect cell function. Typically, the nucleus is stained with dyes or molecules which intercalate DNA, potentially disrupting normal processes within the nucleus.[189]

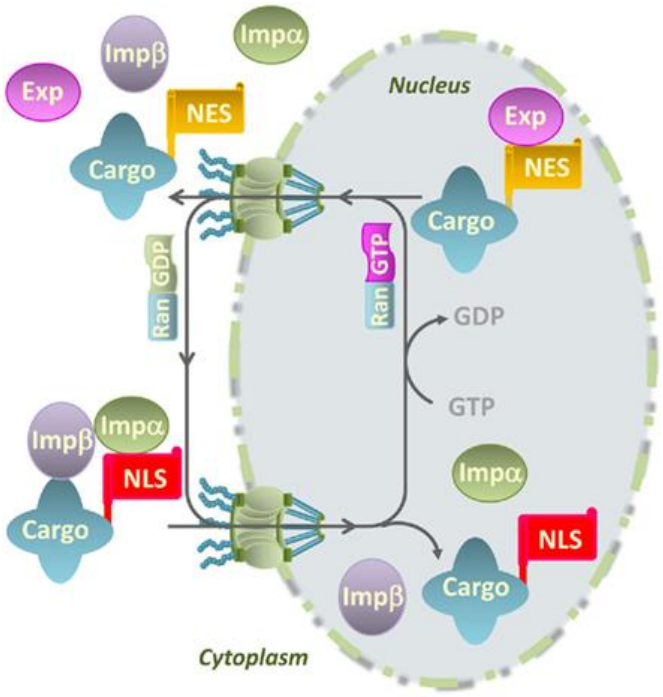

Figure 66: Cargoes can be transported into the nucleus by use of a nuclear localisation sequence (NLS) and its association with importin-α and importin-β. The complex is transported through nuclear porins which span the double lipid bilayer of the nucleus. Ras-related nuclear protein (Ran) dictates the directionality of the transport by binding with GDP in the cytoplasm for import or GTP in the nucleus for export of cargoes. Reprinted from Rivas and Genin, open access publication.[190] Copyright 2011 Rivas and Genin.

Mitochondria are the powerhouses of eukaryotic cells, producing energy through oxidative phosphorylation and lipid oxidation. Mitochondria have an outer membrane and highly folded inner membrane which increases the surface area on

which adenosine triphosphate (ATP, a cell's main energy source) can be synthesised.[191] The function of the mitochondria is not limited to energy production; control of the cell metabolism by calcium storage and signalling[192] and regulation of reactive oxygen species[193] are also roles played by these subcellular organelles (**Figure 67**). The number of mitochondria within a cell depends widely on the type of tissue and the organism itself. Unicellular organisms often contain a single mitochondrion[194] whereas there can be 1000–2000 mitochondria per human liver cell.[195]

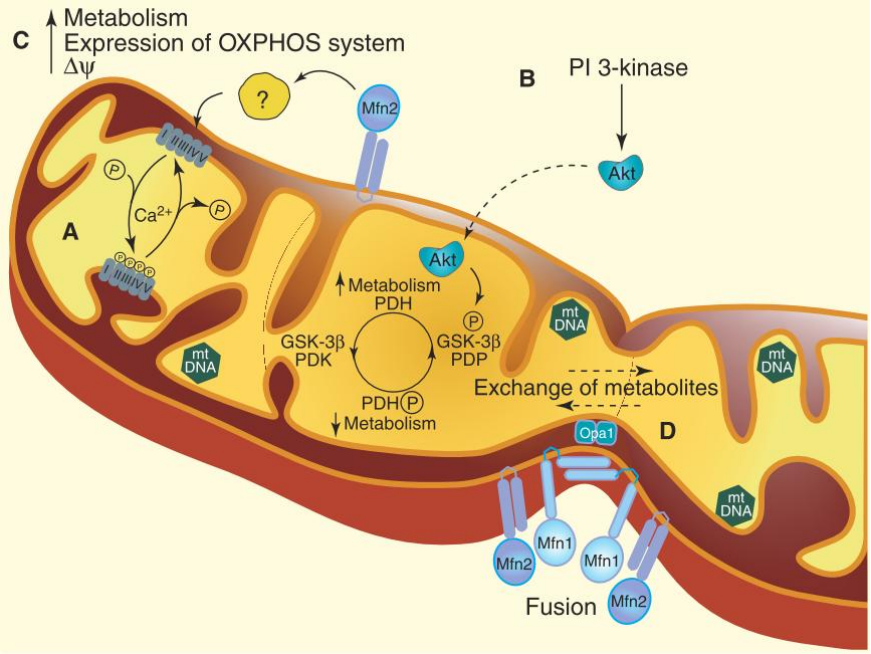

Figure 67: Regulation of key cell processes are carried out by mitochondria; (A) calcium-mediated signaling control the phosphorylation and dephosphorylation of enzymes; (B) Energy metabolism within the mitochondria occurs on the highly folded inner membrane; (C) Unknown signaling partners regulate electrochemical potential and expression of respiratory complexes; (D) membrane fusion proteins facilitate the propagation of metabolites, e.g. calcium, reactive oxygen species and mitochondrial DNA. Reprinted with permission from McBride.[196] Copyright 2006 Elsevier Ltd.

Mitochondria possess their own independent genome, different from that of the nucleus of the cell in which resides maternal mitochondrial DNA. Mutations in this DNA or defects in enzymes which control mitochondrial DNA replication can lead

to a number of mitochondrial-based diseases, e.g. mitochondrial myopathy, Leigh syndrome.[197] The UK government legalised controversial treatment of mitochondrial disease in 2015 whereby a healthy donor egg is used to host nuclear DNA from a patient with a mitochondrial disease.[198] Currently, imaging of mitochondria is based on small molecule fluorescent probes, e.g. Mitotracker® (**Figure 68**) and although live cell staining is efficient, the probes are not well retained in fixed cells.[199]

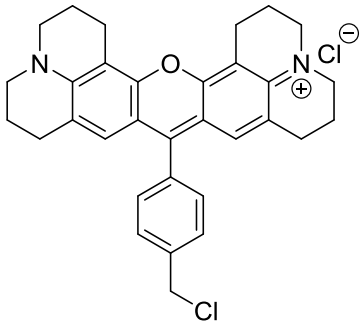

Figure 68: Mitotracker® Red Chloromethyl X Rosamine (λ_{ex} 578, λ_{em} 598 in MeOH)

Currently, optical imaging of live cells relies heavily on the fluorescence output of traditional small molecule fluorophores. Many of these organic molecules are cytotoxic, have low solubility in water and may aggregate within cells thereby causing self-quenching (attributable to the π-stacking of aromatic fluorophores which significantly decreases their fluorescence output). Fluorophores may also interact with the components within cells making them difficult to detect amid the autofluorescence of cell components or the tissue. Photobleaching of fluorophores also remains an issue for some fluorophores.[200] Carbon dots, which overcome some of these limitations provide an attractive alternative to small molecule fluorophores and their use *in vitro* and *in vivo* has been reported.[201] The aim of the work in this chapter was to ascertain whether **CD-P1** was suitable for conjugation to nuclei and mitochondrial targeting molecules. Another aim was to use **CD-P1** in conjunction with a peptide with the carbon dot quenching an 'IR-dye'.

4.2 Conjugation Studies

The XPS of **CD-P1** indicated amino groups were present on the surface of the carbon dots. This surface functionalisation allows easy conjugation to molecules with free carboxylic acid groups via amide bond formation. The carboxylic acid group of methyl red thus allows conjugation to **CD-P1** through an amide bond. A large excess of methyl red was dissolved in DMF and Oxyma/DIC used to activate the carboxylic acid. The solution was then added to a suspension of **CD-P1** and stirred for 1 h. Excess methyl red and other reagents were removed by dialysis in MeOH and H_2O before the solvent was removed to give the methyl red-carbon dot conjugate. To ascertain whether or not the coupling had been successful, the fluorescence spectra of a 0.1 mg mL^{-1} aqueous solution of conjugated and unconjugated **CD-P1** were measured (**Figure 69**). On excitation at 360 nm, **CD-P1** conjugated to methyl red showed a 45-fold reduction in fluorescence compared to the unconjugated carbon dots. The fluorescence spectra of the conjugated carbon dots showed the same excitation dependent emission as the unconjugated dots with the reduction in fluorescence intensity showing effective quenching of the carbon dot.

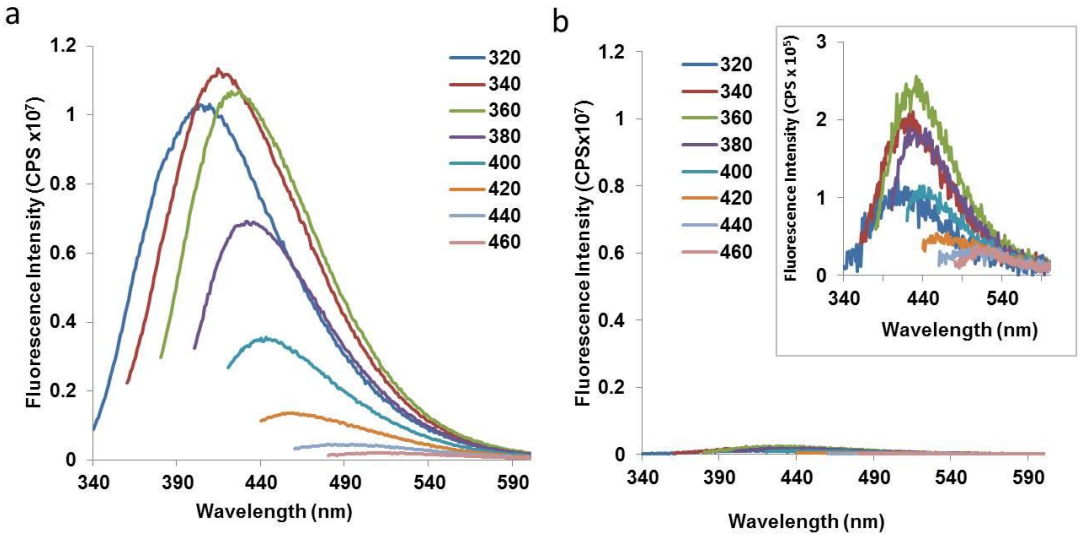

Figure 69: Fluorescence spectra of (a) unconjugated **CD-P1** (b) **CD-P1** conjugated with methyl red, (inset) emission spectra of **CD-P1** conjugated with methyl red shown on a different scale (max = 3 x 10^5 CPS) showing excitation wavelength dependent emission; excitation between 320–460 nm in 20 nm increments; concentration 0.1 mg mL^{-1}.

4.3 Targeting the Cell Nucleus

To verify whether carbon dots could successfully be transported through the nuclear membrane, a carbon dot-peptide conjugate probe based on the known NLS (PKKKRKV) was designed (**Figure 70**).

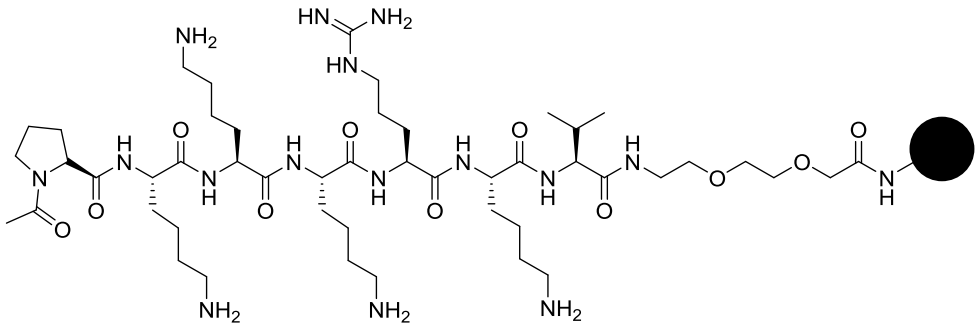

Figure 70: Structure of **CD-P1–NLS** conjugate (Ac-PKKKRKV-CD-P1)

The NLS with a PEG spacer was synthesised on 2-chlorotrityl polystyrene resin (1.0 mmol g^{-1}, 100-200 mesh with the PEG spacer (Fmoc-PEG-OH) attached as the first residue. The linker was activated with $SOCl_2$ and the Fmoc-PEG-OH spacer coupled using DIPEA under dry conditions. Any remaining free sites were capped using MeOH. The spacer increased the distance between the carbon dot and the NLS in order to make the sequence more accessible. The amine group of 2-(aminoethoxy)ethanol was protected with benzyl bromide followed by *O*-alkylation with bromoacetic acid and excess NaH to introduce the acid moiety in moderate yields. Debenzylation of the amine by hydrogenation using a Pd/C catalyst yielded the free amine in high yield which was Fmoc protected to make the spacer compatible with standard solid phase synthesis (**Figure 71**).

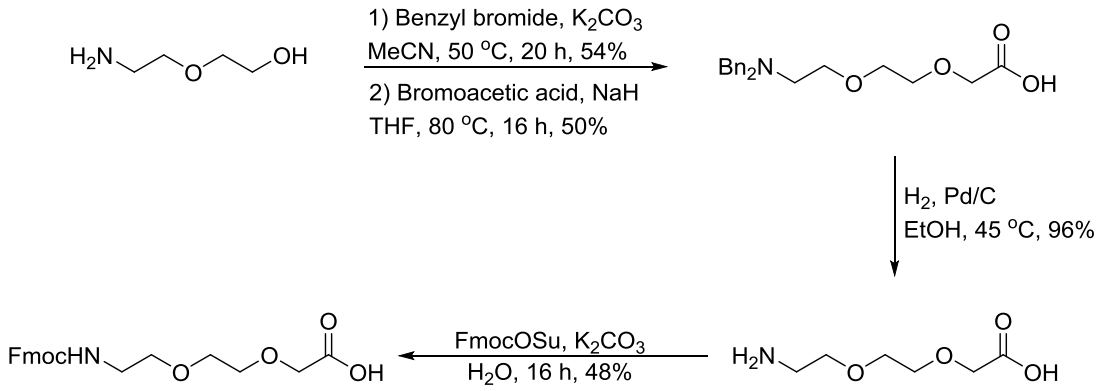

Figure 71: PEG linker synthesis from 2-(aminoethoxy)ethanol

The Fmoc group was removed using 20% piperidine in DMF and confirmation of the removal was given by the Ninhydrin test. Subsequent Fmoc protected amino acids (with orthogonally protected side chains) were coupled using Oxyma and DIC with confirmation of their coupling given by the Ninhydrin or Chloranil tests. The peptide was cleaved from the resin using dilute acid (1% TFA in DCM) and precipitated from water to give the protected peptide (**Figure 72**). The peptide was analysed by MALDI-TOF mass spectrometry and the purity assessed by HPLC (>99% pure). The chlorotrityl linker allows the peptide to be cleaved from the resin with side chain protecting groups intact, thus leaving the free acid for future conjugation.

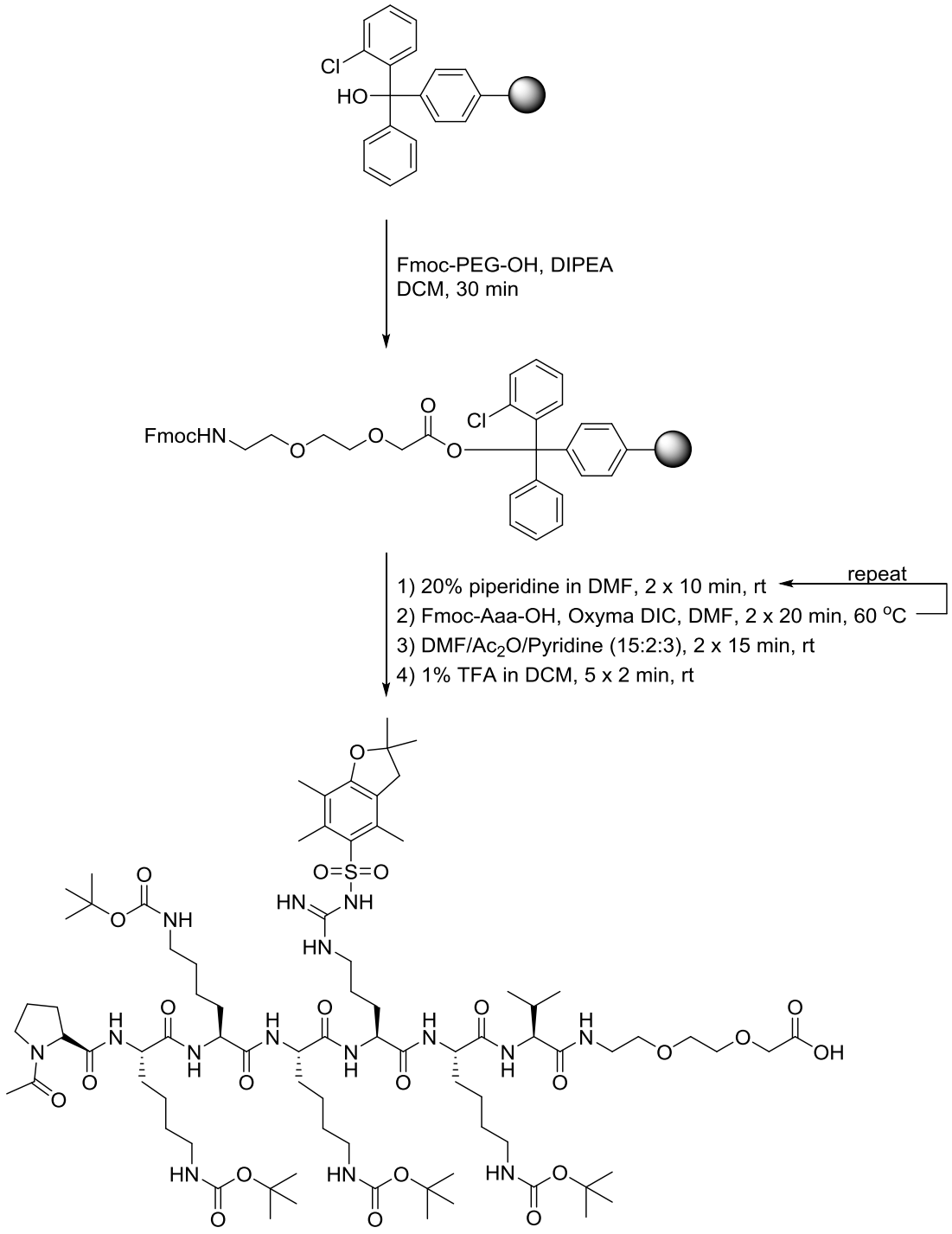

Figure 72: Solid phase strategy for the synthesis of the protected NLS peptide on 2-chlorotrityl chloride polystyrene resin.

The stability of the carbon dots to acidic conditions was investigated. No noticeable loss of fluorescence was seen when **CD-P1** was dispersed in neat TFA. On excitation at 360 nm, the carbon dots showed fluorescence intensities within the same order of magnitude with the difference attributed to minor variations in the exact concentrations of the solutions (**Figure 73**). The TFA was removed by evaporation and the carbon dots suspended in water. The fluorescence spectrum showed that there was no loss of fluorescence and confirmed that **CD-P1** was compatible with the acidic conditions that would be used in the cleavage of the side chain protecting groups.

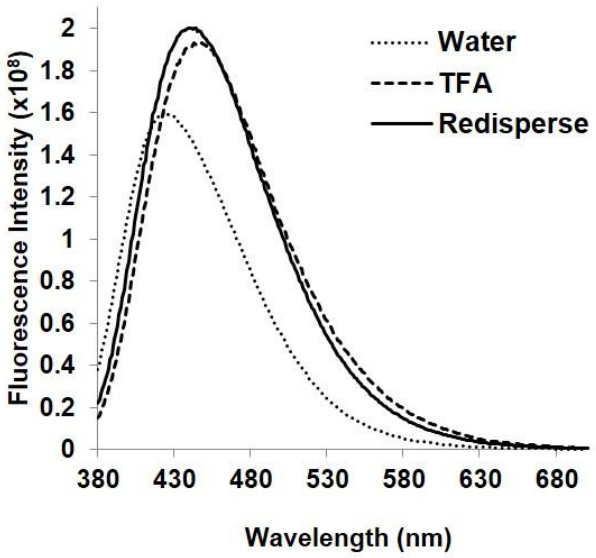

Figure 73: Fluorescence spectra of **CD-P1** (1 mg mL^{-1}) in water (dotted line) and TFA (dashed line) show no loss of fluorescence on addition of neat TFA. Further dispersal of **CD-P1** in water after evaporation of TFA (solid line) shows fluorescence in maintained (λ_{ex} 360 nm).

The protected NLS peptide was coupled to **CD-P1** using Oxyma/DIC in DMF. Although more volatile solvents such as DCM, THF or dioxane would have been easier to remove after the coupling, **CD-P1** does not easily disperse in these solvents and are thus unsuitable for solution phase couplings. DMF was chosen, therefore, as

both the carbon dots and the peptide are soluble in this solvent. **CD-P1** and the activated peptide were reacted for 1 h at room temperature after which the solvent was removed *in vacuo*. The residue was treated with TFA-TIS-H_2O (95:2.5:2.5) for 3 h to remove the side chain protecting groups. After removal of the solution *in vacuo*, the carbon dot conjugates were dispersed in water, dialysed against a large volume of water and dried to give the carbon dot-NLS conjugate (**CD-P1-NLS**) (31 mg). Based on the increase in mass after addition of the NLS sequence, the **CD-P1** were estimated to have an amine loading of 1.96 mmol g^{-1}.

To test the ability of **CD-P1-NLS** to target the nucleus, PC3 cells were treated with the probe. PC3 cells were chosen as a robust cell line and it was previously shown that these cells take up **CD-P1**. SYTO17, a red nucleic acid dye was chosen as a counterstain for the blue fluorescent carbon dots. **CD-P1-NLS** (1 mg mL^{-1}) were incubated with PC3 cells for 5 h before fixation and staining with SYTO17 for a further 2 h. The cells were washed and imaged by confocal microscopy (**Figure 74**).

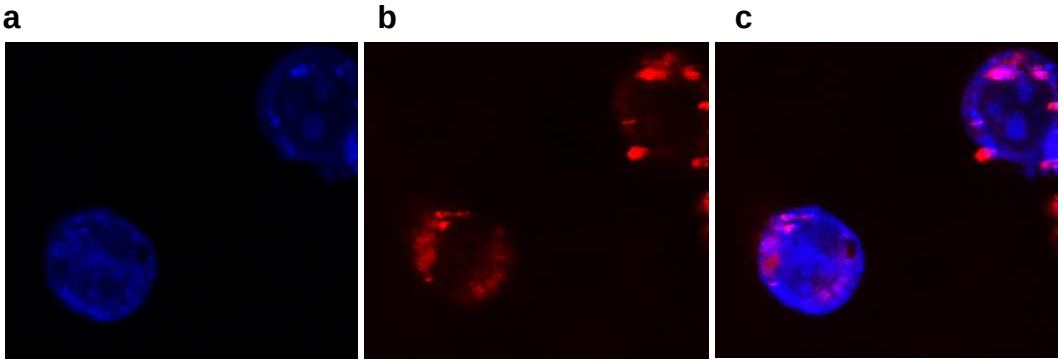

Figure 74: Confocal microscopy images of (a) **CD-P1-NLS** in the nucleus of PC3 cells (b) SYTO17 counterstain inside the nucleus of PC3 cells, (c) merged image of **CD-P1-NLS** and SYTO17. The structure of SYTO17 had not been disclosed at time of writing.

Confocal microscopy of **CD-P1-NLS** inside PC3 cells showed localisation in the nucleus. The fluorescent area was consistent with the expected diameter of the cell nucleus. Previous uptake experiments showed little uptake of **CD-P1** within the nucleus (see Chapter 3.6.2). The red fluorescent SYTO17 stain was shown to localise in the nucleus and the merged image confirmed colocalisation with **CD-P1-NLS**.

4.4 Mitochondrial Labelling

Lipophilic cations, such as triphenylphosphonium ions, have been widely used to target mitochondria.[202,203] Their uptake across the mitochondrial membrane is enhanced by the membrane potential with a predicted ~10 fold increase in uptake for every ~60 mV increase in the potential.[204] Due to its extensive use and the relative ease of conjugation, a triphenylphosphonium-based carbon dot conjugate was designed (**Figure 75**).

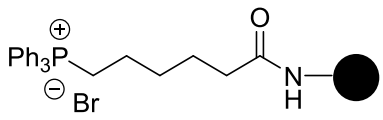

CD-P1-MITO

Figure 75: Structure of the CD-P1-MITO conjugate

5-Carboxypentyltriphosphonium bromide was prepared from 6-bromohexanoic acid and triphenylphosphine in quantitative yield and subsequently converted to an NHS-ester by addition of a solution of *N*-hydroxysuccinimide and DIC in DCM. The synthesis of the isolable active ester was followed by conjugation to **CD-P1** without the need for additional coupling reagents. Coupling of the cation to **CD-P1** (11 mg) was achieved in DMF with the use of DIPEA and stirring for 1 h at room temperature to afford the mitochondria targeting conjugate (**CD-P1-MITO**) (22 mg) (**Figure 76**). The theoretical loading based on the mass increase was 2.4 mmol/g.

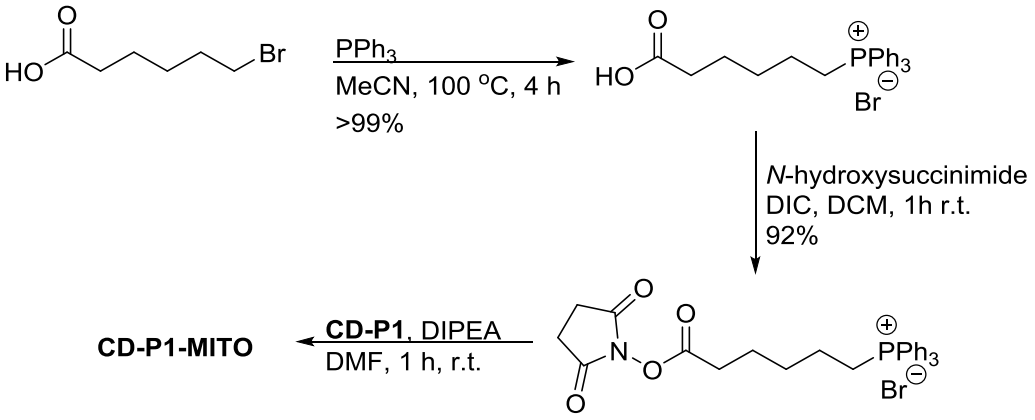

Figure 76: CD-P1-MITO synthesis from 6-bromohexanoic acid.

PC3 cells were treated with **CD-P1-MITO** at a concentration of 1 mg mL^{-1} and incubated for 5 hours. The cells were stained with Mitotracker Red to give a contrast to the blue fluorescent carbon dots before fixation. The cells were washed and imaged by confocal microscopy (**Figure 77**).

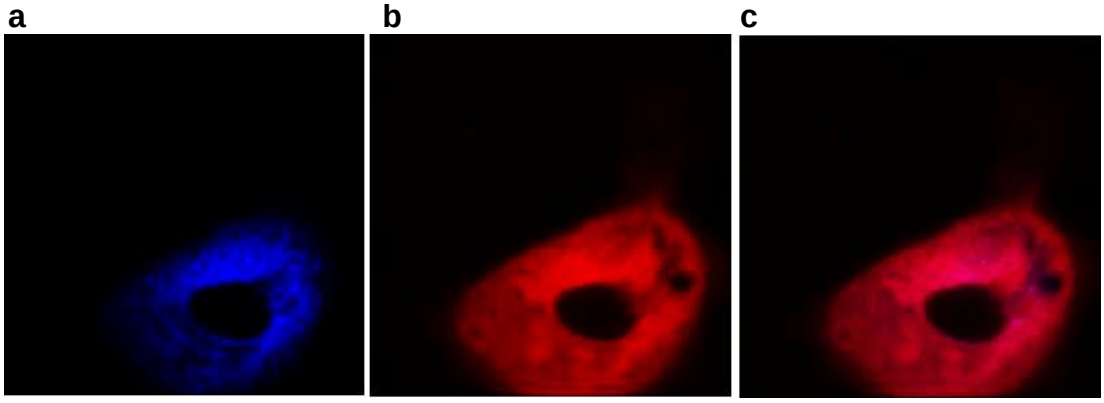

Figure 77: Confocal microscopy images of (a) **CD-P1-MITO** in PC3 cells (b) Mitotracker counterstain inside PC3 cells, (c) merged image of **CD-P1-MITO** and Mitotracker Red.

The diffuse staining of the Mitotracker counterstain made identification of the mitochondria difficult, however there was no fluorescence signal from either **CD-P1-MITO** or Mitotracker in the nucleus. The **CD-P1-MITO** signal was less intense

around the cell membrane and images of **CD-P1-MITO** showed more punctate staining often associated with mitochondrial localisation.

4.5 Peptide Conjugates

The ability to conjugate targeting moieties to the amine functionalised **CD-P1** and the uptake properties of the carbon dots presents a useful strategy for peptide based probes. In an extension of the conjugation studies of methyl red to the carbon dots, a short peptide sequence (AAPV) known to be cleaved by Human Neutrophil Elastase (HNE) was introduced.[205] HNE is a serine protease with broad specificity which is released by neutrophils predominantly during immune defence responses. Methyl red effectively quenches the fluorescence of **CD-P1** when in close proximity. On introduction of HNE it was expected that cleavage of the short peptide would result in an increase in the fluorescence intensity of the carbon dots (**Figure 78**).

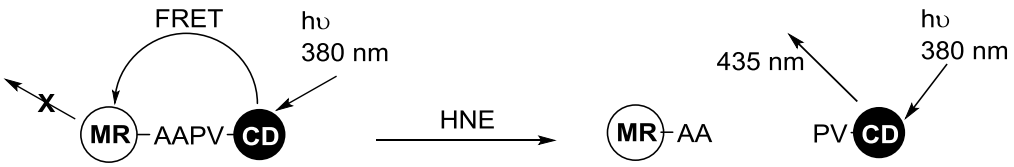

Figure 78: Principle of the carbon dot (CD)/HNE sequence (AAPV)/Methyl Red (MR) FRET system showing the quenching of the fluorescence of the carbon dot when excited at 380 nm and emission at 435nm on cleavage of the peptide sequence by HNE.

The peptide was synthesised by solid phase synthesis using polystyrene resin functionalised with a 2-chlorotrityl chloride linker, thus ensuring the peptide sequence had a carboxylic acid group at the C-terminus. As before, after activation and coupling of the spacer (DIPEA, dry DCM), coupling of each Fmoc protected amino acid was achieved using Oxyma/DIC as the coupling reagents and a solution of 20% piperidine in DMF was used for Fmoc deprotection. After coupling of the

four amino acids, 2-(*N*,*N*-dimethyl-4-aminophenyl)azobenzenecarboxylic acid (methyl red) was coupled using Oxyma/DIC. The peptide was cleaved from the resin (1% TFA in DCM) and precipitated as a dark purple solid without the need for further purification. The peptide was analysed by mass spectrometry and HPLC. The peptide was conjugated to **CD-P1** using Oxyma/DIC in DMF and stirring for 1 h at room temperature before dialysis against water to yield the product **MR-AAPV-CD-P1** (**Figure 79**).

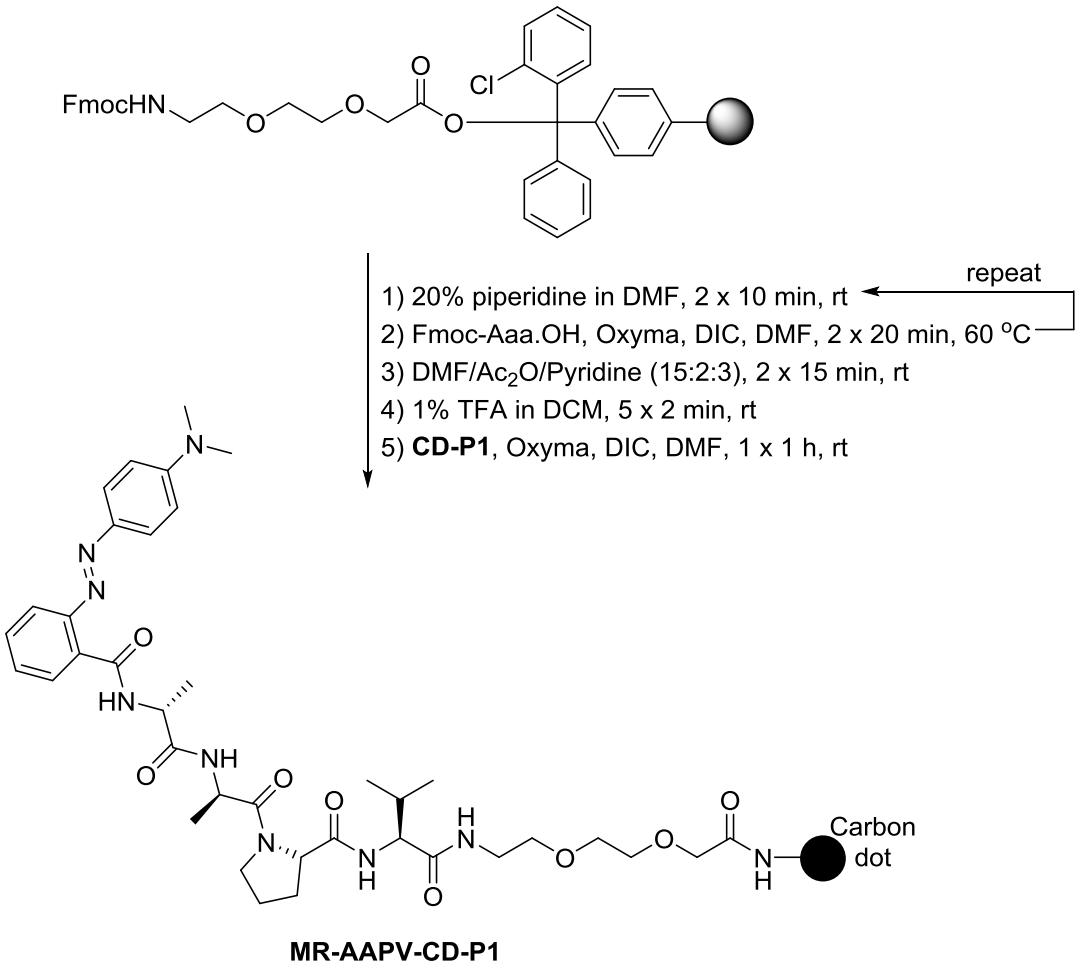

Figure 79: Solid phase strategy for synthesis of AAPV peptide on 2-chlorotrityl polystyrene resin.

The emission spectra of **MR-AAPV-CD-P1** was recorded and the fluorescence emission intensity when excited at 360 nm was significantly less than unconjugated **CD-P1** (~10 fold). On addition of HNE, however, the cleavage of the peptide sequence resulted in an increase in fluorescence intensity from the carbon dot due to removal of the quenching by methyl red (**Figure 80**).

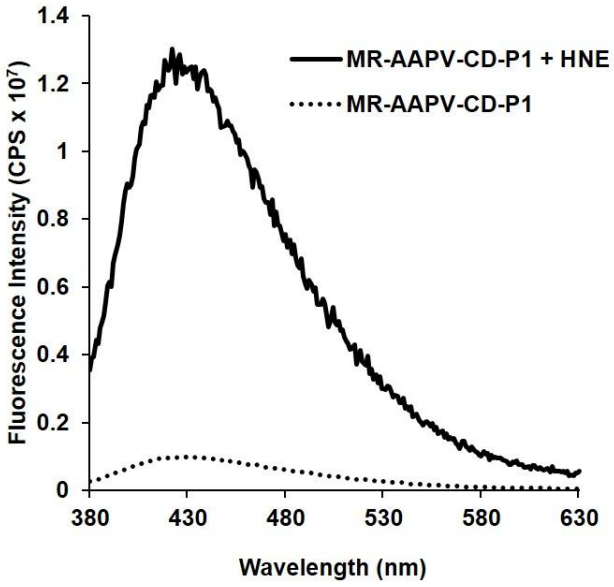

Figure 80: Fluorescence spectra of **MR-AAPV-PEG-CD-P1** (0.1 mg mL^{-1}) (dashed line) in buffer and after the addition of HNE (solid line) shows an increase (~10 fold) in fluorescence intensity (λ_{ex} 360 nm).

The carbon dots were envisaged as being broad resorbers and so could be used to quench IR signals. By coupling the alkyne, propiolic acid, instead of methyl red, the probe would contain an IR signature and it was hoped that the IR signal associated with the alkyne would be quenched and subsequently restored on addition of HNE. The peptide was synthesised in the same manner as **MR-AAPV-PEG-OH** on polystyrene resin with a 2-chlorotrityl chloride linker. After coupling of the PEG spacer and four amino acids, the alkyne, propiolic acid was coupled using Oxyma/DIC. The peptide was cleaved from the resin (1% TFA in DCM) and precipitated as an off white solid without the need for further purification. The

peptide was analysed by mass spectrometry and HPLC (>99% pure). The peptide was conjugated to **CD-P1** using Oxyma/DIC in DMF and stirring for 1 h at room temperature before dialysis against water to yield the product **Alkyne-AAPV-CD-P1** (**Figure 81**).

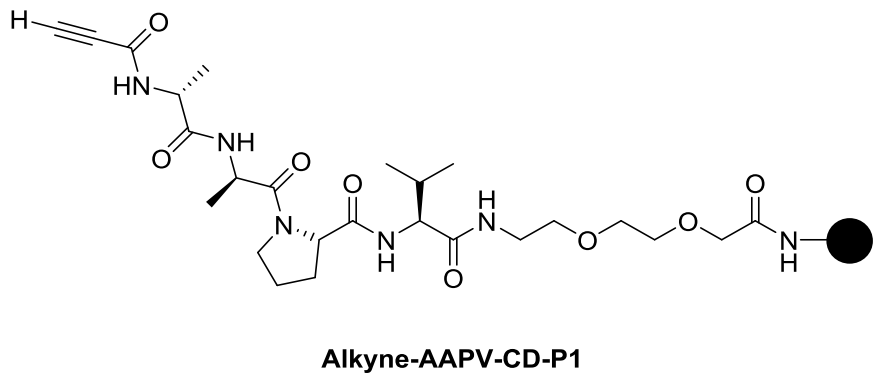

Alkyne-AAPV-CD-P1

Figure 81: Structure of the AAPV-carbon dot conjugate with propiolic acid (alkyne) at the N-terminus.

The successful coupling of the alkyne-functionalised peptide to **CD-P1** was confirmed by the increase in mass after dialysis. The peak attributed to the triple bond stretch of the alkyne (2152 cm^{-1}, see **Figure 82**) did not appear in the IR spectrum of the **Alkyne-AAPV-CD-P1** (see **Figure 83**).

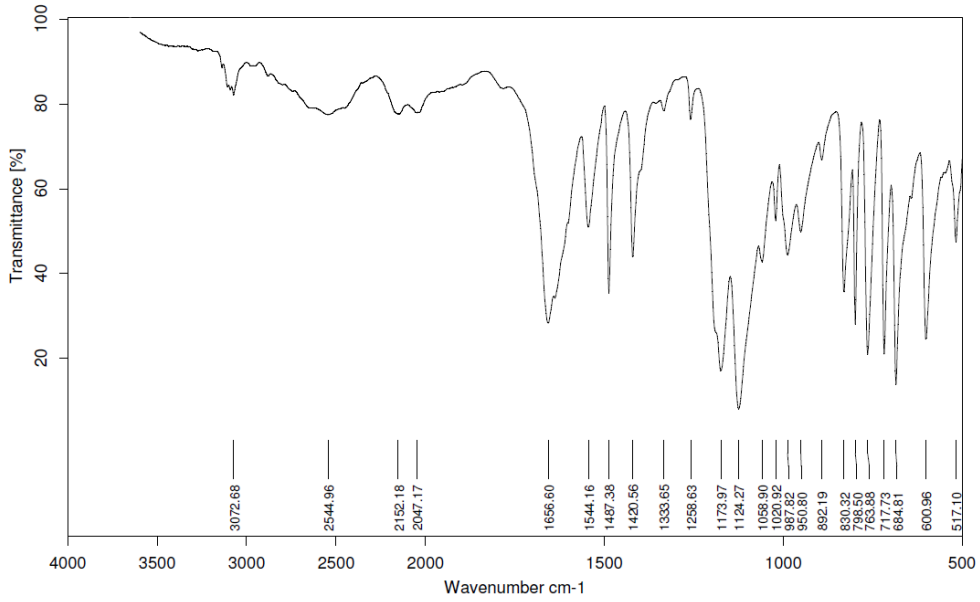

Figure 82: IR spectrum of **Alkyne-AAPV-PEG-OH** showing a C≡C stretch at 2152/2047 cm^{-1} and characteristic amine peak at 1657 cm^{-1}

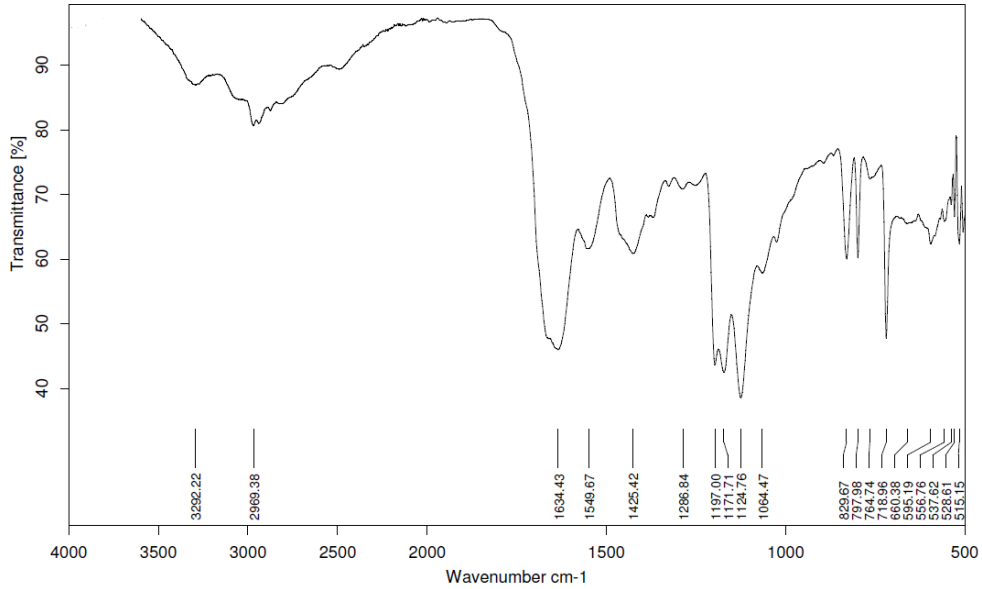

Figure 83: IR spectrum of **Alkyne-AAPV-PEG-CD-P1** showing an absence of the C≡C stretch around 2100 cm^{-1} and characteristic amine peak at 1634 cm^{-1}

The close proximity of the IR absorbing carbon dot was able to quench the IR signal from the alkyne. On subsequent addition of HNE, a weak signal attributed to the alkyne was visible at 2128 cm^{-1} (see **Figure 84**) confirming cleavage of the probe.

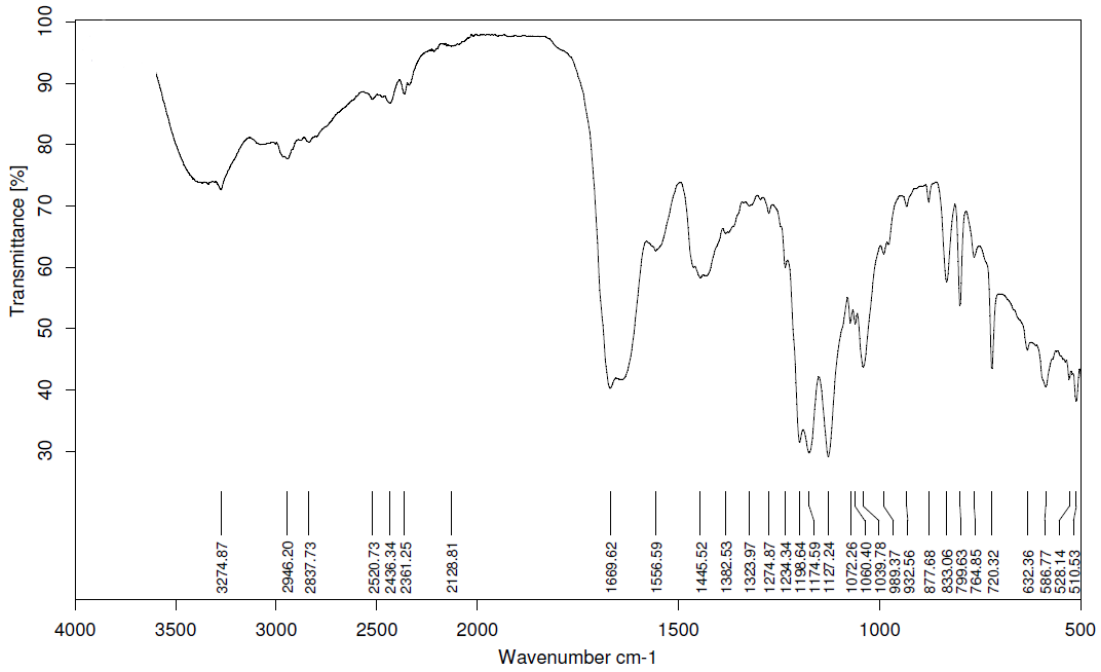

Figure 84: IR spectrum of **Alkyne-AAPV-PEG-CD-P1** after cleavage by HNE showing a C≡C stretch at 2128 cm^{-1}

4.6 Conclusions

The ability to use the amino groups of **CD-P1** to conjugate these nanoparticles to biologically relevant molecules presents a valuable starting point in the application of these carbon dots to real biological situations. In addition to the amino functionality which provides a convenient conjugation site, their stability in acidic conditions allows conjugation to peptides before deprotection of the side chain protecting groups. **CD-P1** were investigated in FRET systems with methyl red used as the quencher. The emission of **CD-P1** was shown to be reduced on conjugation to methyl red, demonstrating not only that conjugation to these nanoparticles was

achievable, but also that their fluorescence could be quenched. Exploiting their cell entry capabilities, **CD-P1** were conjugated to an NLS and shown to localise inside the nucleus of PC3 cells. Conjugation with a mitochondria targeting molecule also showed carbon dots accumulated within cells.

Coupling of a small peptide known to be cleaved by human neutrophil elastase (HNE) was confirmed by two approaches; IR and a conventional FRET system. **CD-P1** were investigated as broad resorbers coupling to the small peptide (**Alkyne-AAPV-PEG-OH**). The absence of the expected alkyne peak in the IR spectrum of the conjugate indicated that the IR signal of the alkyne was quenched by the carbon dot. On cleavage with HNE the alkyne peak reappeared. A similar system using the quencher, methyl red, showed an increase in fluorescence intensity of the carbon dots on treatment of the methyl red conjugate, **MR-AAPV-PEG-CD-P1** with HNE. These systems show that these carbon dots are able to quench and be quenched and hence may offer applications in the optical imaging arena.

Chapter 5:

Conclusion and Future Work

The thermal synthesis of carbon dots from 1,4-addition polymers resulted in fluorescent nanoparticles of the desired shape and size (<10 nm) by TEM which was scalable (from 10 mg to 100 mg of carbon dots). The optical properties of these carbon nanoparticles compared favourably with literature carbon dot syntheses with a maximum emission of 450 nm when excited at 380 nm. The carbon dots showed excitation wavelength dependence and increasing nitrogen content correlated well with the fluorescence intensity of the carbon dots. The optimal carbon dots were non-cytotoxic, while the quantum yield of the most fluorescent carbon dot sample (**CD-P1**) was 26% and **CD-P1** was chosen to be taken forward for cell experiments. They were readily taken up by PC3, MCF7 and RAW cells with results verified by flow cytometry with **CD-P1** in PC3 cells – a 100% population shift was recorded.

The up-conversion properties of **CD-P1** were tested. At first, the carbon dots appeared to up-convert light of shorter wavelengths with emission in the visible region. When a long-pass filter was used, however, there was no emission in the visible region as would have been expected with two-photon excitation. The coexistence of second order diffraction light was assumed to be responsible for the emission. The scepticism around up-conversion of carbon nanoparticles requires further research.

The biocompatibility of **CD-P1** was also evaluated. It was shown that **CD-P1** could be conjugated to biologically relevant molecules via amide bonds with the amine groups on the surface of the dots (calculated loading ~2 mmol g^{-1} based on the mass increase of **CD-P1-NLS** and **CD-P1-MITO**). Methyl red was conjugated to the carbon dots and shown to reduce the fluorescence intensity of **CD-P1**. Conjugates based on a nuclear localisation sequence and a mitochondrial targeting molecule

were synthesised and shown to target their respective cell organelles. Two further probes based on the short peptide sequence, AAPV, known to be cleaved by Human Neutrophil Elastase, were also synthesised. On cleavage of the probes by HNE, the fluorescence intensity of a methyl red quenched probe increased and an alkyne signal was visible in an IR based probe indicating that these carbon dots have use as both quenchers and as fluorescent IR probes. The next logical step is to use these HNE probes inside cells and to use the carbon dots as an indicator of the level of HNE within activated neutrophils.

Although only in its infancy, the research into carbon dots has expanded rapidly over the last ten years. The work contained in this thesis is a useful addition to the field, particularly with respect to the area of carbon dots as alternatives to traditional small molecules fluorophores.

Chapter 6:

Experimental section

General information

Solvents and reagents were obtained from commercial suppliers and used as received. Reactions involving moisture sensitive reagents were performed under a positive pressure of nitrogen, and the glassware used was oven dried and cooled under nitrogen prior to the experiment. Reactions involving light sensitive compounds were kept under aluminium foil at all times. Evaporation of solvents was performed at reduced pressure, using a Büchi rotary evaporator.

Microwave assisted heating reactions were performed in sealed heavy-walled Pyrex tubes using a Biotage Initiatior Microwave. Microwave irradiation was conducted at 2.45 Hz for a fixed temperature and pressure unless otherwise specified.

Thin layer chromatography was carried out on aluminium sheets precoated with silica gel 60 F254 with visualisation at 254 nm/345 nm and/or stained with ninhydrin (0.3% ninhydrin in n-butanol and 3% acetic acid). **Column chromatography** was performed in glass columns using silica gel 60 (mesh 0.040–0.063).

Solid-phase synthesis was carried out using polypropylene Isolute filtration reservoirs as the reaction vessel, equipped with polyethylene frits (Argonaut Technologies Inc.). Amino acids were Fmoc protected at the *N*-terminus, with suitable acid labile protecting groups on the side chains.

^{1}H and ^{13}C nuclear magnetic resonance spectra were recorded on automated Bruker instruments: AV500 (500 and 125 MHz respectively). Chemical shifts (δ_H and δ_C) are quoted in parts per million (ppm) relative to the residual solvent signal with all coupling constants (*J*) given in Hertz (Hz). Resonances were characterised as singlet (s), doublet (d), triplet (t) or multiplet (m).

Electrospray ionization mass spectrometry (ESI–MS) analyses were acquired on a VG platform single Quadrupole MS-electrospray ionization $(ES)^+$ or $(ES)^-$ mode.

Analytical HPLC spectra were obtained using an Agilent 1100 series system coupled to a Polymer Lab 100 ES Evaporative Scattering Detector (ELSD) and UV detector with detection at 220, 254, 260, 282 and 495 nm. A Supelco Discovery ® C18, 5 µm, 5 cm column was used with two HPLC grade eluents:

Eluent A: MeCN + 0.1% formic acid, Eluent B: H_2O + 0.1% formic acid

Method 1: 5% to 95% A over 3 min; isocratic 95% over 1 min

Method 2: 5% to 95% A over 6 min; isocratic 95% over 3 min

Matrix assisted laser desorption ionisation-time of flight (MALDI-TOF) mass spectrometry was carried out using an Applied Biosystems Voyager-DE™ STR and analysed with the Voyager Instrument Control Panel software. Sinapic acid was used as a matrix (10 mg/mL) in 50% MeCN in water with 0.1% TFA.

Dynamic Light Scattering (DLS) was performed using a Malvern Instruments Zetasizer, Nanoseries. 1 µL of carbon nanoparticles suspended in water was mixed with 1 mL water (refractive index = 1.330; viscosity = 0.886), sonicated for 5 min and transferred to a disposable 1 cm plastic sizing cuvette. Three repeat measurements were taken at 25 °C with sonication of the sample for 1 min between measurements.

X-ray photoelectron spectra (XPS) were obtained at the National EPSRC XPS User's Service (NEXUS) at Newcastle University, an EPSRC Mid-Range Facility.

Cell experiments were carried out in a HERAsafe KS 18 class II negative-flow cabinet from Heraeus. Cell cultures were performed in a HERAcell 150 incubator from Heraeus at 37 °C with 5% CO_2. Cellular experiments were carried out with cells passaged between 4- and 20-times.

Fourier transform infrared (IR) spectra were recorded on a Bruker Tensor 27 with a golden gate accessory for solid samples.

Chapter 2 Synthesis

Carbon dots from glycerol, citric acid and PEG_{1500} (thermal)[140]

Glycerol (3 mL, 41 mmol) and PEG_{1500} (0.2 g, 0.13 mmol) were sealed in a 5 mL glass microwave vial and heated to 270 °C on a hotplate with stirring. When the solution reached 270 °C the vial was unsealed, citric acid (0.2 g, 1.0 mmol) was added quickly and the vial resealed. The reaction continued for a further 3 h at 270 °C with stirring before cooling to room temperature. The light brown solution was dialysed (Sigma-Aldrich cellulose membrane dialysis tube, MWCO = 14,000) against deionised water (3 × 1 h), before evaporation of the solvent and redispersal in water. The product was analysed by fluorescence spectroscopy (Edinburgh Instruments), TEM (Philips / FEI CM120 Biotwin transmission electron microscope operating at 100 kV) and DLS (Zetasizer Nanoseries).

Carbon dots from glycerol, citric acid and PEG_{1500} (microwave)

PEG_{1500} (0.2 g, 0.13 mmol) was dissolved in glycerol (3 mL, 41 mmol) in a 5 mL glass microwave vial and citric acid (0.2 g, 1.0 mmol) added. The mixture was microwave irradiated at 250 °C for 3 × 1 h to afford a straw coloured viscous liquid. The solution was dialysed (Sigma-Aldrich cellulose membrane dialysis tube, MWCO = 14,000) against deionised water (3 × 1 h), before evaporation of the solvent and redispersal in water. The product was analysed by fluorescence spectroscopy.

Carbon dots from P_2O_5 and acetic acid[141]

In a 25 mL glass beaker, a solution of acetic acid (1.0 mL, 17.5 mmol) and water (80 μL, 0.56 μmol) was added to P_2O_5 (2.5 g, 8.8 mmol) without stirring. After 5 min, the mixture had ceased bubbling and was allowed to cool to room temperature before addition of water (40 mL). The product was analysed by fluorescence spectroscopy, fluorescence microscopy, UV-Vis absorbance (recorded on an Varian Cary 50 Scan Spectrophotometer using 100% water as a blank), TEM and DLS.

Carbon dots from glucose and PEG_{400} (microwave)[99]

Glucose (2 g, 11.1 mmol) was dissolved in H_2O (3 mL) and PEG_{400} (10 mL, 28.2 mmol) was added and the mixture vortexed. The mixture was microwave irradiated (Biotage Initiator) for a total time of 80 min (3 × 10 min, 120 °C; 2 × 15 min, 150 °C; 1 × 20 min, 150 °C) to give a dark brown solution. The carbon dots were purified by attempted size separation or dialysis. In the case of size separation the carbon nanoparticles were dispersed in a mixture of H_2O/EtOH/$CHCl_3$ (1:3:1, 1 mL) and centrifuged sequentially at 4,000, 5,000, 6,000, 8,000 and 16,000 rpm for 10 minutes. The solid material was collected and disposed of after each centrifugation until no solid remained. The solvent was evaporated *in vacuo*. In the case of dialysis, the reaction mixture was dialysed against deionised water for 36 h (Sigma-Aldrich cellulose membrane dialysis tube, MWCO = 14,000) then against MeOH for 3 h (MWCO = 14,000). The solvent was evaporated overnight and the carbon dots precipitated with the addition of acetone. The carbon dots were centrifuged (14,000 rpm, 10 min) and collected. The product was analysed by DLS, TEM fluorescence spectroscopy.

Carbon dots from sucrose and phosphoric acid[151]

In a 5 mL glass microwave vessel, sucrose (0.2 g, 0.6 mmol) was dissolved in water (0.8 mL) and H_3PO_4 (4.0 mL, 77 mmol) was added. The solution was microwave irradiated (Biotage Initiator) for 75 s at 100 °C. After cooling to room temperature, the sample was diluted with H_2O (10 mL). The crude suspension was centrifuged (4,000 rpm, 10 min) and the brown solid removed by gravity filtration. The light brown solution was dialysed against deionised water for 3 h (Sigma-Aldrich cellulose membrane dialysis tube, MWCO = 14,000). The procedure was repeated with microwave irradiation for a) 90s at 100 °C, b) 105 s at 100 °C, c) 120 s at 100 °C, d) 90s at 75 °C, e) 90s at 125 °C and f) 90s at 150 °C. The products were analysed by TEM and DLS.

Carbon dots from glucose and PEG_{400} (thermal)

Glucose (2 g, 11.1 mmol) was dissolved in H_2O (3 mL) in a 5 mL glass vial and PEG400 (10 mL, 28.2 mmol) was added before being sealed. The mixture was heated for 3 h at 270 °C with stirring on a hotplate to give a dark brown solution. After cooling to room temperature, the reaction mixture was dialysed against deionised water for 36 h (Sigma-Aldrich cellulose membrane dialysis tube, MWCO = 14,000). The solvent was evaporated overnight and the carbon dots re-dispersed in water. The product was analysed by DLS and fluorescence spectroscopy.

Chapter 3 Synthesis

Polymer Synthesis

Synthesis of Polymer 1 (**P1**): A mixture of piperazine (0.45 g, 5 mmol), BHEEDA (0.74 g, 5 mmol), MBA (1.54 g, 10 mmol) and water (3 mL) was purged with N_2 for 30 min and then heated at 40 °C for 12 h. The water was removed by lyophilisation, and the residue dissolved in $CHCl_3$ (8 mL). The product was precipitated by addition of hexane (40 mL), collected by centrifugation, and dried in a vacuum oven at 50 °C for 16 h to give 2.58 g of purified polymer.

Synthesis of Polymer 2 (**P2**): A mixture of TEGDA (0.45 g, 10 mmol) and DTT (1.54 g, 10 mmol) was purged with N_2 for 30 min and then heated at 40 °C for 12 h. The residue was dissolved in $CHCl_3$ (8 mL) and the product was precipitated by addition of hexane (40 mL), collected by centrifugation, and dried in a vacuum oven at 50 °C for 16 h to give 2.12 g of purified polymer.

Synthesis of Polymer 3 (**P3**): A mixture of TEGDA (0.45 g, 10 mmol) and piperazine (1.54 g, 10 mmol) was purged with N_2 for 30 min and then heated at 40 °C for 12 h. The residue was dissolved in $CHCl_3$ (8 mL) and the product was precipitated by addition of hexane (40 mL), collected by centrifugation, and dried in a vacuum oven at 50 °C for 16 h to give 3.17 g of purified polymer.

Synthesis of Polymer 4 (**P4**): A mixture of MBA (0.74 g, 10 mmol), DTT (1.54 g, 10 mmol) and water (3 mL) was purged with N_2 for 30 min and then heated at 40 °C for 12 h. The water was removed by lyophilisation, and the residue dissolved in $CHCl_3$ (8 mL). The product was precipitated by addition of hexane (40 mL), collected by centrifugation, and dried in a vacuum oven at 50 °C for 16 h to give 2.83 g of purified polymer.

Synthesis of Polymer 5 (**P5**): A mixture of MBA (0.74 g, 10 mmol), piperazine (1.54 g, 10 mmol) and water (3 mL) was purged with N_2 for 30 min and then heated at 40 °C for 12 h. The water was removed by lyophilisation, and the residue dissolved in $CHCl_3$ (8 mL). The product was precipitated by addition of hexane (40 mL), collected by centrifugation, and dried in a vacuum oven at 50 °C for 16 h to give 2.56 g of purified polymer.

Polymers **P1**–**P5** were analysed by gel permeation chromatography (GPC) on an Agilent 1100 with a PLgel MIXED-C column (300 × 7.5 mm ID, Polymer Laboratories) and a refractive index detector using NMP as an eluent at a flow rate of 1.0 mL min^{-1}. The molecular weights (M_w) and polydispersities (PDI) of the polymers are reported relative to monodisperse polystyrene standards.

Carbon dot synthesis

Carbon dots were synthesised by thermopyrolysis of P1–P5. Neat polymer (0.1 g) was placed in a reaction vessel and purged with N_2 for 30 min, and heated at 250 °C in a sealed tube for 2 h. The crude product was suspended in water (5 mL) and centrifuged at 14,000 rpm for 30 min. The supernatant was collected and filtered by ultrafiltration (Amicon Ultra-0.5 centrifugal filters, regenerated cellulose membrane, MWCO = 50,000) at 14,000 rpm for 15 min. The filtrates were collected and concentrated to ~1 mL in vacuo, and dialysed against distilled water (Sigma-Aldrich, cellulose membrane dialysis tube, MWCO = 14,000) to give ~10 mg of the purified carbon dots **CD-P1** to **CD-P5** in 10% yield by weight. Transmission Electron Microscopy (TEM) images of **CD-P1** were taken on FEI Tecnai F20 transmission electron microscope operating at 400 kV. TEM images of **CD-P2**–**CD-P5** were taken

using a Philips / FEI CM120 Biotwin transmission electron microscope operating at 100 kV. Samples were prepared by sonicating the carbon dot solutions (~1% w/v in acetone) for 30 min and depositing on a formvar/carbon support film 200 mesh copper grid and dried.

Fluorescence of the carbon dot samples was measured on an Edinburgh Instruments Spectrometer using 100% solvent as a blank. Quantum yields were obtained on a Fluoromax-P spectrofluorimeter (Horiba-Jobin-Yvon) and a Varian Cary 50 Scan Spectrophotometer using 4',6-diamidino-2-phenylindole (DAPI) in DMSO as a standard and calculated using the formula below:

$$\Phi_X = \Phi_{ST}\left(\frac{Grad_X}{Grad_{ST}}\right)\left(\frac{\eta_X^2}{\eta_{ST}^2}\right)$$

Where the ST and X subscripts denote the standard and test respectively, Φ is the quantum yield (Φ_{DAPI} in DMSO = 0.58), Grad is the gradient from the straight line graph of integrated fluorescence vs absorbance and η the refractive index of the solvent (DMSO η = 1.48, H_2O η = 1.33).

Cellular Uptake

Cells were cultured in Dulbecco's Modified Essential Medium (DMEM) supplemented with 10% FBS, penicillin (20 units mL^{-1}), streptomycin (20 μg mL^{-1}) and L-glutamine (4 mM) at 37 °C in an atmosphere of 5% CO_2. For uptake experiments, 12-well plates of PC3, MCF7 or RAW cells were seeded at ~100,000 cell/well and grown overnight until ~80% confluent. The media was changed and **CD-P1** added at 1 mg mL^{-1}. After incubation for 5 h, the cells were washed three times with PBS and imaged by fluorescent microscopy using a Zeiss semi-confocal microscope (excitation 340–395 nm, emission 430–505 nm, band-pass filter). For flow cytometry analysis, PC3 cells were grown in a 12-well plate as described above and **CD-P1** added at 2, 1 and 0.1 mg mL^{-1} (n = 3), and cultured overnight. After washing with PBS and trypsination, uptake was evaluated using a BD LSR Flow Cytometer and data plotted using the FlowJo Version 7.6.3 software for analysis.

Cytotoxicity Assay

Cells were cultured in complete DMEM (supplemented with 10% FBS, penicillin (20 units/mL), streptomycin (20 μg mL^{-1}) and L-glutamine (4 mM) at 37 °C in an atmosphere of 5% CO_2. 96-well plates of PC3 cells were seeded at ~10,000 cells per well and cultured until ~80% confluent. A 10 mg mL^{-1} carbon dot solution in deionised water was sterilised and diluted with complete DMEM to give solutions of **CD-P1**–**CD-P5** in 2, 1 and 0.1 mg mL^{-1}. Media was removed from the cells and replaced with the compound (100 μL) per well. The cells were incubated with the carbon dot solution for 5 h before removal of the solution. The cells were washed (2 × media, 2 × PBS). MTT (5 mg) was dissolved in DMEM (10 mL) and was added to each well (100 μL). The plate was incubated at 37 °C for a further 4 h before solubilisation of the formazan crystals with 10% Triton X 100 plus 0.1 N HCl in isopropanol. The absorbance of the solution at 540 nm was recorded using a microplate reader Synergy HT Reader and the Gen 5 (1.11) software. For data analysis, background corrected absorption values were averaged and expressed as '% viability' compared to healthy untreated PC3 cells.

Chapter 4 Synthesis

Conjugation Studies

CD-P1–MR *conjugate*

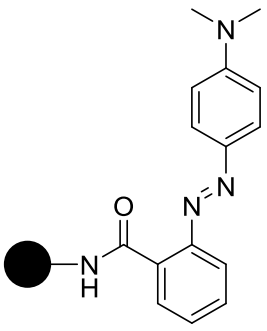

To a solution of 2-(*N*,*N*-dimethyl-4-aminophenyl)azobenzenecarboxylic acid (methyl red, 95 mg, 0.36 mmol) in DMF (1 mL), Oxyma (50 mg, 0.36 mmol) and DIC (55

μL, 0.36 mmol) were added and the solution stirred for 5 min. **CD-P1** (10 mg, 0.12 mmol based on 20% elemental composition of nitrogen, 1 eq) was added to the coupling solution in a 1 mL plastic vial and the reaction stirred for 1 h at r.t. The reaction mixture was transferred to a cellulose dialysis tubing (MWCO = 14,000) and dialysed overnight against MeOH to remove excess methyl red. The light brown solution was dialysed against deionised water and dried in a vacuum oven to give the **CD-P1–MR** conjugate (~1 mg).

Acid stability of CD-P1

CD-P1 (1 mg) were dispersed in H_2O (1 mL) or neat TFA (1 mL) at r.t. After 3 h the fluorescence intensity was measured between 380 nm–700 nm (λ_{ex} 360 nm). The TFA was fully removed by evaporation under a flow of nitrogen and the residue was dispersed in H_2O (1 mL). The fluorescence intensity was measured again between 380 nm–700 nm (λ_{ex} 360 nm) and compared to the fluorescence intensity of an aqueous solution of **CD-P1** (1 mg mL^{-1}) recorded over the same wavelengths.

Synthesis of PEG spacer[206]

2-[(Dibenzylamino)ethoxy]ethanol

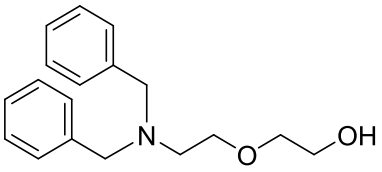

A mixture of 2-(aminoethoxy)ethanol (9.5 mL, 95.0 mmol), K_2CO_3 (32.0 g, 237.5 mmol) and benzyl bromide (27.2 mL, 190.0 mmol) in MeCN (500 mL) was stirred at 50 °C overnight. The solid was removed by filtration and the solvent removed *in vacuo*. The residue was dissolved in aqueous HCl (0.1 M, 50 mL) and washed with EtOAc (2 × 50 mL). The aqueous layer was made basic with aqueous NaOH (1 M) and extracted with DCM (4 × 50 mL). The organic phase was dried over $MgSO_4$ and removed under vacuum to yield 2-[(dibenzylamino)ethoxy]ethanol (14.8 g, 54%) which was used without further purification.

^{1}H NMR (500 MHz, $CDCl_3$): δ_H 7.37–7.24 (m, 10H, ar), 3.71–3.69 (m, 2H, CH_2-O-**CH_2**), 3.68 (s, 4H, N-**CH_2**-ar), 3.58 (t, 2H, *J* = 5.9 Hz, -**CH_2**-OH), 3.50–3.47 (m, 2H, **CH_2**-O-CH_2), 2.70 (t, 2H, *J* = 5.9 Hz, N-**CH_2**-CH_2)

^{13}C NMR (125 MHz, $CDCl_3$): δ_C 139.4, 128.9, 127.0, 72.0, 69.7, 61.9, 59.0, 53.0

MS (ES)$^+$: 286.0 ($[M+H]^+$, 100%)

Data in agreement with literature.[206]

2-[(Dibenzylaminoethoxy)ethoxy]acetic acid

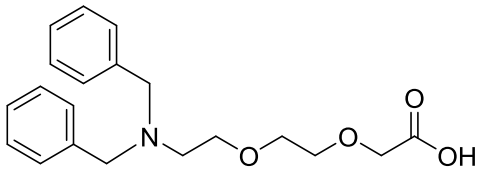

2-[(Dibenzylamino)ethoxy]ethanol (14.7 g, 51.5 mmol) was dissolved in dry THF (120 mL) and cooled in an ice bath to 0 °C. NaH (6.9 g, 206.0 mmol; 60% dispersion in oil) was added in portions followed by α-bromoacetic acid (10.7 g, 77.3 mmol). The suspension was heated at reflux under nitrogen overnight. H_2O (5 mL) was added carefully and the reaction stirred for 5 min before addition of H_2O (120 mL). The aqueous layer was washed with a mixture of hexane/Et_2O 1:1 (2 × 75 mL). The aqueous solution was acidified to pH 2 with aqueous HCl (1 M) and washed with Et_2O (3 × 75 mL). The aqueous solution was then neutralised to pH 6–7 with aqueous NaOH (1 M), solid NaCl was added and the mixture extracted with DCM (5 × 100 mL). The organic layer was dried over $MgSO_4$ and the solvent *removed in vacuo* to give the product which was used without further purification (8.9 g, 50%).

^{1}H NMR (500 MHz, $CDCl_3$): δ_H 7.45–7.26 (m, 10H, ar), 4.09 (s, 2H, -O-C**H_2**-COOH), 3.87 (s, 4H, N-C**H_2**-ar), 3.70–3.63 (m, 4H, -O-C**H_2**-C**H_2**-O-), 3.57–3.53 (m, 2H, -N-CH_2-C**H_2**-O), 2.85–2.80 (m, 2H, N-C**H_2**-CH_2)

^{13}C NMR (125 MHz, $CDCl_3$): δ_C 136.8, 129.6, 128.5, 127.7, 70.6, 70.0, 68.7, 58.5, 53.5, 51.9

MS (ES)$^+$: 344.4 ($[M+H]^+$, 100%)

Data in agreement with literature.[206]

[2-(2-aminoethoxy)ethoxy]acetic acid

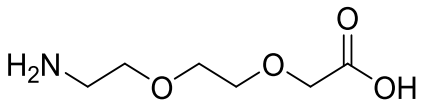

[2-(Dibenzylaminoethoxy)ethoxy]acetic acid (8.9 g, 25.8 mmol) was dissolved in EtOH (150 mL), Pd/C (0.89 g, 10%) was added and the mixture was stirred under a hydrogen atmosphere at 45 °C for 48 h. The catalyst was removed by filtration through a celite pad and the solvent removed *in vacuo*. The residue was triturated with Et_2O (100 mL) and collected by vacuum filtration to give the product (3.9 g, 96%).

^{1}H NMR (500 MHz, $CDCl_3$): δ_H 3.90 (s, 2H, -O-C**H$_2$**-COOH), 3.75–3.58 (m, 6H, -C**H$_2$**-O-C**H$_2$**-C**H$_2$**-O-), 3.11–3.07 (m, 2H, H_2N-C**H$_2$**-)
^{13}C NMR (125 MHz, $CDCl_3$): δ_C 68.6, 68.3, 68.1, 65.0, 37.5
MS (ES)$^+$: 164.2 ($[M+H]^+$, 100%)
Data in agreement with literature.[206]

{2-[3-(9H-fluoren-9-ylmethoxy)-3-oxopropoxy]ethoxy} acetic acid

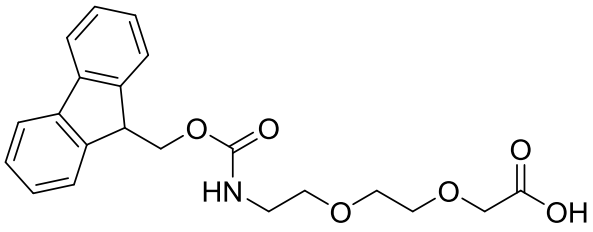

[2-(2-Aminoethoxy)ethoxy]acetic acid (3.8 g, 23.3 mmol) was suspended in H_2O (50 mL) and K_2CO_3(6.4 g, 46.6 mmol) added and the resulting mixture stirred at room temperature for 10 min. To the mixture, *N*-(9-fluorenylmethoxycarbonyl) succinimide (7.9 g, 23.3 mmol) was added and the reaction stirred for 16 h. The mixture was washed with Et_2O (2 × 15 mL) and the aqueous solution acidified to pH 1 with neat HCl and then extracted with DCM (5 × 50 mL). The solvent was dried over $MgSO_4$, removed under vacuum and the crude product purified by column

chromatography eluting with DCM/MeOH 9:1 + 0.1% acetic acid to afford the product as a white powder (4.3 g, 48%).

^{1}H NMR (500 MHz, $CDCl_3$): δ_H 7.76 (d, 2H, *J* = 7.5 Hz, ar), 7.61 (d, 2H, *J* = 7.4 Hz, ar), 7.40 (t, 2H, *J* = 7.4 Hz, ar), 7.32 (dt, 2H, *J* = 1.1 Hz, *J* = 7.4 Hz, ar), 4.41 (d, 2H, *J* = 7.0 Hz, -NH(CO)-O-C**H$_2$**), 4.23 (t, 1H, *J* = 7.0 Hz, -NH(CO)-O-CH$_2$-C**H**), 4.16 (s, 2H, O-C**H$_2$**-COOH), 3.80–3.60 (m 6H, -C**H$_2$**-O-C**H$_2$**-C**H$_2$**-O-), 3.43–3.40 (m, 2H, -NH-C**H$_2$**-)

^{13}C NMR (125 MHz, $CDCl_3$): δ_C 156.5, 143.9, 141.3, 127.7, 127.1, 125.1, 120.0, 71.5, 70.4, 69.9, 68.8, 66.8, 47.2, 40.7

MS (ES)$^+$: 385.9 ($[M]^+$, 10%); ($[M+Na]^+$, 100%)

HPLC t_R: 4.281 min, purity >99% by ELSD (Method 2)

Data in agreement with literature.[206]

Nucleus targeting

Protected NLS peptide

[Ac-Pro-Lys(Boc)-Lys(Boc)-Lys(Boc)-Arg(Pbf)-Lys(Boc)-Val-PEG-H]

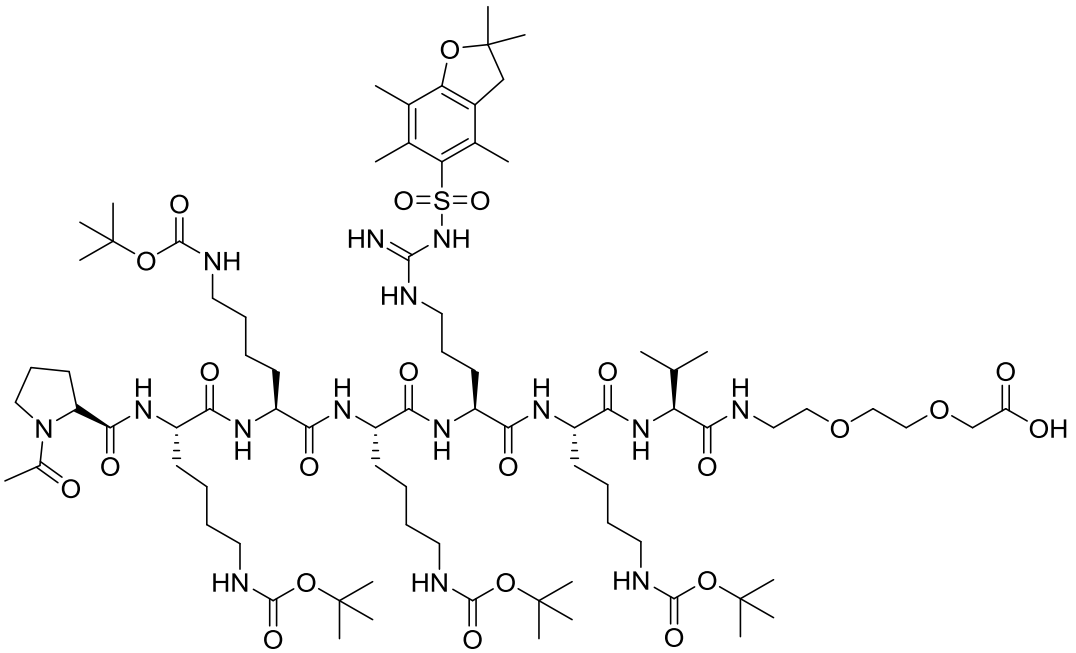

Pre-treatment of Resin

2-Chlorotrityl chloride polystyrene resin (CLTR-PS; 200 mg, 0.2 mmol, 1.0 mmol g-1, 100–200 mesh) was placed in a 6 mL Isolute filtration reservoir fitted with a polyethylene porous frit (20 µm). The resin was swollen in dry DCM, filtered and a solution of thionyl chloride in DCM (1:2 v/v, 2 mL) was added and the reaction stirred for 30 min. The resin was then washed with dry DCM (2 × 5 mL).

Attachment of Spacer

A solution of Fmoc-PEG-OH (3 eq) and DIPEA (3 eq) in dry DCM (0.1 M) was added to CLTR (200 mg, 1 eq) and the mixture stirred for 30 min. The mixture was filtered and washed with dry DMF (2 × 2 min). To the resin, DCM/MeOH/DIPEA ((80:15:5), 3 mL) was added and the mixture shaken for 5 min, filtered and washed with DMF (3 × 5 mL).

Amino acid coupling procedure

The resin was swollen in DCM (3 mL) for 5 min in a 6 mL reaction vessel and filtered. A solution of 20% piperidine in DMF (v/v, 3 mL) was added and the reaction stirred at r.t. (2 × 10 min). The resin was isolated by filtration and washed with DMF (3 × 3 mL), DCM (3 × 3 mL) and MeOH (3 × 3 mL). The resin was dried under vacuum and deprotection was confirmed by a Ninhydrin solid phase test (positive). To a solution of the appropriate Fmoc protected amino acid (3 eq) in DMF (0.1 M), Oxyma (3 eq) was added and the solution stirred for 2 min. DIC (3 eq) was added and the solution stirred for a further 5 min. The coupling solution as then added to the CLTR-PS resin (1 eq) pre-swollen in DCM and stirred at 60 °C for 20 min. The coupling solution was removed by filtration, a fresh coupling solution added and the mixture stirred at 60 °C for 20 min. The resin was isolated by filtration, washed with DMF (3 × 3 mL), DCM (3 × 3 mL) and MeOH (3 × 3 mL). The resin was dried under vacuum and the coupling was confirmed by a Ninhydrin solid phase test (negative).

Qualitative ninhydrin test:

3 drops of reagent A and 1 drop of reagent B were added to a small quantity of the resin of interest and heated at 110 °C for 3 min. Solution A (1.3 mg KCN in water (2

mL), phenol : EtOH (8 : 2: 50 mL), freshly distilled pyridine (100 mL)) and Solution B (2.5 g ninhydrin in EtOH (50 mL)).

Procedure for Coupling to Proline

The resin was swollen in DCM (3 mL) for 5 min in a 6 mL reaction vessel and filtered. A solution of 20% piperidine in DMF (v/v, 3 mL) was added and the reaction stirred at r.t. (2 × 10 min). The resin was isolated by filtration and washed with DMF (3 × 3 mL), DCM (3 × 3 mL) and MeOH (3 × 3 mL). The resin was dried under vacuum and deprotection was confirmed by a Chloranil solid phase test (positive). To a solution of Fmoc-Pro-OH (3 eq) in DMF (0.1 M), Oxyma (3 eq) was added and the solution stirred for 2 min. DIC (3 eq) was added and the solution stirred for a further 5 min. The coupling solution as then added to the CLTR-PS resin (1 eq) pre-swollen in DCM and stirred at 60 °C for 20 min. The coupling solution was removed by filtration, a fresh coupling solution added and the mixture stirred at 60 °C for 20 min. The resin was isolated by filtration, washed with DMF (3 × 3 mL), DCM (3 × 3 mL) and MeOH (3 × 3 mL). The resin was dried under vacuum and the coupling was confirmed by a Chloranil solid phase test (negative).

Qualitative chloranil test

3 drops of reagent A and 3 drops of B are added to a small quantity of the resin of interest and left at room temperature for 5 min. Solution A (2% acetaldyhyde in DMF) and Solution B (2% chloranil in DMF).

Acetylation Procedure

A solution of DMF/acetic acid/pyridine ((15:2:3), 10 mL g^{-1}) was added to preswollen CLTR-PS resin (1 eq) and stirred (2 × 15 min) at r.t. The resin was isolated by filtration and washed with DMF (3 × 3 mL), DCM (3 × 3 mL) and MeOH (3 × 3 mL). Confirmation of acetylation was confirmed by the Chloranil test.

Cleavage of Protected Peptide

A solution of 1% TFA in dry DCM (10 mL g^{-1}) was added to pre-swollen CLTR-PS resin and the mixture shaken to 2 min. The solution was filtered into a flask containing 10% pyridine in MeOH (2 mL g^{-1}). The cleavage solution was added,

shaken for 2 min and filtered a further 4 times and the resin washed with DCM (3 x 1 mL), MeOH (3 × 1 mL), DCM (2 × 1 mL) and MeOH (3 × 1 mL). The filtrates were evaporated under vacuum and H_2O was added to the residue. The mixture was cooled on ice to aid precipitation of the product as a white solid (67 mg).

^{1}H NMR: Unable to identify peaks due to presence of pyridine
MS (ES)$^+$: 1723.7 ([M+H]$^+$, 100%)
MALDI-TOF: $C_{81}H_{139}N_{15}O_{23}S_1K_1$ calculated $[M+K]^+$ 1760.952; found 1761.378
HPLC t_R: 6.69 min, purity >99% by ELSD (Method 2)

CD-P1–NLS

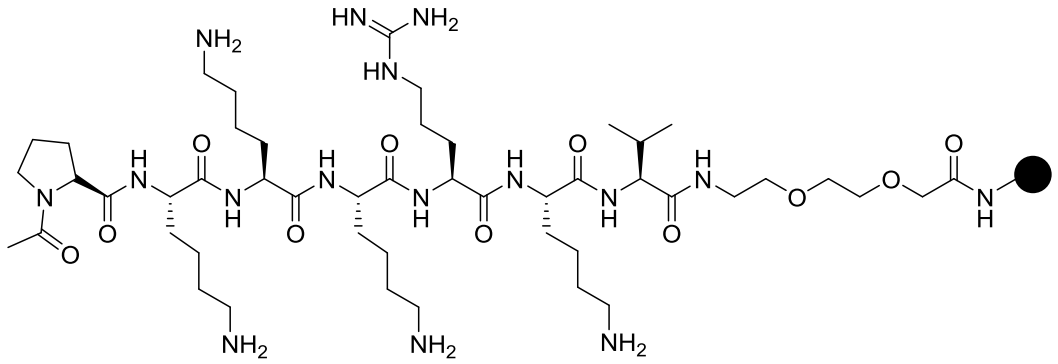

To a solution of protected NLS peptide (40 mg, 23 μmol) in DMF (400 μL), Oxyma (10 mg, 70 μmol) and DIC (10 μL, 70 μmol) were added and the solution stirred for 5 min. **CD-P1** (10 mg) was added to the coupling solution and the reaction shaken for 1 h at r.t. The solvent was removed *in vacuo* and the product suspended in TFA/TIS/H_2O (95:2.5:2.5, 500 μL) and shaken for 3 h. After removal of the cleavage cocktail under a flow of nitrogen, the carbon dot conjugates were suspended in water and dialysed against deionised water (1 × 1 h), MeOH (1 × 1 h) and water (1 × 1 h). The solvent was removed in a vacuum oven overnight (125 °C) to give the **CD-P1–NLS** conjugate (31 mg).

Confocal microscopy

In 6-well plates, coverslips were coated with poly-lysine (0.01% solution in water) for 10 min at r.t. The coverslips were washed (2 × media, 2 × PBS) and PBS added. The coverslips were sterilised under UV irradiation for 15 min and washed with PBS. Prostate cancer (PC3) cells were cultured on the poly-lysine coated coverslips in 6-well plates in complete DMEM (10% fetal bovine serum, 1% L-glutamine, 100 units L^{-1}, penicillin, 100 μg mL^{-1} streptomycin) incubated at 37 °C and 5% CO_2 until ~60% confluent. **CD-P1-NLS** (1 mg mL^{-1}) in DMEM media was added to the cells and incubated for 5 h at 37 °C and 5% CO_2. The media was removed and the cells fixed with 4% paraformaldehyde for 20 min at r.t. After washing with PBS, SYTO 17 red fluorescent nucleic acid stain was then added to the cells at 5 μM for 2 h. The cells were then washed (2 × media, 2 × PBS) and PBS added. The cells were imaged using a Zeiss 1sm 510 meta confocal microscope, 405 nm (DAPI) and 543 nm (rhodamine), Zeiss Meta software was used for digital acquisition and Image J for data analysis.

Mitochondria Targeting

5-Carboxypentyl triphenylphosphonium bromide[207]

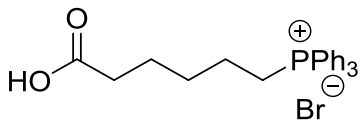

A solution of 6-bromohexanoic acid (1.5 g, 7.7 mmol) and triphenylphosphine (2.1 g, 8.1 mmol) was heated at reflux under a nitrogen atmosphere for 4 h. On cooling to room temperature, the product crystallised. The product was collected by vacuum filtration, washed with Et_2O (2 × 5 mL) and dried to give a white crystalline powder (3.49 g, >99%).

^{1}H NMR (500 MHz, $CDCl_3$): δ_H 7.84–7.77 (m, 9H, ar), 7.75–7.69 (m, 6H, ar), 3.69–3.60 (m, 2H, -C**H$_2$**-PPh_3), 2.44–2.38 (m, 2H, -O(CO)-C**H$_2$**-), 1.72–1.63 (m, 6H, CH_2-(C**H$_2$**)$_3$-CH_2-P).

^{13}C NMR (125 MHz, $CDCl_3$): δ_C 175.9, 135.4, 133.9, 130.9, 118.8, 34.5, 29.8, 24.2, 23.0, 22.1

MS (ES)$^+$: 377.1 ($[M]^+$, 100%)

HPLC t_R: 4.89 min, purity >99% by ELSD (Method 2)

Data in agreement with literature.[207]

5-carboxypentyl triphenylphosphonium bromide

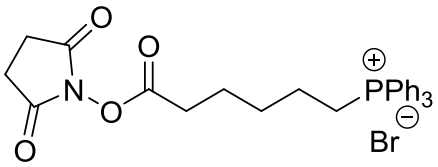

To a solution of 5-carboxypentyl triphenylphosphonium bromide (100 mg, 0.21 mmol) and *N*-hydroxysuccinimide (31 mg, 0.27 mmol) in DCM (5 mL) was added DIC (43 μL, 0.27 mmol) and the reaction stirred for 1 h at room temperature. The solvent was removed in vacuo and the residue washed extensively with EtOAc and dried to give the product as a white powder (112 mg, 92%) which was used without further purification.

^{1}H NMR (500 MHz, $CDCl_3$): δ_H 7.90–7.84 (m, 6H, ar), 7.82–7.78 (m, 3H, ar), 7.74–7.68 (m, 6H, ar), 3.94–3.87 (m, 2H, -C**H$_2$**-PPh_3), 2.82 (s, 4H, -(CO)-C**H$_2$**-C**H$_2$**-(CO)-) 2.59 (t, 2H, J = 7.1 Hz, -O(CO)-C**H$_2$**-), 1.71–1.64 (m, 6H, CH_2-(C**H$_2$**)$_3$-CH_2-P).

^{13}C NMR (125 MHz, $CDCl_3$): δ_C 169.3, 168.8, 135.2, 133.9, 130.7, 188.9, 42.4, 30.8, 25.8, 24.4, 23.7, 22.5

MS (ES)$^+$: 474.1 ($[M]^+$, 100%)

HPLC t_R: 4.98 min, purity >99% by ELSD (Method 2)

CD-P1-MITO

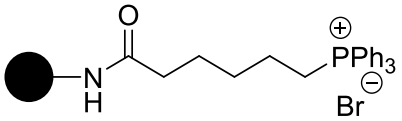

To a solution of **CD-P1** (11 mg) in DMF (500 μL) was added DIPEA (10 μL) and the solution stirred for 5 min. 5-Carboxypentyl triphenylphosphonium bromide NHS ester (40 mg, 0.07 mmol) in DMF (500 μL) was added and the reaction shaken for 1 h at r.t. The crude product was dialysed against deionised water (3 × 1 h) and the solvent was removed in a vacuum oven overnight (125 °C) to give the **CD-P1–MITO** conjugate (22 mg).

Confocal studies

Prostate cancer (PC3) cells were cultured on poly-lysine coated coverslips in 6-well plates as previously described until ~80% confluent. **CD-P1-MITO** (1 mg mL^{-1}) in DMEM media was added to the cells and incubated for 5 h at 37 °C and 5% CO_2. After washing with PBS, Mitotracker Red was then added to the cells at a concentration of 5 μM and incubated at 37 °C and 5% CO_2 for 30 min. The media was removed and the cells fixed with 4% paraformaldehyde. The cells were washed (2 × media, 2 × PBS) and PBS added. The cells were imaged using a Zeiss 1sm 510 meta confocal microscope under 405 nm (DAPI) and 543 (rhodamine), Zeiss Meta software was used for digital acquisition and Image J for data analysis.

Human Neutrophil Elastase (HNE) probes

MR-AAPV-PEG-OH

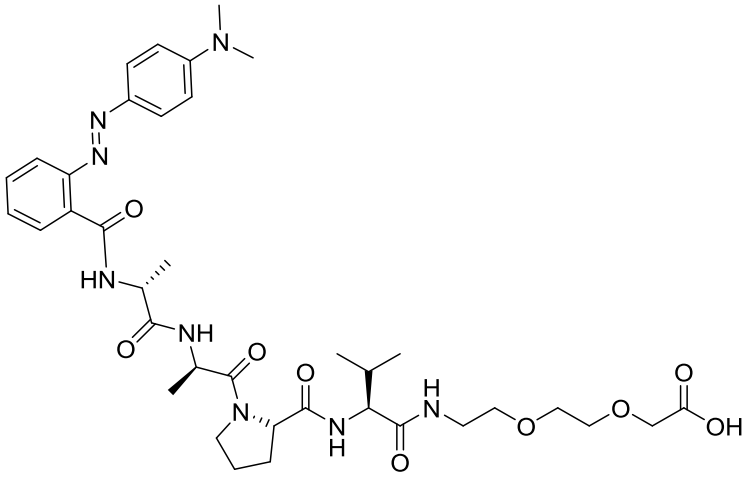

MR-AAPV-PEG-OH

2-Chlorotrityl chloride polystyrene resin (CLTR-PS; 150 mg, 0.2 mmol, 1.0 mmolg^{-1}) was pre-treated with thionyl chloride (2 mL). Fmoc-PEG-OH (3 eq) was activated with DIPEA (3 eq) in dry DCM, added to the resin and stirred for 30 min. The resin was washed and capped as previously described. The Fmoc group was deprotected with 20% piperidine in DMF (v/v) and subsequent amino acids and methyl red (3 eq) coupled with Oxyma/DIC (3 eq) in DMF as previously described with confirmation using the Ninhydrin or Chloranil tests as appropriate. The peptide was cleaved with a solution of 1% TFA in dry DCM (10 mL g^{-1}) as previously described and the solution was lyophilised to afford the product as a purple solid (22 mg).

^{1}H NMR: Unable to identify peaks due to presence of pyridine
MS (ES)$^+$: 753.2 ([M+H]$^+$, 60%); 275.1 ([M+3Na]$^{3+}$, 100%
HPLC t_R: 5.45 min, purity >99% by ELSD

MR-AAPV-CD-P1

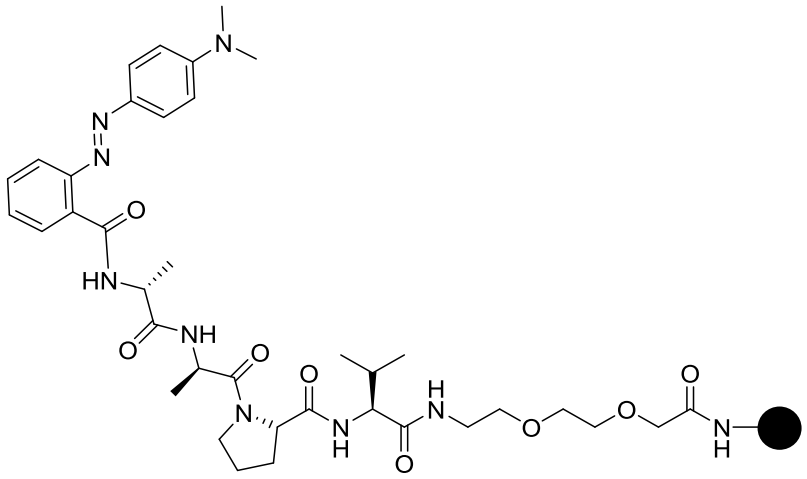

MR-AAPV-CD-P1

To a solution of **MR-AAPV-PEG-OH** (40 mg, 27 μmol) in DMF (300 μL), Oxyma (4 mg, 27 μmol) and DIC (4 μL, 27 μmol) were added and the solution stirred for 5 min. **CD-P1** (5 mg) was added to the coupling solution and the reaction shaken for 1 h at r.t. The solvent was removed *in vacuo* and the product was suspended in water

and dialysed against deionised water (3 × 1 h). The solvent was removed in a vacuum oven overnight (125 °C) to give the **MR-AAPV-CD-P1** conjugate (7 mg).
Fluorescence spectroscopy of **MR-AAPV-CD-P1** was recorded in HNE buffer (50 mM HEPES (4-(2-hydroxyethyl)-1-piperazineethanesulfonic acid) + 0.75 M NaCl + 0.05% IGEPAL (not denaturing detergent) at 1 mg mL^{-1}. HNE (10 µL, 10 µg/mL) was added to the methyl red conjugate and incubated for 10 min at 37 °C and the fluorescence spectrum was recorded.

Alkyne-AAPV-PEG-OH

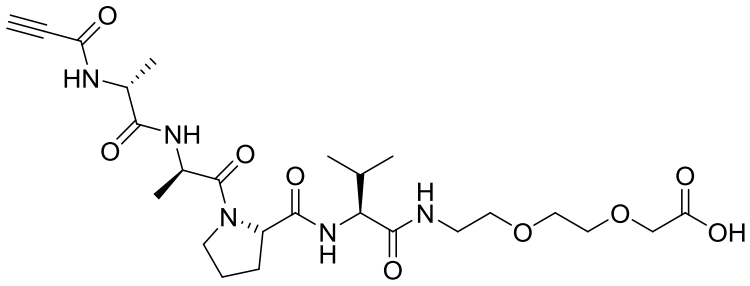

Alkyne-AAPV-PEG-OH

2-Chlorotrityl chloride polystyrene resin (CLTR-PS; 150 mg, 0.2 mmol, 1.0 mmol/g) was pre-treated with thionyl chloride (2 mL). Fmoc-PEG-OH (4, 3 eq) was activated with DIPEA (3 eq) in dry DCM and added to the resin and stirred for 30 min. The resin was washed and capped as previously described. The Fmoc group was deprotected with 20% piperidine in DMF (v/v) and subsequent amino acids and propiolic acid (3 eq) coupled with Oxyma/DIC (3 eq) in DMF as previously described with confirmation using the Ninhydrin or Chloranil tests as appropriate. The peptide was cleaved with a solution of 1% TFA in dry DCM (10 mL g^{-1}) as previously described and the solution was lyophilised to afford the product as an off-white solid (18 mg).

MS (ES)$^+$: 554.2 ($[M+H]^+$, 60%)
HPLC t_R: 3.99 min, purity >99% by ELSD

Alkyne-AAPV-CD-P1

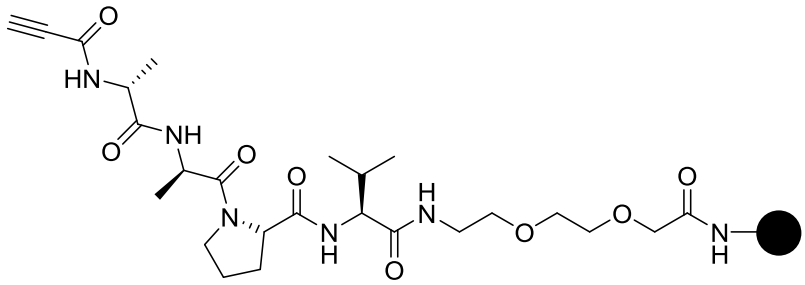

Alkyne-AAPV-CD-P1

To a solution of **Alkyne-AAPV-PEG-OH** (20 mg, 36 μmol) in DMF (300 μL), Oxyma (5 mg, 36 μmol) and DIC (5 μL, 36 μmol) were added and the solution stirred for 5 min. **CD-P1** (5 mg) was added to the coupling solution and the reaction shaken for 1 h at r.t. The solvent was removed *in vacuo* and the product was suspended in water and dialysed against deionised water (3 × 1 h). The solvent was removed in a vacuum oven overnight (125 °C) to give the **Alkyne-AAPV-CD-P1** conjugate (6 mg). The IR spectrum of solid **Alkyne-AAPV-CD-P1** was recorded and HNE (10 μL, 10 μg mL^{-1}) in buffer (50 mM HEPES (4-(2-hydroxyethyl)-1-piperazineethanesulfonic acid) + 0.75 M NaCl + 0.05% IGEPAL (not denaturing detergent) was added and the vial incubated for 10 min at 37 °C before removal of the buffer in a vacuum oven. The IR spectrum was recorded again to confirm cleavage.

Appendices

Copyright permissions: All published material used in this thesis was used with permissions to reprint on paper and electronically. A summary of all the acquired permissions is listed below.

Chapter 1: Figure 1, copyright the National Cancer Institute, Office of Cancer Nanotechnology Research. Image can be found at http://nano.cancer.gov/learn/understanding/

Figure 2, Sigma Aldrich. Image can be found at http://www.sigmaaldrich.com/materials-science/nanomaterials/quantum-dots.html

Figure 3, copyright 2012 American Chemical Society, published in Saha, K.; Agasti, S. S.; Kim, C.; Li, X.; Rotello, V. M. *Chemical Reviews* **2012**, *112*, 2739

Figure 4, copyright 2008 Nature Publishing Group, published in Qian, X., Peng, X.-H., Ansari, D. O., Yin-Goen, Q., Chen, G. Z., Shin, D. M., Yang, L., Young, A. N., Wang, M. D., Nie, S. *Nature Biotechnology* **2008**, *26*, 83

Figure 5, copyright 2009 Spring Science+Business Media B.V., published in Lara, H. H., Ayala-Núñez, N. V., Ixtepan Turrent, L. D. C., Rodríguez Padilla, C. *World Journal of Microbiology and Biotechnology* **2009**, *26*, 615

Figure 6, copyright 2010 AIP Publishing LLC, published in Rabias, I., Tsitrouli, D., Karakosta, E., Kehagias, T., Diamantopoulos, G., Fardis, M., Stamopoulos, D., Maris, T. G., Falaras, P., Zouridakis, N., Diamantis, N., Panayotou, G., Verganelakis, D. A., Drossopoulou, G. I., Tsilibari, E. C., Papavassiliou, G. *Biomicrofluidics* **2010**, *4*

Figure 7, copyright 2006 American Heart Association Inc, published in Nahrendorf, M., Jaffer, F., Kelly, K., Sosnovik, D. E., Aikawa, E., Libby, P., Weissleder, R. *Circulation* **2006**, *114*, 1504

Figure 8, copyright 2010 The Royal Society of Chemistry, published in He, C., Zhu, W., Xu, Y., Zhong, Y., Zhou, J., Qian, X. *Journal of Materials Chemistry* **2010**, *20*, 10755

Figure 11, copyright 2010 The Royal Society of Chemistry, published in Zrahevskiy, P., Sena, M., Gao, X. *Chemical Society Reviews* **2010**, *39*, 4326

Figure 14, copyright 2004 American Chemical Society, published in Xu, X.,Ray, R., Gu, Y., Ploehn, H. J., Gearheart, L., Raker, K.; Scrivens, W. *Journal of the American Chemical Society* **2004**, *126*, 12736

Figure 17a, copyright 2007 Wiley-VCH Verlag GmBH & Co, published in Liu, H., Ye, T., Mao, C. *Angewandte Chemie International Edition* **2007**, *46*, 6473

Figure 17b, copyright 2008 The Royal Society of Chemistry, published in Zhao, Q.-L., Zhang, Z.-L., Huang, B.-H., Peng, J., Zhang, M., Pang, D.-W. *Chemical Communications* **2008**, 5116

Figure 18, copyright 2012 The Royal Society of Chemistry, published in Guo, X., Wang, C.-F., Yu, Z.-Y., Chen, L., Chen, S. *Chemical Communications* **2012**, 2692

Figure 19, copyright 2012 The Royal Society of Chemistry, published in Jia, X., Li, J., Wang, E. *Nanoscale* **2012**, *4*, 5572

Figure 20, copyright 2012 Wiley-VCH Verlag GmbH & Co., published in Qu, S., Wang, X., Lu, Q., Liu, X., Wang, L. *Angewandte Chemie International Edition* **2012**, *51*, 12215

Figure 21, copyright 2014 American Chemical Society, published in Gao, X., Ding, C., Zhu, A., Tian, Y. *Analytical Chemistry* **2014**, *86*, 7071

Chapter 4: Figure 67, copyright 2006 Elsevier Ltd, published in McBride, H. M., Neuspiel, M., Wasiak, S. *Current Biology*, **2006**, *16*, 551

ChemPubSoc Europe
DOI: 10.1002/chem.201403076
CHEMISTRY A European Journal Full Paper

Nanoparticles

Photoluminescent Carbon Dots from 1,4-Addition Polymers

Zhiqiang Jiang,*[a, b] Andrew Nolan,[a] Jeffrey G. A. Walton,[a] Annamaria Lilienkampf,[a] Rong Zhang,[c] and Mark Bradley*[a]

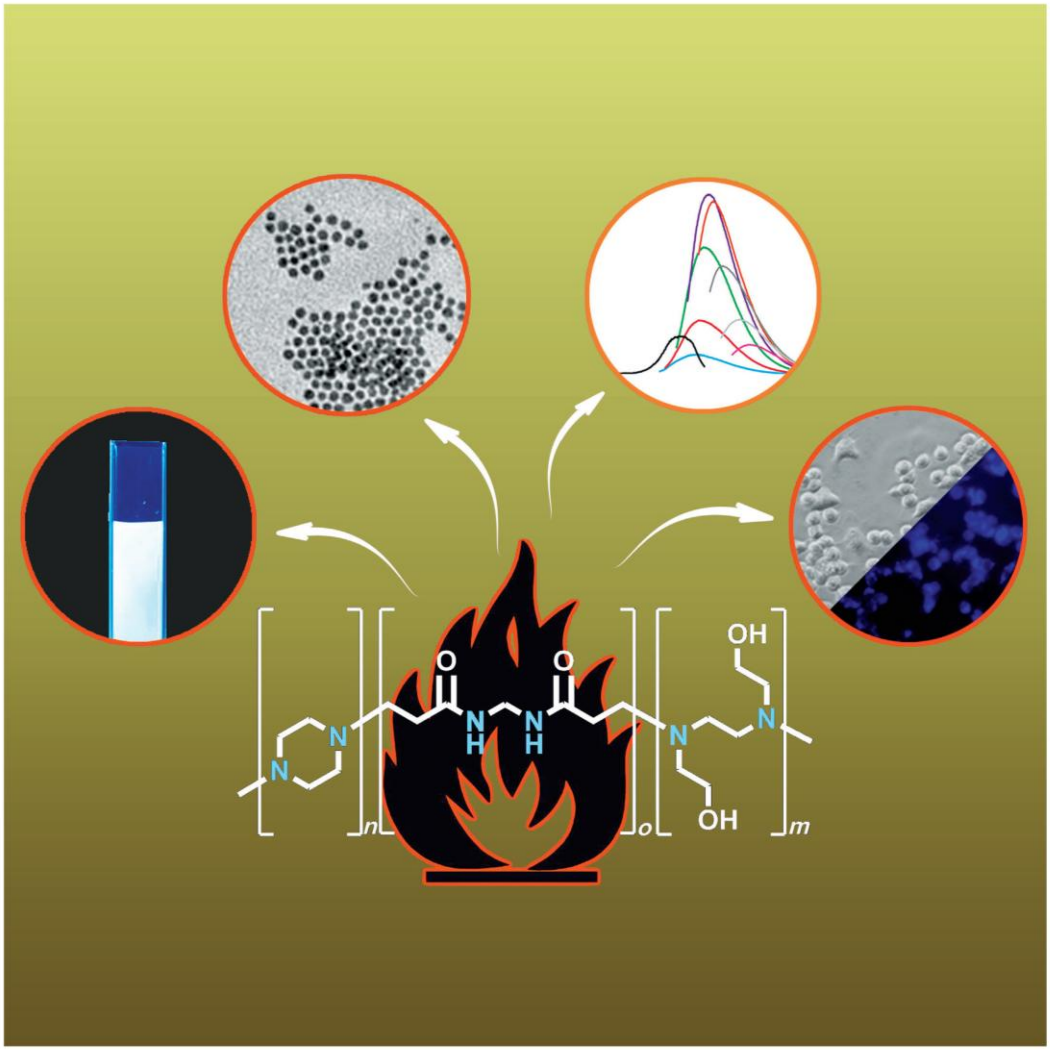

ChemPubSoc Europe

CHEMISTRY
A European Journal
Full Paper

Abstract: Photoluminescent carbon dots were synthesised directly by thermopyrolysis of 1,4-addition polymers, allowing precise control of their properties. The effect of polymer composition on the properties of the carbon dots was investigated by TEM, IR, XPS, elemental analysis and fluorescence analysis, with carbon dots synthesised from nitrogen-containing polymers showing the highest fluorescence. The carbon dots with high nitrogen content were observed to have strong fluorescence in the visible region, and culture with cells showed that the carbon dots were non-cytotoxic and readily taken up by three different cell lines.

Introduction

Photoluminescent nanoparticles have a multitude of uses as sensors,[1,2] in bioimaging,[3–6] and in a number of cell-based applications such as tagging/tracking and flow cytometry.[7] The most widely studied photoluminescent nanoparticles are quantum dots, based on cadmium selenide, which have been intensively studied as alternatives to traditional small-molecule fluorophores. However, quantum dots derived from heavy metals raise concerns about potential toxicities.[8,9] Photoluminescent carbon dots, which are predominantly composed of carbon, are thus an attractive alternative, offering biocompatibility and non-blinking emission.[10–12] In addition, it has been suggested that carbon dots have "up-converting" properties,[13] which would make them ideal for in vivo and light-harvesting-based applications.[14]

Carbon dots have been synthesised by a number of approaches including laser ablation of graphite,[15] electrochemical exfoliation from carbon paste electrodes,[16] nitric acid oxidation of candle soot,[17] thermal carbonisation of organic compounds,[18,19] microwave pyrolysis of glucose,[20] glycerol[21] or egg-shell membranes,[22] ultrasonic treatment of glucose,[23] and plasma treatment of egg proteins.[24] Carbon-based dots, produced by templated synthesis of polymeric structures, have also been offered as an alternative to quantum dots.[25] The mode of formation and the mechanism of photoluminescence of carbon dots is not clear, and although several mechanisms have been proposed to explain their optical characteristics,[17,19,26] the rationale behind their fluorescence remains open to debate. Undoubtedly, the nature of the precursor plays a vital role in the formation and properties of the carbon dots. Egg-white- and yolk-derived carbon dots have similar quantum yields (8 and 6%, respectively),[24] whereas the quantum yields of citric acid derived carbon dots generated by pyrolysis with either urea or 1-hexadecylamine were 53[27] and 14%,[28] respectively. It has been reported that the incorporation of heteroatoms, such as phosphorus, nitrogen or sulfur into the carbon dots may alter their structure, photoluminescence and potential up-conversion properties.[29,30]

Here, we report the generation and characterisation of a series of fluorescent carbon dots derived directly from 1,4-addition polymers, which were synthesised using monomers including piperazine, dithiothreitol (DTT), *N,N'*-bis(2-hydroxyethyl)-ethylenediamine (BHEEDA), *N,N'*-methylenebisacrylamide (MBA) and tetra(ethylene glycol)diacrylate (TEGDA). Nitrogen-containing carbon dots (up to 17% by weight) showed higher fluorescence than those not containing nitrogen. 1,4-Addition polymers conceptually offer a scaffold that defines the size and properties of the "carbon dots". The controlled and rapid synthesis of defined carbon dots from inexpensive starting materials offers an advantage over previously reported methods, and enables their use in various applications.

Results and Discussion

Polymers **P1–P5** (Supporting Information, Figure S1) were synthesised by a 1,4-addition polymerisation using the monomers shown in Table 1. Equimolar ratios of diacrylates with dithiols or diamines were used to give addition polymers with molecular weights up to 22 kDa and polydispersity indices (PDIs) between 1.4 and 2.1. Polymers containing MBA (**P1**, **P4** and **P5**) were obtained as off-white solids, whereas **P2** formed a sticky gel-like polymer and **P3** a viscous oil.

The carbon dots were synthesised by a thermopyrolysis of the polymers **P1–P5** at 250 °C. Over time, the neat polymers changed from colourless to brown and then black; indicating the formation of carbon dots. Isolation and purification of the carbon dots was achieved by size exclusion and dialysis. First, the crude carbon dots were centrifuged to remove visible solid material generated during pyrolysis, and then further refined by ultracentrifugation to remove particles larger than 50 kDa. Dialysis (M_w cut-off 14 kDa) ensured removal of unreacted monomers, before drying overnight at 125 °C to yield the carbon dots as a dark-brown solids.

Aqueous solutions of the carbon dots displayed varying degrees of blue fluorescence under UV irradiation (λ_{Ex} 365 nm) (Figure 1). More detailed fluorescence analysis showed **CD-P1**

[a] *Dr. Z. Jiang,[+] A. Nolan,[+] Dr. J. G. A. Walton, Dr. A. Lilienkampf, Prof. M. Bradley*
EaStCHEM, School of Chemistry University of Edinburgh
Joseph Black Building, West Mains Road
Edinburgh, EH9 3JJ (UK)
E-mail: mark.bradley@ed.ac.uk

[b] *Dr. Z. Jiang[+]*
School of Materials Science and Engineering
Ningbo University of Technology
201 Fenghua Road, Ningbo, Zhejiang, 315211 (P.R. China)
E-mail: jiangzqiang@hotmail.com

[c] *Dr. R. Zhang*
School of Materials Science and Engineering
Changzhou University
Changzhou 2213164, Jiangsu (P.R. China)

[+] *These authors contributed equally to this work.*

Supporting information for this article is available on the WWW under http://dx.doi.org/10.1002/chem.201403076.

ChemPubSoc Europe

CHEMISTRY
A European Journal
Full Paper

Table 1. Monomers and the molar ratios [mmol] used in the synthesis of the 1,4-addition polymers, and polymer characterisation.

	Monomer A	Monomer B	Monomer C	Molar Ratio	M_n	M_w	PDI
P1	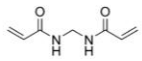		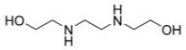	2:1:1	8500	17300	2.0
P2	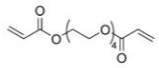	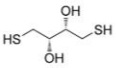		1:1	10300	21700	2.1
P3	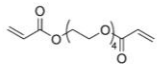			1:1	5000	8500	1.7
P4	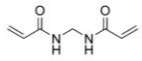	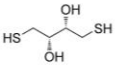		1:1	5600	10400	1.9
P5	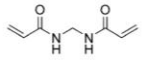			1:1	12500	18000	1.4

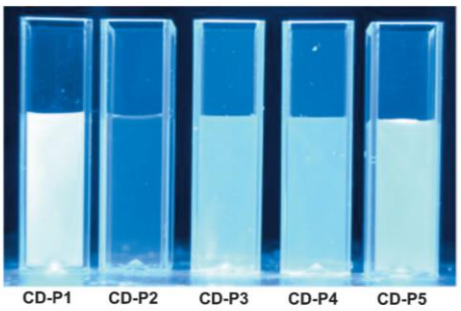

Figure 1. Aqueous solutions of carbon dots **CD-P1** to **CD-P5** (0.1% w/v) excited at 365 nm.

had the highest fluorescence intensity, closely followed by **CD-P5** with quantum yields (λ_{Ex} 380 nm) of 26 and 20%, respectively. **CD-P3** and **CD-P4** also exhibited fluorescence, but **CD-P2** had negligible fluorescence (Table 2). Elemental analysis showed that all carbon dots contained similar weight percentages of carbon and hydrogen but varying amounts of nitrogen, oxygen and sulfur, with the weight percentages of these heteroatoms in the carbon dots correlating reasonably well with the heteroatom content in the corresponding precursor monomers.

When the elemental composition of the dots was compared to the fluorescence intensities, no noticeable trend was seen with the levels of oxygen and sulfur. However, a greater percentage of nitrogen led to an increase in the fluorescence intensity of the carbon dots, as seen with **CD-P1** and **CD-P5** (Table 2). **CD-P2** (no noticeable fluorescence) was the only carbon dot not to contain nitrogen, suggesting that the polymer precursors play a role in the properties of the particles.

Carbon dots formed from MBA-containing polymers (**CD-P1**, **CD-P4** and **CD-P5**) showed greater fluorescence and quantum yields compared to those containing TEGDA (**CD-P2** and **CD-P3**). An increase in fluorescence was also seen when piperazine was used instead of DTT (**CD-P4** vs. **CD-P5** and **CD-P2** vs. **CD-P3**). Incorporation of BHEEDA (**P1**) seemed particularly beneficial, yielding **CD-P1**, the most fluorescent particles. These results suggest that the fluorescence of the carbon dots can be tuned by altering the nature of the polymer precursors. **CD-P1** was identified as the most promising particles and examined in greater depth.

Based on TEM analysis, **CD-P1** were spherical with a diameter of ≈5 nm and a lattice spacing of 0.21 nm, which was consistent with (100) diffraction planes of nano-crystalline graphite[31] (Figure 2). Similarly, TEM analysis of **CD-P2**–**CD-P5** showed the

Table 2. Quantum yield (in aqueous solution) and elemental analysis of the carbon dots.

	Size [nm]	Quantum Yield[a] [%]	Elemental Analysis [%]				
			C	H	N	O	S
CD-P1[b]	4.7±0.6	26	57.7	8.0	17.0	18.3	0.0
CD-P2	5.3±0.8	2	53.2	7.4	0.0	31.7	7.0
CD-P3	4.2±0.5	13	57.5	8.0	7.3	28.2	0.0
CD-P4	3.7±0.9	16	58.6	5.2	10.1	10.4	14.1
CD-P5	3.9±0.7	20	56.8	7.4	17.1	16.4	0.0

[a] Quantum yields were calculated using excitation wavelength of 330 nm and standardised against DAPI in DMSO. [b] **CD-PX** denote the carbon dots derived from polymer X in Table 1 ($n=3$).

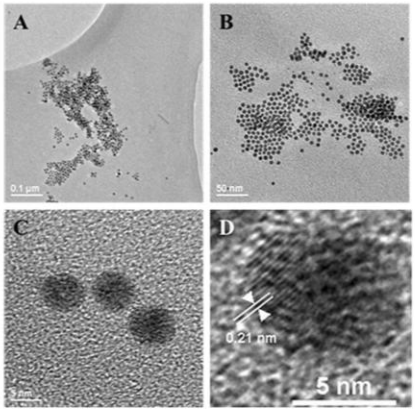

Figure 2. TEM images of **CD-P1** at A) ×10000, B) ×40000 and C) ×200000 magnification; D) high-resolution TEM image of an individual carbon dot.

ChemPubSoc Europe

CHEMISTRY
A European Journal
Full Paper

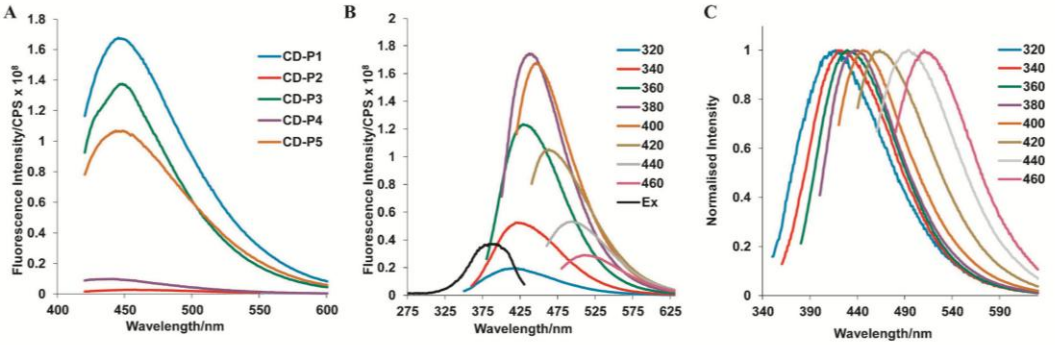

Figure 3. A) Overlapping fluorescence spectra of **CD-P1**–**CD-P5** (λ_{Ex} 400 nm). B) Fluorescence spectrum of aqueous solution of **CD-P1** (excitation wavelength from 320 nm to 460 nm in 20 nm increments) and corresponding excitation spectrum (black line). C) Normalised emission spectral intensities of **CD-P1** showing the change in emission at increasing excitation wavelengths. The legends show the corresponding excitation wavelengths.

carbon nanoparticles to be spherical and of the desired size (Supporting Information, Figure S2).

For all carbon dots, the fluorescence emission was highly dependent on the excitation energy. The emission of **CD-P1**, **CD-P3** and **CD-P5** reached maxima at 437, 443 and 433 nm, respectively, when excited at 380 nm. However, the sulfur-containing **CD-P2** and **CD-P4** reached maxima at 442 and 381 nm when excited at lower wavelengths (360 and 340 nm, respectively). The maximum emission wavelength for the carbon dots ranged from 419 (**CD-P4**) to 443 nm (**CD-P3**), when excited at 380 nm. Increasing nitrogen content did not appear to affect the maximum emission (Figure 3a). When **CD-P1** was excited at different wavelengths, multi-colour emissions were observed (Figure 3b and c), with the λ_{max} of emission shifting from 417 to 510 nm when changing the excitation wavelength from 320 to 460 nm. The fluorescence of aqueous solutions of carbon dots (λ_{Ex} = 380 nm) remained stable over a pH range of 4 to 9 with only very minor variations observed (Supporting Information, Figure S3).

To investigate the ability of the polymer derived carbon dots to up-convert low energy radiation and emit light in the visible region, a suggested property of carbon dots,[13] aqueous solutions of **CD-P1** were excited with light in the near-infrared region. On excitation at wavelengths between 650–900 nm, the maximum emitted intensity appeared at 480 nm (λ_{Ex} = 850 nm) (Supporting Information, Figure S5). However, when the experiment was repeated with a 455 nm long-pass filter, no emission was observed in the visible region (Figure 4), suggesting that the emission in the absence of the filter arose not from up-conversion but as a result of co-existence of second-order diffraction light.

Cellular uptake studies of the carbon dots were carried out on prostate cancer cells (PC3), breast cancer cells (MCF7) and macrophages (RAW). **CD-P1** did not show any cytotoxicity on PC3 cells in an MTT assay up to 2 mg mL^{-1} concentration (Figure 5a). Similarly, **CD-P2**, **CD-P3** and **CD-P5** did not show notable cytotoxicity up to 2 mg mL^{-1}, and **CD-P4** only showed minor cytotoxicity (70% cell viability at 2 mg mL^{-1}) (Supporting Information, Figure S4). Visualisation of MCF7, PC3 and RAW cells by semi-confocal microscopy after incubation with **CD-P1** for 5 h clearly showed cellular uptake of the particles (Figure 5b), which was verified by flow cytometry analysis of PC3 (Figure 5c). The good cellular uptake of these non-toxic carbon dots suggests their compatibility with cell-based applications.

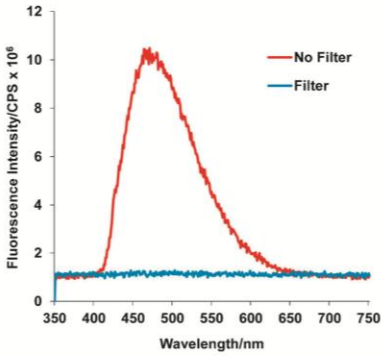

Figure 4. Fluorescence spectra of aqueous solution of **CD-P1** (0.1% w/v) excited in the near infrared region (850 nm) with and without a 455 nm long-pass filter.

Conclusion

Photoluminescent carbon dots were directly synthesised by thermopyrolysis of a series of 1,4-addition polymers without the need for surface activation/passivation. Fluorescence intensity and quantum yields of the carbon dots were dependent on the chemical composition of the starting polymer precursors, with incorporation of nitrogen-containing precursors giving materials with good quantum yields. This approach may provide a basis for fine tuning the luminescence of carbon dots based on inclusion of different heteroatoms.

ChemPubSoc Europe

CHEMISTRY A European Journal Full Paper

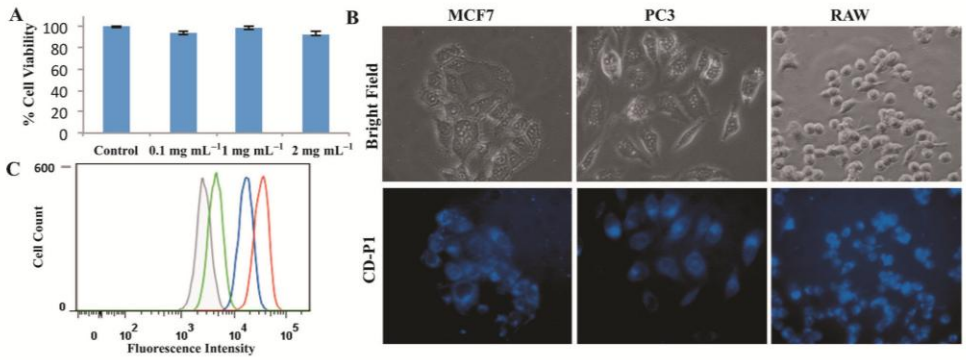

Figure 5. A) Cell viability of PC3 cells with increasing amounts of **CD-P1** (MTT assay, $n=8$). B) Bright field and fluorescence (λ_{Ex} 340–395 nm, 430–505 nm band-pass filter) images (×40) of MCF7, PC3 and RAW cells incubated with **CD-P1** (1 mg mL^{-1}) for 5 h. C) Flow cytometry analysis of PC3 cells incubated with **CD-P1** at 0.1 mg mL^{-1} (green), 1 mg mL^{-1} (blue), and 2 mg mL^{-1} (red).

CD-P1 showed the highest quantum yield (26%) and was taken forward for further studies. The carbon dots dispersed well in aqueous solutions and displayed stable fluorescence properties. TEM analysis showed **CD-P1** were spherical and uniform in shape, and showed lattice spacing consistent with that of nanocrystalline graphite. The photoluminescence properties of **CD-P1** showed a maximum emission at 450 nm when excited at 380 nm; however, the broad emission peak could indicate size variation in the nano-sized material.[31] **CD-P1** were readily taken up by three different cell lines without apparent cytotoxicity. These carbon dots constitute promising materials with possible bioimaging applications due to their good water dispersity, good cell permeability, low cytotoxicity, and strong fluorescent properties.

Experimental Section

Materials

Piperazine, dithiothreitol (DTT), *N,N'*-methylenebisacrylamide (MBA), *N,N'*-bis(2-hydroxyethyl)ethylenediamine (BHEEDA) and tetra(ethyleneglycol) diacrylate (TEGDA) were purchased from Sigma–Aldrich and used without further purification.

Polymer synthesis

Synthesis of polymer-1 (**P1**): A mixture of piperazine (0.45 g, 5 mmol), BHEEDA (0.74 g, 5 mmol), MBA (1.54 g, 10 mmol) and water (3 mL) was purged with N_2 for 30 min and then heated at 40 °C for 12 h. The water was removed by lyophilisation, and the residue dissolved in $CHCl_3$ (8 mL). The product was precipitated by addition of hexane (40 mL), collected by centrifugation, and dried in a vacuum oven at 50 °C for 16 h to give 2.58 g of purified polymer. **P4** (yield 2.83 g) and **P5** (yield 2.56 g) were synthesised in a similar manner. The syntheses of **P2** (yield 2.12 g) and **P3** (yield 3.17 g) were carried out with a similar method but without the addition of water. See Table 1 for the polymers synthesised and characterisation.

Carbon dot synthesis

Carbon dots were synthesised by thermopyrolysis of **P1**–**P5**. Neat polymer (0.1 g) was placed in a reaction vessel and purged with N_2 for 30 min, and heated at 250 °C in a sealed tube for 2 h. The crude product was suspended in water (5 mL) and centrifuged at 14000×g for 30 min. The supernatant was collected and filtered by ultrafiltration (Amicon Ultra-0.5 centrifugal filters, regenerated cellulose membrane, MWCO = 50000) at 14000×g for 15 min. The filtrates were collected and concentrated to ≈1 mL in vacuo, and dialysed against distilled water (Sigma–Aldrich, cellulose membrane dialysis tube, MWCO = 14000) to give ≈10 mg of the purified carbon dots **CD-P1** to **CD-P5** in 10% yield.

Cellular uptake

Cells were cultured in Dulbecco's modified essential medium (DMEM) supplemented with 10% FBS, penicillin (20 units/mL), streptomycin (20 μg mL^{-1}) and L-glutamine (4 mM) at 37 °C in an atmosphere of 5% CO_2. For uptake experiments, 12-well plates of PC3, MCF7 or RAW cells were seeded at ≈100000 cells per well and grown overnight until ≈80% confluent. The media was changed and **CD-P1** added at 1 mg mL^{-1}. After incubation for 5 h, the cells were washed three times with PBS and imaged by fluorescent microscopy using a Zeiss semi-confocal microscope (excitation 340–395 nm, emission 430–505 nm, band-pass filter). For flow cytometry analysis, PC3 cells were grown in a 12-well plate as described above and **CD-P1** added at 2, 1 and 0.1 mg mL^{-1} ($n=3$) and cultured overnight. After washing with PBS and trypsination, uptake was evaluated using a BD LSR flow cytometer and data plotted using the software FlowJo.

Acknowledgements

The authors would like to thank the EU for a Marie Curie International Incoming Fellowship to Z.J. (Project No. PIIF-GA-2010–27103108) and Intra-European Fellowship for career development for A.L. (Project No. PIEF-GA-2010–276116). The Medical Research Council UK and the Ministry of Science and Technology of the People's Republic of China (Project No. 1106) are thanked for funding, Mr. Andrea Venturato for help with the

ChemPubSoc Europe

CHEMISTRY
A European Journal
Full Paper

cover image, and Drs Nicolaos Avlonitis and Marc Vendrell Escobar for helpful discussions. The authors would also like to thank the reviewers and Dr Gareth Williams for valuable insights into the up-conversion experiments.

Keywords: carbon · imaging · luminescence · nanoparticles · polymers

[1] E. R. Goldman, A. R. Clapp, G. P. Anderson, H. T. Uyeda, J. M. Mauro, I. L. Medintz, H. Mattoussi, *Anal. Chem.* **2004**, *76*, 684–688.
[2] D. Gerion, F. Chen, B. Kannan, A. Fu, W. J. Parak, D. J. Chen, A. Majumdar, A. P. Alivisatos, *Anal. Chem.* **2003**, *75*, 4766–4772.
[3] F. Thielbeer, S. V. Chankeshwara, E. Johansson, N. Norouzi, M. Bradley, *Chem. Sci.* **2013**, *4*, 425–431.
[4] I. Schick, S. Lorenz, D. Gehrig, A.-M. Schilmann, H. Bauer, M. Panthöfer, K. Fischer, D. Strand, F. Laquai, W. Tremel, *J. Am. Chem. Soc.* **2014**, *136*, 2473–2483.
[5] L. Cao, X. Wang, M. J. Meziani, F. Lu, H. Wang, P. G. Luo, Y. Lin, B. A. Harruff, L. M. Veca, D. Murray, S.-Y. Xie, Y.-P. Sun, *J. Am. Chem. Soc.* **2007**, *129*, 11318–11319.
[6] J. Li, J.-J. Zhu, *Analyst* **2013**, *138*, 2506–2515.
[7] P. K. Chattopadhyay, D. A. Price, T. F. Harper, M. R. Betts, J. Yu, E. Gostick, S. P. Perfetto, P. Goepfert, R. A. Koup, S. C. De Rosa, M. P. Bruchez, M. Roederer, *Nat. Med.* **2006**, *12*, 972–977.
[8] J. Geys, A. Nemmar, E. Verbeken, E. Smolders, M. Ratoi, M. F. Hoylaerts, B. Nemery, P. H. M. Hoet, *Environ. Health Perspect.* **2008**, *116*, 1607–1613.
[9] A. M. Derfus, W. C. W. Chan, S. N. Bhatia, *Nano Lett.* **2004**, *4*, 11–18.
[10] R. Liu, D. Wu, S. Liu, K. Koynov, W. Knoll, Q. Li, *Angew. Chem.* **2009**, *121*, 4668–4671; *Angew. Chem. Int. Ed.* **2009**, *48*, 4598–4601.
[11] S. C. Ray, A. Saha, N. R. Jana, R. Sarkar, *J. Phys. Chem. C* **2009**, *113*, 18546–18551.
[12] S. N. Baker, G. A. Baker, *Angew. Chem.* **2010**, *122*, 6876–6896; *Angew. Chem. Int. Ed.* **2010**, *49*, 6726–6744.
[13] X. Jia, J. Li, E. Wang, *Nanoscale* **2012**, *4*, 5572–5575.
[14] R. Narayanan, M. Deepa, A. K. Srivastava, *J. Mater. Chem. A* **2013**, *1*, 3907–3918.
[15] Y.-P. Sun, B. Zhou, Y. Lin, W. Wang, K. Fernando, P. Pathak, M. Meziani, B. Harruff, X. Wang, H. Wang, P. Luo, H. Yang, M. Kose, B. Chen, L. Veca, S.-Y. Xie, *J. Am. Chem. Soc.* **2006**, *128*, 7756–7757.
[16] Y.-M. Long, C.-H. Zhou, Z.-L. Zhang, Z.-Q. Tian, L. Bao, Y. Lin, D.-W. Pang, *J. Mater. Chem.* **2012**, *22*, 5917–5920.
[17] H. Liu, T. Ye, C. Mao, *Angew. Chem.* **2007**, *119*, 6593–6595; *Angew. Chem. Int. Ed.* **2007**, *46*, 6473–6475.
[18] P.-C. Hsu, H.-T. Chang, *Chem. Commun.* **2012**, *48*, 3984–3986.
[19] A. Bourlinos, A. Stassinopoulos, D. Angelos, R. Zboril, V. Georgeakilas, E. Giannelis, *Chem. Mater.* **2008**, *20*, 4539–4541.
[20] H. Zhu, X. Wang, Y. Li, Z. Wang, F. Yang, X. Yang, *Chem. Commun.* **2009**, 5118–5120.
[21] X. Wang, K. Qu, B. Xu, J. Ren, X. Qu, *J. Mater. Chem.* **2011**, *21*, 2445–2450.
[22] Q. Wang, X. Liu, L. Zhang, Y. Lv, *Analyst* **2012**, *137*, 5392–5397.
[23] H. Li, X. He, Y. Liu, H. Huang, S. Lian, S.-T. Lee, Z. Kang, *Carbon* **2011**, *49*, 605–609.
[24] J. Wang, C.-F. Wang, S. Chen, *Angew. Chem.* **2012**, *124*, 9431–9435; *Angew. Chem. Int. Ed.* **2012**, *51*, 9297–9301.
[25] Z.-A. Qiao, Q. Huo, M. Chi, G. Veith, A. Binder, S. Dai, *Adv. Mater.* **2012**, *24*, 6017–6021.
[26] Y. Lu, L. Zhang, H. Lin, *Chem. Eur. J.* **2014**, *20*, 4246–4250.
[27] F. Wang, S. Pang, L. Wang, Q. Li, M. Kreiter, C.-y. Liu, *Chem. Mater.* **2010**, *22*, 4528–4530.
[28] S. Qu, X. Wang, Q. Lu, X. Liu, L. Wang, *Angew. Chem.* **2012**, *124*, 12381–12384; *Angew. Chem. Int. Ed.* **2012**, *51*, 12215–12218.
[29] J. Niu, H. Gao, L. Wang, S. Xin, G. Zhang, Q. Wang, L. Guo, W. Liu, X. Gao, Y. Wang, *New J. Chem.* **2014**, *38*, 1522–1527.
[30] Y. Xu, M. Wu, Y. Liu, X.-Z. Feng, X.-B. Yin, X.-W. He, Y.-K. Zhang, *Chem. Eur. J.* **2013**, *19*, 2276–2283.
[31] H. Li, X. He, Z. Kang, H. Huang, Y. Liu, J. Liu, S. Lian, C. H. A. Tsang, X. Yang, S.-T. Lee, *Angew. Chem.* **2010**, *122*, 4532–4536.

Received: April 14, 2014
Published online on August 5, 2014

References

(1) NSTC. *The National Nanotechnology Initiative - Strategic Plan, December 2007*; 2007.

(2) Czaban, J.; Thompson, D. *Nanotechnology* **2010**, *21*, 134005.

(3) Seeman, N. C. *Biochemistry* **2003**, *42*, 7259.

(4) European Commission. *Towards a European Strategy for Nanotechnology*; 2004.

(5) The National Cancer Institute http://nano.cancer.gov/learn/understanding/ (accessed Nov 21, 2014).

(6) Goesmann, H.; Feldmann, C. *Angewandte Chemie International Edition* **2010**, *49*, 1362.

(7) Chukwuocha, E. O.; Onyeaju, M. C.; Harry, T. S. T. *World Journal of Condensed Matter Physics* **2012**, *2*, 96.

(8) Hodes, G. *Advanced Materials* **2007**, *19*, 639.

(9) Kaiser, J.-P.; Diener, L.; Wick, P. *Journal of Physics: Conference Series* **2013**, *429*, 012036.

(10) Smijs, T. G.; Pavel, S. *Nanotechnology, Science and Applications* **2011**, *4*, 95.

(11) Pardeike, J.; Hommoss, A.; Müller, R. H. *International Journal of Pharmaceutics* **2009**, *366*, 170.

(12) Sigma Aldrich Quantum Dots http://www.sigmaaldrich.com/materials-science/nanomaterials/quantum-dots.html (accessed Nov 21, 2014).

(13) Tassa, C.; Shaw, S. Y.; Weissleder, R. *Accounts of Chemical Research* **2011**, *44*, 842.

(14) Tai, S.-P.; Wu, Y.; Shieh, D.-B.; Chen, L.-J.; Lin, K.-J.; Yu, C.-H.; Chu, S.-W.; Chang, C.-H.; Shi, X.-Y.; Wen, Y.-C.; Lin, K.-H.; Liu, T.-M.; Sun, C.-K. *Advanced Materials* **2007**, *19*, 4520.

(15) Meiser, F.; Cortez, C.; Caruso, F. *Angewandte Chemie International Edition* **2004**, *43*, 5954.

(16) Lu, Y.; Wang, L.; Chen, D.; Wang, G. *Langmuir* **2012**, *28*, 9282.

(17) Turkevich, J.; Stevenson, P. C.; Hillier, J. *Discussions of the Faraday Society* **1951**, *11*, 55.

(18) Radwan, S. H.; Azzazy, H. M. E. *Expert Review of Molecular Diagnostics* **2009**, *9*, 511.

(19) Jain, P. K.; Lee, K. S.; El-Sayed, I. H.; El-Sayed, M. *The Journal of Physical Chemistry. B* **2006**, *110*, 7238.

(20) Hutter, E.; Fendler, J. H. *Advanced Materials* **2004**, *16*, 1685.

(21) Homola, J. *Chemical Reviews* **2008**, *108*, 462.

(22) Wu, L.; Chen, J.; Du, D.; Ju, H. *Electrochimica Acta* **2006**, *51*, 1208.

(23) Nagatani, N.; Tanaka, R.; Yuhi, T.; Endo, T.; Kerman, K.; Takamura, Y.; Tamiya, E. *Science and Technology of Advanced Materials* **2006**, *7*, 270.

(24) Ruedas-Rama, M. J.; Walters, J. D.; Orte, A.; Hall, E. A. H. *Analytica Chimica Acta* **2012**, *751*, 1.

(25) Saha, K.; Agasti, S. S.; Kim, C.; Li, X.; Rotello, V. M. *Chemical Reviews* **2012**, *112*, 2739.

(26) Cai, W.; Gao, T.; Hong, H.; Sun, J. *Nanotechnology, Science and Applications* **2008**, *2008*, 17.

(27) Qian, X.; Peng, X.-H.; Ansari, D. O.; Yin-Goen, Q.; Chen, G. Z.; Shin, D. M.; Yang, L.; Young, A. N.; Wang, M. D.; Nie, S. *Nature Biotechnology* **2008**, *26*, 83.

(28) Huang, X.; El-Sayed, I. H.; Qian, W.; El-Sayed, M. a. *Journal of the American Chemical Society* **2006**, *128*, 2115.

(29) Ali, M. E.; Hashim, U.; Mustafa, S.; Che Man, Y. B.; Islam, K. N. *Journal of Nanomaterials* **2012**, 1.

(30) Alshehri, A. H.; Jakubowska, M.; Anna, M.; Horaczek, M.; Rudka, D.; Free, C.; Carey, J. D. *Applied Materials and Interfaces* **2012**, *4*, 7007.

(31) Mcfarland, A. D.; Duyne, R. P. Van. *Nano letters* **2003**, *3*, 1057.

(32) Mandal, A.; Sekar, S.; Mohamed, K.; Meera, S.; Mukherjee, A.; Sastry, T. P.; Mandal, A. B. *Physical Chemistry Chemical Physics* **2014**, *16*, 20175.

(33) Iravani, S.; Korbekandi, H.; Mirmohammadi, S. V; Zolfaghari, B. *Research in Pharmaceutical Sciences* **2013**, *9*, 385.

(34) Domènech, B.; Muñoz, M.; Muraviev, D. N.; Macanás, J. In *Microbial Pathogens and Strategies for Combating them: Science, Technology and Education*; Méndex-Vilas, A., Ed.; 2013; pp. 630–640.

(35) Lara, H. H.; Ayala-Núñez, N. V.; Ixtepan Turrent, L. D. C.; Rodríguez Padilla, C. *World Journal of Microbiology and Biotechnology* **2009**, *26*, 615.

(36) Shin, J.; Anisur, R. M.; Ko, M. K.; Im, G. H.; Lee, J. H.; Lee, I. S. *Angewandte Chemie International Edition* **2009**, *48*, 321.

(37) Li, L.; Jiang, W.; Luo, K.; Song, H.; Lan, F.; Wu, Y.; Gu, Z. *Theranostics* **2013**, *3*, 595.

(38) Yang, H.; Li, X.; Zhou, H.; Zhuang, Y.; Hu, H.; Wu, H.; Yang, S. *Journal of Alloys and Compounds* **2011**, *509*, 1217.

(39) Parkes, L. M.; Hodgson, R.; Lu, L. T.; Tung, L. D.; Robinson, I.; Fernig, D. G.; Thanh, N. T. K. *Contrast Media & Molecular Imaging* **2008**, *3*, 150.

(40) Colombo, M.; Carregal-Romero, S.; Casula, M. F.; Gutiérrez, L.; Morales, M. P.; Böhm, I. B.; Heverhagen, J. T.; Prosperi, D.; Parak, W. J. *Chemical Society Reviews* **2012**, *41*, 4306.

(41) Lu, A.-H.; Salabas, E. L.; Schüth, F. *Angewandte Chemie International Edition* **2007**, *46*, 1222.

(42) Rabias, I.; Tsitrouli, D.; Karakosta, E.; Kehagias, T.; Diamantopoulos, G.; Fardis, M.; Stamopoulos, D.; Maris, T. G.; Falaras, P.; Zouridakis, N.; Diamantis, N.; Panayotou, G.; Verganelakis, D. a; Drossopoulou, G. I.; Tsilibari, E. C.; Papavassiliou, G. *Biomicrofluidics* **2010**, *4*.

(43) Perazella, M. A. *Current Drug Safety* **2008**, *3*, 67.

(44) Nahrendorf, M.; Jaffer, F. a; Kelly, K. a; Sosnovik, D. E.; Aikawa, E.; Libby, P.; Weissleder, R. *Circulation* **2006**, *114*, 1504.

(45) Koehler, F. M.; Rossier, M.; Waelle, M.; Athanassiou, E. K.; Limbach, L. K.; Grass, R. N.; Günther, D.; Stark, W. J. *Chemical Communications* **2009**, 4862.

(46) Singh, N.; Jenkins, G. J. S.; Asadi, R.; Doak, S. H. *Nano Reviews* **2010**, *1*, 5358.

(47) Press, D. *International Journal of Nanomedicine* **2014**, *9*, 1393.

(48) Berry, C. C.; Wells, S.; Charles, S.; Aitchison, G.; Curtis, A. S. G. *Biomaterials* **2004**, *25*, 5405.

(49) Sokolov, K. V; Emelianov, S. Y. *Nanotechnology* **2011**, *22*, 415105.

(50) Gupta, A. K.; Gupta, M. *Biomaterials* **2005**, *26*, 1565.

(51) Lunov, O.; Syrovets, T.; Röcker, C.; Tron, K.; Nienhaus, G. U.; Rasche, V.; Mailänder, V.; Landfester, K.; Simmet, T. *Biomaterials* **2010**, *31*, 9015.

(52) Ahamed, M.; Akhtar, M. J.; Siddiqui, M. a; Ahmad, J.; Musarrat, J.; Al-Khedhairy, A. a; AlSalhi, M. S.; Alrokayan, S. a. *Toxicology* **2011**, *283*, 101.

(53) Mahmoudi, M.; Hofmann, H.; Rothen-Rutishauser, B.; Petri-Fink, A. *Chemical Reviews* **2012**, *112*, 2323.

(54) Voinov, M. A.; Paga, J. O. S.; Morrison, E.; Smirnova, T. I.; Smirnov, A. I. *Journal of the American Chemical Society* **2011**, *133*, 35.

(55) Starke, P. E.; Farbers, L. *Journal of Biological Chemistry* **1985**, *260*, 10099.

(56) Rasmussen, J. W.; Martinez, E.; Louka, P.; Wingett, D. G. *Expert Opinion in Drug Delivery* **2011**, *7*, 1063.

(57) Santra, S.; Malhotra, A. *Wiley Interdisciplinary Reviews. Nanomedicine and Nanobiotechnology* **2011**, 501.

(58) Russin, T. J.; Kaiser, J. M.; Barth, B. M.; Eklund, P. C.; Kester, M.; Adair, J. H. *ACS Nano* **2008**, *2*, 2075.

(59) Kobayashi, H.; Kosaka, N.; Ogawa, M.; Morgan, N. Y.; Smith, P. D.; Murray, C. B.; Ye, X.; Collins, J.; Kumar, G. A.; Bell, H.; Choyke, P. L. *Journal of Materials Chemistry* **2009**, *19*, 6481.

(60) Febvay, S.; Marini, D. M.; Belcher, A. M.; Clapham, D. E. *Nano Letters* **2010**, *10*, 2211.

(61) Cho, E.-B.; Volkov, D. O.; Sokolov, I. *Advanced Functional Materials* **2011**, *21*, 3129.

(62) Huh, S.; Wiench, J. W.; Yoo, J.; Pruski, M.; Lin, V. S. *Chemistry of Materials* **2003**, *15*, 4247.

(63) He, C.; Zhu, W.; Xu, Y.; Zhong, Y.; Zhou, J.; Qian, X. *Journal of Materials Chemistry* **2010**, *20*, 10755.

(64) Singh, N.; Karambelkar, A.; Gu, L.; Lin, K.; Miller, J. S.; Chen, C. S.; Sailor, M. J.; Bhatia, S. N. *Journal of the American Chemical Society* **2011**, *133*, 19582.

(65) Tung, C.; Mahmood, U.; Bredow, S.; Weissleder, R. *Cancer Research* **2000**, *60*, 4953.

(66) Mérian, J.; Gravier, J.; Navarro, F.; Texier, I. *Molecules* **2012**, *17*, 5564.

(67) Kim, J. Y.; Voznyy, O.; Zhitomirsky, D.; Sargent, E. H. *Advanced Materials* **2013**, *25*, 4986.

(68) Unl, H. In *Low Dimensional Semiconductor Structures*; Ünlü, H.; Horing, N. J. M., Eds.; NanoScience and Technology; Springer Berlin Heidelberg: Berlin, Heidelberg, 2013; pp. 1–17.

(69) Ekimov, A. I.; Onushchenko, A. A. *JETP Letters* **1981**, *34*, 363.

(70) Rossetti, R.; Nakahara, S.; Brus, L. E. *The Journal of Chemical Physics* **1983**, *79*, 1086.

(71) Murray, C. B.; Noms, D. J.; Bawendi, M. G. *Journal of the American Chemical Society* **1993**, *115*, 8706.

(72) Demchenko, A. P. *Methods and Applications in Fluorescence* **2013**, *1*, 022001.

(73) Zrazhevskiy, P.; Sena, M.; Gao, X. *Chemical Society Reviews* **2010**, *39*, 4326.

(74) Jensen, K. F.; Mattoussi, H.; Michel, J.; Dabbousi, B. O.; Bawendi, M. G. *Applied Phsyical Letters* **1997**, *70*, 2132.

(75) Hines, M. A.; Guyot-Sionnest, P. *Journal of Physical Chemistry* **1996**, *100*, 468.

(76) Resch-Genger, U.; Grabolle, M.; Cavaliere-Jaricot, S.; Nitschke, R.; Nann, T. *Nature Methods* **2008**, *5*, 763.

(77) Sweeney, E.; Ward, T. H.; Gray, N.; Womack, C.; Jayson, G.; Hughes, A.; Dive, C.; Byers, R. *Biochemical and Biophysical Research Communications* **2008**, *374*, 181.

(78) Chan, W. C. W.; Maxwell, D. J.; Gao, X.; Bailey, R. E.; Han, M.; Nie, S. *Current Opinion in Biotechnology* **2002**, *13*, 40.

(79) Medintz, I. L.; Uyeda, H. T.; Goldman, E. R.; Mattoussi, H. *Nature Materials* **2005**, *4*, 435.

(80) Su, S.; Fan, J.; Xue, B.; Yuwen, L.; Liu, X.; Pan, D.; Fan, C.; Wang, L. *Applied Materials and Interfaces* **2014**, *6*, 1152.

(81) Gao, X.; Cui, Y.; Levenson, R. M.; Chung, L. W. K.; Nie, S. *Nature Biotechnology* **2004**, *22*, 969.

(82) Peng, L.; He, M.; Chen, B.; Wu, Q.; Zhang, Z.; Pang, D.; Zhu, Y.; Hu, B. *Biomaterials* **2013**, *34*, 9545.

(83) Derfus, A. M.; Chan, W. C. W.; Bhatia, S. N. *Nano Letters* **2004**, *4*, 11.

(84) Kim, M. R.; Chung, J. H.; Lee, M.; Lee, S.; Jang, D.-J. *Journal of Colloid and Interface science* **2010**, *350*, 5.

(85) Baker, S. N.; Baker, G. a. *Angewandte Chemie International Edition* **2010**, *49*, 6726.

(86) Xu, X.; Ray, R.; Gu, Y.; Ploehn, H. J.; Gearheart, L.; Raker, K.; Scrivens, W. a. *Journal of the American Chemical Society* **2004**, *126*, 12736.

(87) Sun, Y. P.; Zhou, B.; Lin, Y.; Wang, W.; Fernando, K. a S.; Pathak, P.; Meziani, M. J.; Harruff, B. a.; Wang, X.; Wang, H.; Luo, P. G.; Yang, H.; Kose, M. E.; Chen, B.; Veca, L. M.; Xie, S. Y. *Journal of the American Chemical Society* **2006**, *128*, 7756.

(88) Hu, S.-L.; Niu, K.-Y.; Sun, J.; Yang, J.; Zhao, N.-Q.; Du, X.-W. *Journal of Materials Chemistry* **2009**, *19*, 484.

(89) Zhou, J.; Booker, C.; Li, R.; Zhou, X.; Sham, T. *Journal of the American Chemical Society* **2007**, *129*, 744.

(90) Liu, H.; Ye, T.; Mao, C. *Angewandte Chemie International Edition* **2007**, *46*, 6473.

(91) Wang, X.; Qu, K.; Xu, B.; Ren, J.; Qu, X. *Journal of Materials Chemistry* **2011**, *21*, 2445.

(92) Sahu, S.; Behera, B.; Maiti, T. K.; Mohapatra, S. *Chemical Communications* **2012**, *48*, 8835.

(93) Wang, J.; Wang, C. F.; Chen, S. *Angewandte Chemie International Edition* **2012**, *51*, 9297.

(94) Wu, L.; Cai, X.; Nelson, K.; Xing, W.; Xia, J.; Zhang, R.; Stacy, A. J.; Luderer, M.; Lanza, G. M.; Wang, L. V; Shen, B.; Pan, D. *Nano Research* **2013**, *6*, 312.

(95) Jiang, C.; Wu, H.; Song, X.; Ma, X.; Wang, J.; Tan, M. *Talanta* **2014**, *127*, 68.

(96) Bourlinos, A. B.; Stassinopoulos, A.; Anglos, D.; Zboril, R.; Karakassides, M.; Giannelis, E. P. *Small* **2008**, *4*, 455.

(97) Liu, R.; Wu, D.; Liu, S.; Koynov, K.; Knoll, W.; Li, Q. *Angewandte Chemie International Edition* **2009**, *48*, 4598.

(98) Bourlinos, A. B.; Stassinopoulos, A.; Anglos, D.; Zboril, R.; Georgakilas, V.; Giannelis, E. P. *Chemistry of Materials* **2008**, *20*, 4539.

(99) Zhu, H.; Wang, X.; Li, Y.; Wang, Z.; Yang, F.; Yang, X. *Chemical Communications* **2009**, 5118.

(100) Liu, C.; Zhang, P.; Tian, F.; Li, W.; Li, F.; Liu, W. *Journal of Materials Chemistry* **2011**, *21*, 13163.

(101) Linehan, K.; Doyle, H. *Journal of Materials Chemistry C* **2014**, *2*, 6025.

(102) Jiang, J.; He, Y.; Li, S.; Cui, H. *Chemical Communications* **2012**, *48*, 9634.

(103) Lu, Y.; Zhang, L.; Lin, H. *Chemistry A European Journal* **2014**, *20*, 4246.

(104) Lin, Z.; Xue, W.; Chen, H.; Lin, J.-M. *Chemical Communications* **2012**, *48*, 1051.

(105) Bond, C. *Geophysical Research Letters* **2001**, *28*, 4075.

(106) Eda, G.; Lin, Y.-Y.; Mattevi, C.; Yamaguchi, H.; Chen, H.-A.; Chen, I.-S.; Chen, C.-W.; Chhowalla, M. *Advanced Materials* **2010**, *22*, 505.

(107) Li, H.; Kang, Z.; Liu, Y.; Lee, S.-T. *Journal of Materials Chemistry* **2012**, *22*, 24230.

(108) Zheng, L.; Chi, Y.; Dong, Y.; Lin, J.; Wang, B. *Journal of the American Chemical Society* **2009**, *131*, 4564.

(109) Pan, D.; Zhang, J.; Li, Z.; Wu, C.; Yan, X.; Wu, M. *Chemical Communications* **2010**, *46*, 3681.

(110) Zhao, Q.-L.; Zhang, Z.-L.; Huang, B.-H.; Peng, J.; Zhang, M.; Pang, D.-W. *Chemical Communications* **2008**, 5116.

(111) Tian, L.; Ghosh, D.; Chen, W.; Pradhan, S.; Chang, X.; Chen, S. *Chemistry of Materials* **2009**, *21*, 2803.

(112) Guo, X.; Wang, C.-F.; Yu, Z.-Y.; Chen, L.; Chen, S. *Chemical Communications* **2012**, *48*, 2692.

(113) Li, H.; He, X.; Kang, Z.; Huang, H.; Liu, Y.; Liu, J.; Lian, S.; Tsang, C. H. a; Yang, X.; Lee, S. T. *Angewandte Chemie International Edition* **2010**, *49*, 4430.

(114) Li, H.; He, X.; Liu, Y.; Yu, H.; Kang, Z.; Lee, S.-T. *Materials Research Bulletin* **2011**, *46*, 147.

(115) Jia, X.; Li, J.; Wang, E. *Nanoscale* **2012**, *4*, 5572.

(116) Li, H.; Ming, H.; Liu, Y.; Yu, H.; He, X.; Huang, H.; Pan, K.; Kang, Z.; Lee, S.-T. *New Journal of Chemistry* **2011**, *35*, 2666.

(117) Wu, S.; Han, G.; Milliron, D. J.; Aloni, S.; Altoe, V.; Talapin, D. V; Cohen, B. E.; Schuck, P. J. *Proceedings of the National Academy of Sciences* **2009**, *106*, 10917.

(118) Auzel, F. *Chemical Reviews* **2004**, *104*, 139.

(119) Idris, N. M.; Gnanasammandhan, M. K.; Zhang, J.; Ho, P. C.; Mahendran, R.; Zhang, Y. *Nature Medicine* **2012**, *18*, 1580.

(120) Cao, L.; Wang, X.; Meziani, M. J.; Lu, F.; Wang, H.; Luo, P. G.; Lin, Y.; Harruff, B. a.; Veca, L. M.; Murray, D.; Xie, S. Y.; Sun, Y. P. *Journal of the American Chemical Society* **2007**, *129*, 11318.

(121) Pu, S.-C.; Yang, M.-J.; Hsu, C.-C.; Lai, C.-W.; Hsieh, C.-C.; Lin, S. H.; Cheng, Y.-M.; Chou, P.-T. *Small* **2006**, *2*, 1308.

(122) Larson, D. R.; Zipfel, W. R.; Williams, R. M.; Clark, S. W.; Bruchez, M. P.; Wise, F. W.; Webb, W. W. *Science* **2003**, *300*, 1434.

(123) Zhang, Y.-Q.; Ma, D.-K.; Zhuang, Y.; Zhang, X.; Chen, W.; Hong, L.-L.; Yan, Q.-X.; Yu, K.; Huang, S.-M. *Journal of Materials Chemistry* **2012**, *22*, 16714.

(124) Sun, D.; Ban, R.; Zhang, P.-H.; Wu, G.-H.; Zhang, J.-R.; Zhu, J.-J. *Carbon* **2013**, *64*, 424.

(125) Wang, C.; Sun, D.; Zhuo, K.; Zhang, H.; Wang, J. *RSC Advances* **2014**, *4*, 54060.

(126) Niu, J.; Gao, H.; Wang, L.; Xin, S.; Zhang, G.; Wang, Q.; Guo, L.; Liu, W.; Gao, X.; Wang, Y. *New Journal of Chemistry* **2014**, *38*, 1522.

(127) Xu, Y.; Wu, M.; Liu, Y.; Feng, X.-Z.; Yin, X.-B.; He, X.-W.; Zhang, Y.-K. *Chemistry A European Journal* **2013**, *19*, 2276.

(128) Sun, Y.; Wang, X.; Lu, F.; Cao, L.; Meziani, M. J.; Luo, P. G.; Gu, L.; Veca, L. M. *The Journal of Physical Chemistry. C Letters* **2008**, *112*, 18295.

(129) Peng, H.; Travas-Sejdic, J. *Chemistry of Materials* **2009**, *21*, 5563.

(130) Qu, S.; Wang, X.; Lu, Q.; Liu, X.; Wang, L. *Angewandte Chemie International Edition* **2012**, *51*, 12215.

(131) Zhu, S.; Maharjan, S.; Hao, Z.; Song, Y.; Zhao, X.; Jiang, Y.; Yang, B.; Lu, L. *RSC Advances* **2014**.

(132) Li, N.; Liang, X.; Wang, L.; Li, Z.; Li, P.; Zhu, Y.; Song, J. *Journal of Nanoparticle Research* **2012**, *14*, 1177.

(133) Leménager, G.; De Luca, E.; Sun, Y.-P.; Pompa, P. P. *Nanoscale* **2014**, *6*, 8617.

(134) Wang, D.; Wang, X.; Guo, Y.; Liu, W.; Qin, W. *RSC Advances* **2014**, *4*, 51658.

(135) Salinas-Castillo, A.; Ariza-Avidad, M.; Pritz, C.; Camprubí-Robles, M.; Fernández, B.; Ruedas-Rama, M. J.; Megia-Fernández, A.; Lapresta-Fernández, A.; Santoyo-Gonzalez, F.; Schrott-Fischer, A.; Capitan-Vallvey, L. F. *Chemical Communications* **2013**, *49*, 1103.

(136) Hsu, P.-C.; Shih, Z.-Y.; Lee, C.-H.; Chang, H.-T. *Green Chemistry* **2012**, *14*, 917.

(137) Ray, S. C.; Saha, A.; Jana, N. R.; Sarkar, R. *Journal of Physical Chemistry. C* **2009**, *113*, 18546.

(138) Yang, Y.; Cui, J.; Zheng, M.; Hu, C.; Tan, S.; Xiao, Y.; Yang, Q.; Liu, Y. *Chemical Communications* **2012**, *48*, 380.

(139) Gao, X.; Ding, C.; Zhu, A.; Tian, Y. *Analytical Chemistry* **2014**, *86*, 7071.

(140) Wang, F.; Pang, S.; Wang, L.; Li, Q.; Kreiter, M.; Liu, C. *Chemistry of Materials* **2010**, *22*, 4528.

(141) Fang, Y.; Guo, S.; Li, D.; Zhu, C.; Ren, W.; Dong, S.; Wang, E. *ACS Nano* **2012**, *6*, 400.

(142) Liu, Y.; Xiao, N.; Gong, N.; Wang, H.; Shi, X.; Gu, W.; Ye, L. *Carbon* **2014**, *68*, 258.

(143) Jaiswal, A.; Ghosh, S. S.; Chattopadhyay, A. *Chemical Communications* **2012**, *48*, 407.

(144) Mitra, S.; Chandra, S.; Kundu, T.; Banerjee, R.; Pramanik, P.; Goswami, A. *RSC Advances* **2012**, *2*, 12129.

(145) Von Hippel, A. R. *Dielectric Materials and Applications*; MIT Press, Cambridge, MA, 1954.

(146) Giguere, R. J.; Bray, T. L.; Duncan, S. M.; Majctich, G. *Tetrahedron Letters* **1986**, *27*, 4945.

(147) Rousell, J. *Tetrahedron Letters* **1986**, *27*, 279.

(148) Kappe, C. O. *Angewandte Chemie International Edition* **2004**, *43*, 6250.

(149) Zhai, X.; Zhang, P.; Liu, C.; Bai, T.; Li, W.; Dai, L.; Liu, W. *Chemical Communications* **2012**, *48*, 7955.

(150) Login, G. R.; Dvorak, A. M. *Journal of Neuroscience Methods* **1994**, *55*, 173.

(151) Chandra, S.; Das, P.; Bag, S.; Laha, D.; Pramanik, P. *Nanoscale* **2011**, *3*, 1533.

(152) Mather, B. D.; Viswanathan, K.; Miller, K. M.; Long, T. E. *Progress in Polymer Science* **2006**, *31*, 487.

(153) Ferruti, P.; Marchisio, M. A.; Duncan, R. *Macromolecular Rapid Communications* **2002**, *23*, 332.

(154) Ranucci, E.; Spagnoli, G.; Ferruti, P.; Sgouras, D.; Duncan, R. *Journal of Biomaterials Science* **1991**, *2*, 303.

(155) Ferruti, P. *Journal of Polymer Science Part A: Polymer Chemistry* **2013**, *51*, 2319.

(156) Wu, D.; Liu, Y.; He, C.; Chung, T.; Goh, S. *Macromolecules* **2004**, *37*, 6763.

(157) Emilitri, E.; Ferruti, P.; Annunziata, R.; Ranucci, E.; Interdisciplinare, C.; Nanostrutturati, I.; Organica, C.; Venezian, V.; Rossi, M.; Falciola, L.; Mussini, P.; Fisica, C.; Golgi, V.; Chiellini, F.; Bartoli, C.; Udr, B.; Consortium, I.; Industriale, C.; Uni, V. *Macromolecules* **2007**, *40*, 4785.

(158) Lynn, D. M.; Langer, R. *Journal of the American Chemical Society* **2000**, *122*, 10761.

(159) Muralidharan, S.; Ravichandran, S.; Pitchumani, S.; Phani, K. L. N. *Journal of Materials Science Letters* **2000**, *19*, 1299.

(160) Jin, F.; Han, M.; Park, S. *Polymer International* **2006**, *55*, 1265.

(161) Danusso, F.; Ferruti, P. *Polymer* **1970**, *11*, 88.

(162) De, B.; Karak, N. *RSC Advances* **2013**, *3*, 8286.

(163) Wang, Z.; Zhao, Y.; Tait, K.; Liao, X.; Schiferl, D.; Zha, C.; Downs, R. T.; Qian, J.; Zhu, Y.; Shen, T. *Proceedings of the National Academy of Sciences* **2004**, *101*, 13699.

(164) Jolly, W. L.; Hollander, Jack, M. *Accounts of Chemical Research* **1970**, *3*, 193.

(165) Horvath, H. *Atmospheric Environment* **1993**, *27*, 293.

(166) Watson, A. Y.; Valberg, P. a. *American Industrial Hygiene Association Journal* **2001**, *62*, 218.

(167) Andreae, M. O. *Atmospheric Chemistry and Physics Discussions* **2006**, *6*, 3419.

(168) Sun, H.; Biedermann, L.; Bond, T. C. *Geophysical Research Letters* **2007**, *34*, L17813.

(169) Porrès, L.; Holland, A.; Pålsson, L.-O.; Monkman, A. P.; Kemp, C.; Beeby, A. *Journal of Fluorescence* **2006**, *16*, 267.

(170) Brouwer, A. M. *Pure and Applied Chemistry* **2011**, *83*.

(171) Jobin Yvon Horiba. A Guide to Recording Fluorescence Quantum Yields.

(172) Tan, D.; Zhou, S.; Jianrong, Q. *ACS Nano* **2012**, *6*, 6530.

(173) Denk, W.; Svoboda, K. *Neuron* **1997**, *18*, 351.

(174) Xu, C.; Webb, W. W. *Journal of the Optical Society of America B* **1996**, *13*, 481.

(175) Yang, S.; Wang, X.; Wang, H.; Lu, F.; Luo, P. G.; Cao, L.; Meziani, M. J.; Liu, J.; Liu, Y.; Chen, M.; Huang, Y.; Sun, Y. *Journal of Physical Chemistry. C* **2009**, *113*, 18110.

(176) Wang, K.; Gao, Z.; Gao, G.; Wo, Y.; Wang, Y.; Shen, G.; Cui, D. *Nanoscale Research Letters* **2013**, *8*, 122.

(177) Zhu, Y.; Li, W. *Science in China Series B: Chemistry* **2008**, *51*, 1021.

(178) Wang, K.; Gao, Z.; Gao, G.; Wo, Y.; Wang, Y.; Shen, G.; Cui, D. *Nanoscale Research Letters* **2013**, *8*, 122.

(179) Mosmann, T. *Journal of Immunological Methods* **1983**, *65*, 55.

(180) Liu, H.; Wang, Q.; Shen, G.; Zhang, C.; Li, C.; Ji, W.; Wang, C. *Nanoscale Research Letters* **2014**, *9*, 397.

(181) Huang, P.; Lin, J.; Wang, X.; Wang, Z.; Zhang, C.; He, M.; Wang, K.; Chen, F.; Li, Z.; Shen, G.; Cui, D.; Chen, X. *Advanced Materials* **2012**, *24*, 5104.

(182) Li, Q.; Ohulchanskyy, T. Y.; Liu, R.; Koynov, K.; Wu, D.; Best, A.; Kumar, R.; Bonoiu, A.; Prasad, P. N. *Journal of Physical Chemistry. C* **2010**, 12062.

(183) Newport, J. W.; Forbes, D. J. *Annual Review of Biochemistry* **1987**, *56*, 535.

(184) Bataiud, N.; Helser, T.; Fried, H. M. *Journal of Cell Biology* **1990**, *111*, 1571.

(185) Cole, C. N.; Scarcelli, J. J. *Current Opinion in Cell Biology* **2006**, *18*, 299.

(186) Daneholt, B. *Cell* **1997**, *88*, 585.

(187) Wente, S. R.; Rout, M. P. *Cold Spring Harbor Perspectives in Biology* **2010**, *2*, 1.

(188) Kalderon, D.; Roberts, B. L.; Richardson, W. D.; Smith, A. E. *Cell* **1984**, *39*, 499.

(189) Martin, R. M.; Leonhardt, H.; Cardoso, M. C. *Cytometry. Part A* **2005**, *67*, 45.

(190) Rivas, S.; Genin, S. *Frontiers in Plant Science* **2011**, *2*, 104.

(191) Picard, M.; Taivassalo, T.; Gouspillou, G.; Hepple, R. T. *The Journal of Physiology* **2011**, *589*, 4413.

(192) Nicholls, D. G. *Cell Calcium* **2005**, *38*, 311.

(193) Murphy, M. P. *The Biochemical Journal* **2009**, *417*, 1.

(194) Schneider, A. *International Journal for Parasitology* **2001**, *31*, 1403.

(195) Nivala, M.; Korge, P.; Nivala, M.; Weiss, J. N.; Qu, Z. *Biophysical Journal* **2011**, *101*, 2102.

(196) McBride, H. M.; Neuspiel, M.; Wasiak, S. *Current Biology* **2006**, *16*, 551.

(197) Chabi, B.; Adhihetty, P. J.; Ljubicic, V.; Hood, D. a. *Medicine & Science in Sports & Exercise* **2005**, *37*, 2102.

(198) *The Human Fertilisation and Embryology (Mitochondrial Donation) Regulations 2015*; HM Government: UK, 2015.

(199) Gilmore, K.; Wilson, M.; Dioc, J. *Cytometry* **1999**, *36*, 355.

(200) Fei, X.; Gu, Y. *Progress in Natural Science* **2009**, *19*, 1.

(201) Luo, P. G.; Sahu, S.; Yang, S.-T.; Sonkar, S. K.; Wang, J.; Wang, H.; LeCroy, G. E.; Cao, L.; Sun, Y.-P. *Journal of Materials Chemistry B* **2013**, *1*, 2116.

(202) Sheu, S.-S.; Nauduri, D.; Anders, M. W. *Biochimica et Biophysica Acta* **2006**, *1762*, 256.

(203) Smith, R. A. J.; Porteous, C. M.; Coulter, C. V; Murphy, M. P. *European Journal of Biochemistry* **1999**, *263*, 709.

(204) Hardy, M.; Poulhe, F.; Rizzato, E.; Rockenbauer, A.; Banaszak, K.; Karoui, H.; Kalyanaraman, B.; Tordo, P.; Ouari, O. *Chemical Research in Toxicology* **2014**, *27*, 1155.

(205) Aimetti, A. A.; Tibbitt, M. W.; Anseth, K. S. *Biomacromolecules* **2009**, *10*, 1484.

(206) Visintin, C.; Aliev, A. E.; Riddall, D.; Baker, D.; Okuyama, M.; Hoi, P. M.; Hiley, R.; Selwood, D. L. *Organic Letters* **2005**, *7*, 1699.

(207) Deroose, F. D.; Clercq, P. J. De. *Journal of Organic Chemistry* **1996**, *60*, 321.